(NASA-CR-140713) PRELIMINARY DESIGN OF A PRIMARY LOOP PUMP ASSEMBLY (PLPA), USING ELECTROMAGNETIC PUMPS Final Report (Atomics International) 126 p HC $5.75 CSCL 13K G3/37

N75-10458

Unclas 53175

AI-72-54

NASA

FINAL REPORT

PRELIMINARY DESIGN OF A PRIMARY LOOP PUMP ASSEMBLY (PLPA), USING ELECTROMAGNETIC PUMPS

By

T. A. Moss, G. Matlin, L. Donelan, J. L. Johnson, and I. Rowe

ATOMICS INTERNATIONAL DIVISION
ROCKWELL INTERNATIONAL CORPORATION

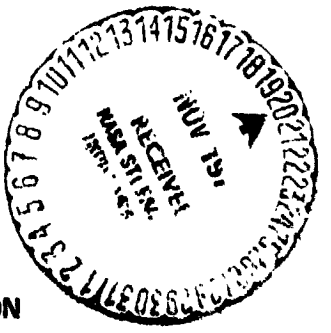

Prepared for
NATIONAL AERONAUTICS AND SPACE ADMINISTRATION
NASA LEWIS RESEARCH CENTER
CONTRACT NAS 3-15342
J. P. Couch, Project Manager

AI-72-54

FINAL REPORT

PRELIMINARY DESIGN OF A PRIMARY LOOP PUMP ASSEMBLY (PLPA), USING ELECTROMAGNETIC PUMPS

By
T. A. Moss, G. Matlin, L. Donelan, J. L. Johnson,
and I. Rowe

ATOMICS INTERNATIONAL DIVISION
ROCKWELL INTERNATIONAL CORPORATION
8900 DeSoto Avenue
Canoga Park, California 91304

Prepared for
NATIONAL AERONAUTICS AND SPACE ADMINISTRATION

SEPTEMBER 1972

CONTRACT NAS 3-15342
NASA LEWIS RESEARCH CENTER
CLEVELAND, OHIO
J. P. Couch, Project Manager

FOREWORD

This report was prepared by Atomics International (AI), a division of North American Rockwell. The activities discussed in the report were conducted under NASA Contract NAS3-15342, with Mr. J. P. Couch, of the Lewis Research Center, as project manager for NASA, and Mr. T. A. Moss as project manager for AI. The primary loop pump assembly study was conducted as part of an overall program to develop a 60- to 80-kwe reactor Brayton space power system.

CONTENTS

CONTENTS

TABLES

FIGURES

FIGURES

FIGURES

FIGURES

ABSTRACT

A preliminary design study of flight-type dc conduction - permanent magnetic, ac helical induction, and ac linear induction pumps for circulating 883°K (1130°F) NaK at 9.1 kg/sec (20 lb/sec) is described. Various electromagnetic pump geometrics are evaluated against hydraulic performance, and the effects of multiple windings and numbers of pumps per assembly on overall reliability were determined. The methods used in the electrical-hydraulic, stress, and thermal analysis are discussed, and the high-temperature electrical materials selected for the application are listed.

SUMMARY

A preliminary design study of dc conduction - permanent magnetic, ac helical induction, and ac linear induction types of pumps was performed, where various geometries were evaluated against performance. The specification in the ZrH reactor - Brayton combined system test (CST) required that the pump assembly produce 48.3 kN/m^2 (7 psi) headrise at 9.1 kg/sec (20 lb/sec) with 610°C (1130°F) NaK. Each pump assembly consisted of either two or three pumps connected in series hydraulically, where one pump in each case was nonoperating or standby to enhance overall reliability.

With the dc-type of pump, the three-pump option proved more efficient, since there was less braking action resulting from the smaller nonoperating pump. In the three-pump option, each pump required ~10,500 amp at ~0.2 v to meet the flow requirements, and operated at 16% efficiency. The total iron and copper weight of the three-pump PLPA was ~345 kg (760 lb).

The Brayton power conversion system produces 440 Hz electrical power, which must be converted to the low voltage, high amperage required for the dc pumps, at an overall conditioning efficiency of~25%. Also associated with the high amperage is high bus loss; therefore, the power conditioning equipment must be in close proximity to the pump in the nuclear shield gallery. This would require that the associated electronic equipment for power conditioning be radiation hardened. Powering the dc pumps with thermoelectric modules was considered, but discarded, since 35 to 40 modules must be tightly packaged into the gallery for the specified flow conditions. As a result of a lack of overall system compatibility, the dc pumps were de-emphasized for the PLPA application.

A reliability analysis of the ac types of PLPA options indicated that there was little difference in the inherent reliabilities between the two-pump option with two windings per pump and the three-pump option with one winding per pump. However, the two-pump options were 20% more efficient than their three-pump counterparts, as a result of higher hydraulic losses in the three-pump configuration. Also, the three-pump option occupied ~80% more volume than the corresponding two-pump option. For these reasons, the three-pump options were de-emphasized about midway through the program.

The dual helical induction pump was selected over the dual linear pump for the PLPA application, since it was more efficient, smaller, and lighter than the linear pump. The dual helical PLPA required 6.6 kwe at 43 v and 46 Hz to produce rated flow while operating at 9.1% efficiency. The efficiency of the dual linear was 7.0%. It was also shown that, because of the stator geometric configurations, the winding temperature of the helical pump was ~65°C (117°F) less than for the linear. Also, heavy external structural members were required to maintain the dimensional integrity of the linear pump, because of its inherent "flat" design.

I. INTRODUCTION

A. SCOPE

This electromagnetic pump study was performed as part of an overall program to develop a PLPA for the ZrH reactor - Brayton cycle combined system test to be run at NASA-LeRC's Space Power Facility.[1-3] This report covers the preliminary design, during which both two-pump and three-pump options of the PLPA were considered for each of three basic types of EM pumps.

The three types of pump which were considered were the permanent magnetic - dc conduction, the ac helical induction, and the ac flat linear induction type. The basic principles of operation of these three types of pumps are shown schematically in Figure 1. In the Faraday dc conduction pump, an electrical current (I) passing horizontally through the fluid in the presence of a magnetic field (B) causes a body force on the fluid in the direction shown. This body force generates a differential pressure in the fluid, causing the conducting fluid to flow in the direction of the force. The pressure generated in the fluid is proportional to the product of the current, flux, and distance. Typically, this type of pump requires a high-amperage (~10,500 amp), low-voltage (0.2 v) power supply.

Also shown in Figure 1 is a schematic of the ac helical induction pump, which is similar to a squirrel cage motor, except that the rotor is replaced with a conducting fluid. The stator windings in the slots carrying ac current generate a rotating magnetic field that induces electrical currents to flow in the liquid metal. The interaction of this induced current and magnetic field creates a body force on the fluid, causing it to rotate tangentially. By imposing a helical vane in the liquid metal channel, a head can be developed in the axial direction.

The flat ac linear induction pump is similar to the helical, except that the stator winding has been flattened out, and divided on either side of the liquid metal duct. Again, the ac winding in the stator slots generates an axially moving magnetic field, which, in turn, induces an electrical current in the liquid metal. The interaction between the induced currents and the magnetic field causes a body force on the conducting fluid, giving a pressure rise in the fluid.

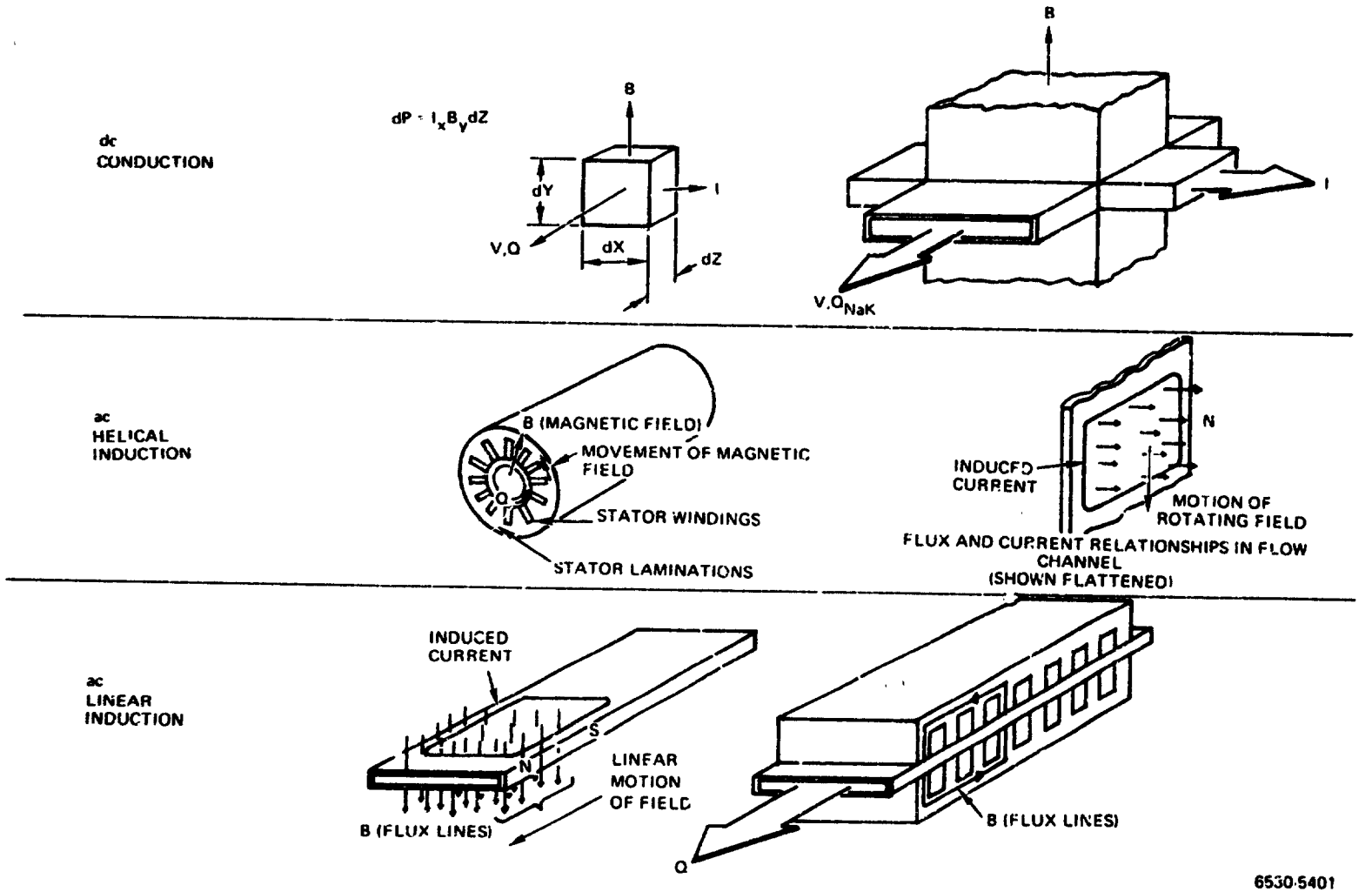

Figure 1. PLPA EM Pump Types

Two other pump concepts were briefly considered, but were rejected as not being competitive with those previously discussed. Consideration was given to the dc electromagnetic field pump, which had the advantages that pressure and flow could be controlled, and eddy current braking on the nonoperating pump was eliminated. In this pump, the permanent magnetic is replaced with an electromagnet. The disadvantage of the concept was that it had all the failure modes associated with both the dc and ac pumps (i.e., bus bar to pump throat joint separation, loss of feedthroughs, coil shorts, and loss of coolant). Since the concept offered no increase in efficiency, and was inherently less reliable, it was dropped from further consideration.

The ac annular linear induction pump was also considered, since it theoretically offered modest improvement in efficiency over the helical and flat linear induction pumps. However, the lack of extensive design, fabrication, or operational experience precluded its being selected for the preliminary design study. The lamination construction for this pump is radial, which is difficult to handle in the stator, and provides a relatively flexible magnetic core construction. This core construction tends to deflect during operation, closing off one side of the gap, due to magnetic pull. The core shift causes an electrical pinch on the fluid, which redistributes the magnetic flux of the machine and could reduce the pump performance.

The two- and three-pump options for the three types of pumps selected are shown schematically in Figure 2. For the dc conduction pump, the options are simply the choice between two large pumps or three smaller pumps in the PLPA, since there are no electrical windings associated with this concept.

In the two-pump option of the ac helical induction pump, two separate concentric windings are contained in each pump. With the failure of Winding 1a or 1b, operation is shifted to 2a and 2b at rated conditions. Failure of 2a or 2b would allow the operation of the PLPA at partial flow conditions, using the unfailed windings in both pumps. In the three-pump option, each pump has one set of windings, each separately contained; however, the electromagnetic end losses and hydraulic losses will be higher than for the two-pump option.

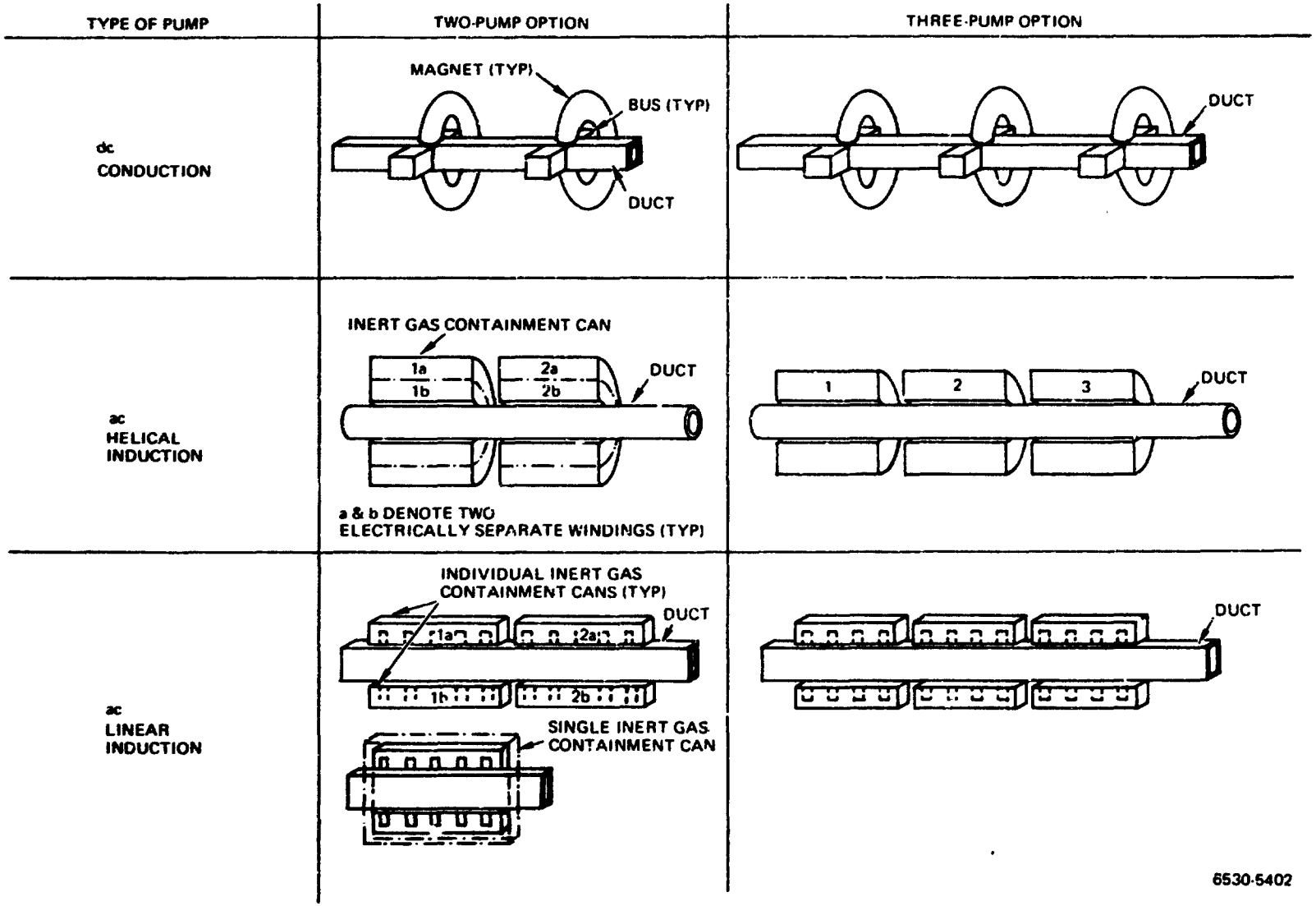

Figure 2. PLPA EM Pump Options

In the two-pump option of the ac linear pump, the two windings of each pump are on separate sides of the fluid duct, and may or may not have separate gas containment. Separate gas containment requires that two thicknesses of metal be added in the air gap, which would reduce overall pump efficiency and introduce severe mechanical design problems. The three-pump option would have single gas containment for each pump; here, again, the three smaller pumps would have slightly higher hydraulic and electromagnetic end losses.

These six concepts were to be carried through the preliminary design phase until they were no longer viable contenders, based upon their relative merits of efficiency, size, controllability, reliability, and system compatibility, at which time they were to be dropped from further consideration.

This report covers the preliminary design study of the dc conduction, ac helical induction, and ac linear induction type pumps performed during the program. Existing AI computer programs were modified, and used to perform the parametric analysis. The programs were changed to account for the two and three pumps in series, encountered in the PLPA application. Using the various parametric curves generated, a set of reference designs were selected and evaluated against the other pump types and system compatibility.

B. OBJECTIVE

The objective of the PLPA program is to design an electromagnetic pump assembly for circulating the primary loop NaK in the SPF reactor - combined system test, Figure 3. The space power system consists of a ZrH reactor heat source cooled with liquid NaK, an inert gas Brayton power conversion system, and an organic-cooled waste heat rejection radiator. There are a number of support systems shown, one of which is the auxiliary NaK loop used to supply coolant to the PLPA electrical windings.

The PLPA is to be situated between the primary nuclear shields surrounding the reactor and secondary disk-shaped shield at the top, as shown in Figure 4. For a given cone angle, the height separating these two shield assemblies has a large effect on overall shield weight, and therefore should be minimized. Throughout the equipment gallery, space is at a premium, and all components should have minimum envelopes. The nuclear environment within the gallery for the 5-year

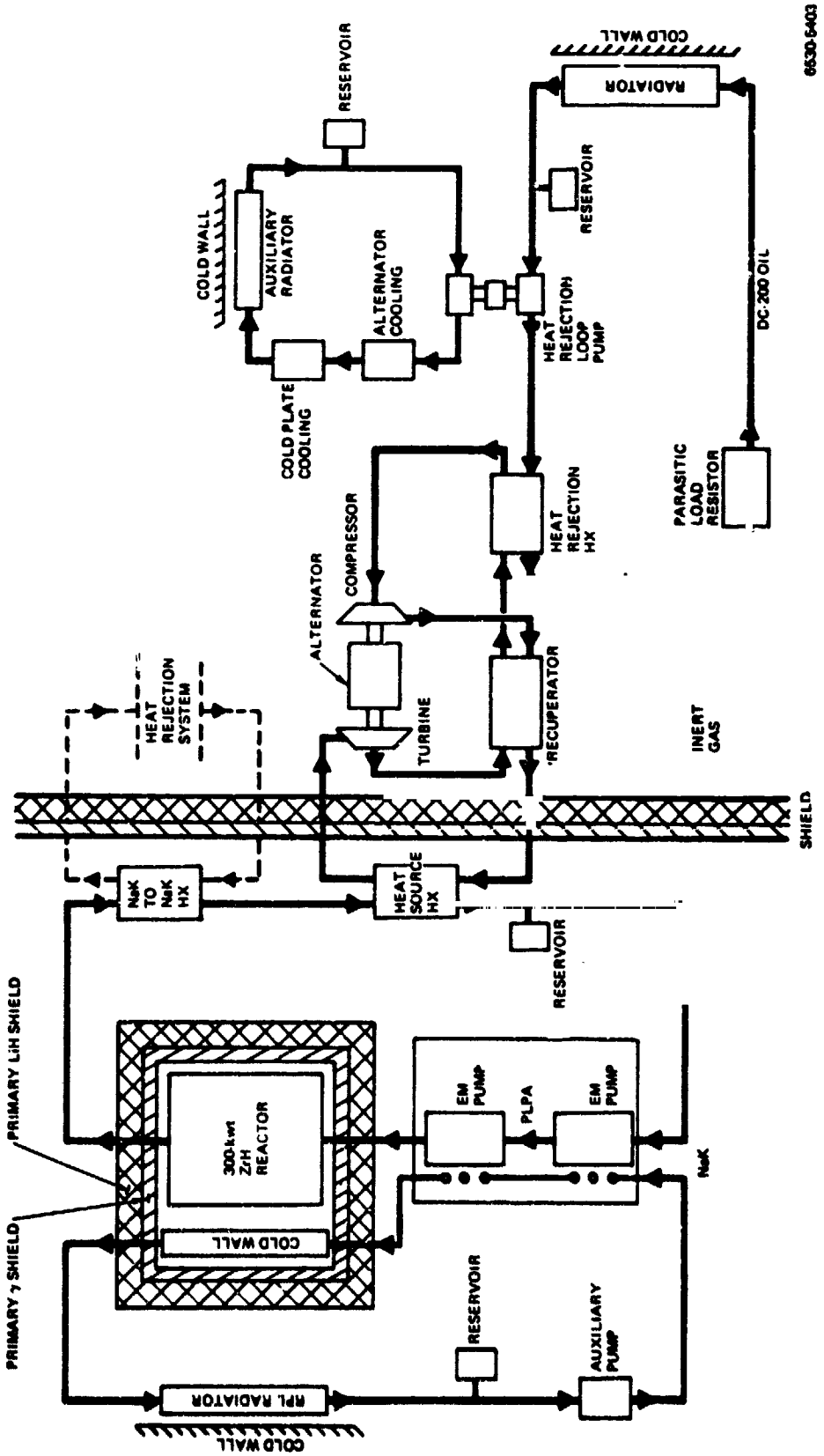

Figure 3. Combined System Test Flow Diagram

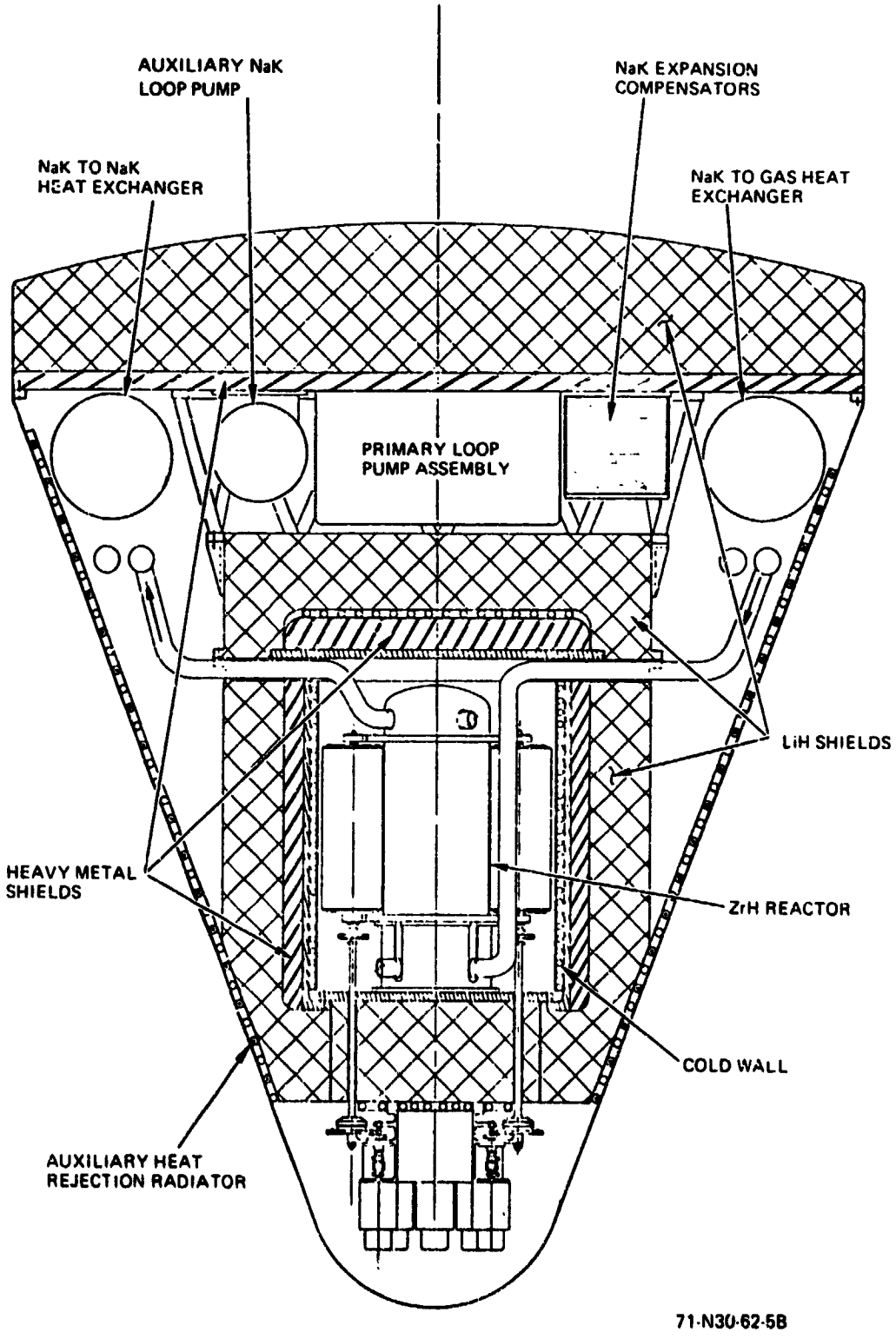

Figure 4. Nuclear Heat Source Assembly

TABLE 1

PRIMARY LOOP PUMP ASSEMBLY SPECIFICATIONS

	Rated Operation	Continuous Off-Design Operation	Short-Term Off-Design Operation
Primary NaK Flow Rate [kg/sec (lbm/sec)]	9.1 (20)	±20% Rated	10 to 120% Rated, 50 hr
Life (years)	5		
Head Rise [kN/m^2 (psi)]	48.3 (7)		
PLPA Input Power [kwe max]	7.6		
Inlet Pressure [kN/m^2 (psi)]	138 (20)	34.5 to 207 (5 to 30)	863 (125 psi) pressure rise in 3 min†
Primary NaK Temperature [°C (°F)]	610 (1130)	593 to 621 (1100 to 1150)	10 to 593 (50 to 1100) in 4 hr 676 (1250), 100 hr
Coolant NaK Inlet Temperature [°C (°F)]	232 (450)	204 to 260 (400 to 500)	232 (450) NaK for Startup
Coolant NaK Flow Rate* [kg/sec (lb/sec)]	0.5 (1.11)		
Coolant NaK Pressure Drop* [kN/m^2 (psi)]	<14 (<2)		
Input Voltage (v)	TBD	±10% Rated	5 to 110% Rated, 50 hr
Height [cm (in.)]	<40.7 (16)		
Environmental Specification	Modified SNAP 8 EGS Spec. 417-2 Rev. C, 6-1-69		
Startup-Shutdowns	100		
Radiation Environment	8×10^9 rad γ 8×10^{17} nvt fast neutrons		

*For one of two redundant circuits

†Emergency — Brayton gas leak

application is expected to be 8×10^9 rad gamma, and 8×10^{17} nvt fast neutrons above 1 Mev. Since the gallery is surrounded by the 204 to 260°C (400 to 500°F) auxiliary NaK heat rejection radiator, there is little possibility of transferring heat by radiation from the PLPA to its surroundings. Therefore, during normal operation, all heat removed from the PLPA is assumed to be rejected only to the primary loop and the NaK auxiliary coolant loops.

The PLPA was to be designed to meet a series of nominal rated, continuous off-design, and emergency short-term conditions shown in Table 1. The unit was to deliver 9.1 kg/sec (20 lbm/sec) of 610°C (1130°F) NaK with a head rise of 48.3 kN/m^2 (7.0 psi), while requiring <7.6 kwe of input power. The PLPA was to be capable of launch, space startup, shutdown and restart, and of continuous operation in space for a minimum of 5 years. It was to consist of two or three electromagnetic pumps connected in series, and to fit inside a rectangular volume with a height of 40.7 cm (16 in.) or less and a minimized length and width. Liquid NaK at 232°C (450°F) was supplied for cooling the electrical windings of each pump.

The primary coolant pressure boundary was to be designed to the "intent" (i.e., no code stamp) of Section III, Class I, Code Case 1331-5 of the ASME Boiler and Pressure Vessel Code. Since a gas leak would not cause failure of the total system, the gas containment surrounding the stator windings was to be designed to the lower requirements of Section III, Class II, by reference to Section VII, Division 2.

Materials which were to be used in the PLPA are shown on Table 2. The selection of the electrical materials is based upon the results of a series of programs to develop high-temperature electromagnetic devices.[4-7] This class of electrical materials is capable of long-term operation at 593°C (1100°F) without serious degradation. A high-thermal-conductivity helium-xenon gas mixture was to be evaluated as a stator gas to reduce winding temperatures.

The following equations were used in determining the properties of sodium-potassium eutectic alloy (NaK):

Vapor Pressure

$$\log_{10} P = 5.7764 - \frac{8103.9}{T} - 0.1125 \log_{10} T, \qquad \ldots(1)$$

where P is in psia and T is in °R. (1 psi = 6.89 kN/m^2; 5/9 $T_R = T_C + 273.15$)

TABLE 2

PLPA SPECIFIED MATERIALS

Primary NaK Piping and Ducts	Type 316 Stainless Steel
Magnetic Material	Hiperco 27
Conductors	Copper or Copper Alloy
Conductor Insulation (end turns)	"S" 994 Glass Tape
Slot Insulation	+99.5 Al_2O_3 Forms
Interlaminar Insulation	Plasma-Sprayed Al_2O_3
Stator Gas*	Argon or Helium-Xenon <5 ppm O_2 and H_2O

*~1 atm at rated conditions

Electrical Resistivity

$$R = 13.49 + 7.463 \times 10^{-3}t + 7.205 \times 10^{-6}t^2 \quad , \qquad \ldots(2)$$

where R is in $\mu\Omega$-in. and T is in °F. (1 in. = 2.540 cm).

Density

$$\rho = 54.67 - 8.349 \times 10^{-3}t \quad , \qquad \ldots(3)$$

where ρ is in lbm/ft^3 and t is in °F. (1 lbm/ft^3 = 11.602 kg/m^3).

Thermal Conductivity

$$k = 12.20 + 6.787 \times 10^{-3}t - 3.793 \times 10^{-6}t^2 \quad , \qquad \ldots(4)$$

where k is in Btu/hr-ft-°F and t is in °F. (1 Btu/hr-ft-°F = 0.01731 w/cm-°C).

Viscosity

$$\log_{10}\mu = 0.6663 + \frac{380.26}{T} - 0.4158 \log_{10}T \quad , \qquad \ldots(5)$$

where μ is in lbm/ft-hr and T is in °R. (1 lbm/ft-hr = 4.134×10^{-4} kg-mass/sec-m).

Specific Heat

$$C_s = 0.2353 - 6.345 \times 10^{-5}t + 4.558 \times 10^{-8}t^2 - 8.573 \times 10^{-12}t^3 \quad , \qquad \ldots(6)$$

where C_s is in Btu/lbm-°F and t is in °F. (1 Btu/lbm-°F = 1 kcal/kg-°C).

Using the preceding guidelines and requirements, conceptual layouts were prepared for the various pump concepts, and parametric studies were performed. Based on trend curves, reference electrical-hydraulic optimum designs were established. Detail layouts were prepared, reflecting the reference design criteria; and, based on the layouts, stress and thermal analyses were performed. Comparative estimated reliability studies on the ac PLPA's were also completed. Finally, recommendations were made regarding the optimum pump type and PLPA configuration. The following sections discuss the results of these studies.

II. dc CONDUCTION PUMPS

A. GENERAL THEORY OF OPERATION

The dc conduction, or Faraday, pump operates on the principle that a conductor carrying current, when placed in a dc magnetic field at right angles to the direction of current flow, will have a force exerted on the conductor in a direction mutually perpendicular to the field and the direction of current. If, then, a conducting fluid contained in a channel is placed in a dc magnetic field at right angles to the axial centerline of the channel, and a current is caused to flow through the channel at right angles to the field and tne axial centerline of the channel, a pressure will be exerted on the fluid in the channel. From Reference 8, the idealized pressure relationship will be of the form:

$$p = \frac{K \varphi I}{w h l} \quad , \qquad \ldots(7)$$

where:

p = pressure rise
φ = total flux
I = total current
w = cross-sectional dimensions of the channel
l = channel length
K = a dimensional constant.

The idealized relationship must be modified to account for current shunting, back emf, and armature reaction. To obtain net pressure rise, hydraulic loss and eddy current braking effects must be subtracted from the developed pressure. In considering overall pump and PLPA performance, bus losses must also be taken into consideration.

The dc magnetic field may be established by a permanent magnet, or may be generated by shunt or series field coils. Studies performed during the initial phase of the PLPA Program indicated that, because of the large conductor cross section required, the use of a series field coil extremely limited the flexibility of the design, and resulted in high bus losses. Also, the use of shunt field coils added potential failure modes without significant improvement of efficiency or

reduction in weight. Therefore, a decision was made, early in the program, to consider only permanent-magnet field pumps.

The dc conduction pump, shown in Figure 5 and used as a model for the study, consists of a straight permanent magnet with a U-shaped iron flux return assembly, and two large copper bus bars brazed to the throat duct. One of the copper bus bars must be curved, to avoid the return iron of the magnet and allow both bus bars to be coupled to the power supply on the same side of the pump. Thermal insulation is required between the 610° C (1130° F) NaK duct and the Alnico V-7 magnets, to maintain their temperature below 482° C (900° F).

The equivalent electrical circuit for the dc conduction pump is shown in Figure 6, along with the basic equation for determining head rise for a given NaK flow rate.

The factor M_1 in Figure 6 is a function of the various wall resistances and pump geometry, which is unique for each design. Factor M_2 is a function of geometry and NaK density, while M_3 also includes NaK resistivity. In this study, the hydraulic losses for the inactive pump were lumped together with the active pump in the factor M_4, using conventional techniques. The final term, M_5 in the equation, was determined from past experimental data on the dc pumps in flowing NaK loops, and is equal to $\sim 1.5 M_3$.

Figure 7 shows the throat configuration of compensated and uncompensated pumps. In the compensated case, the large electrical current is conducted back across the air gap with a copper bar to negate the magnet field setup with a single-pass current. Although the magnetic flux can be nearly cancelled, a large efficiency penalty is incurred by increasing the air gap and bus losses.

B. PARAMETRIC STUDIES

The calculations of the various factors in the pressure equation of Figure 6 were programmed into a computer. In addition to performing arithmetic operations, the program optimizes flux for maximum pressure, and computes magnet dimensions to provide operation at the magnet material maximum energy product point. Printouts are provided of the various pump dimensions, weight, operating conditions, and performance. Table 3 illustrates typical design inputs and variables.

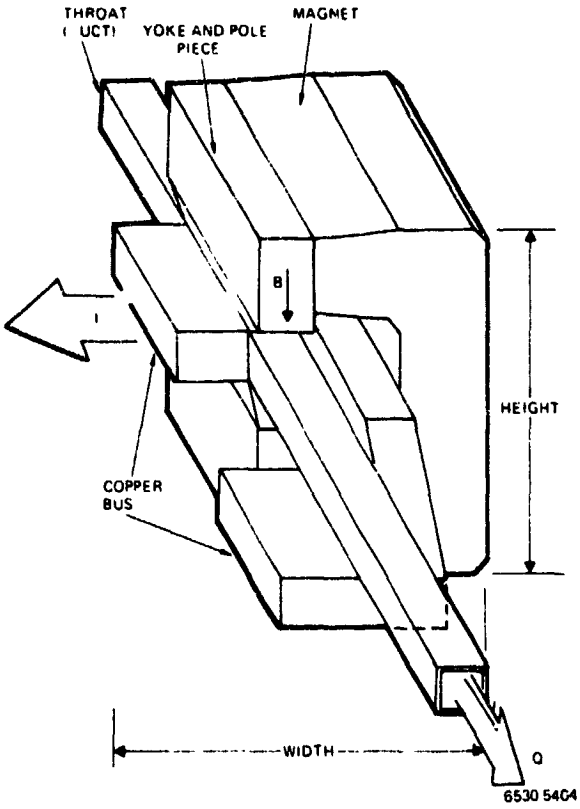

Figure 5. dc Conduction Pump

$$P = M_1GI \times K_{AR} - M_2G^2Q - M_3G^2Q - M_4Q^2 - M_5G^2Q$$

GROSS DEVELOPED PRESSURE	ARMATURE REACTION	BACK emf	EDDY CURRENT LOSSES	HYDRAULIC LOSSES	INACTIVE PUMP BRAKING

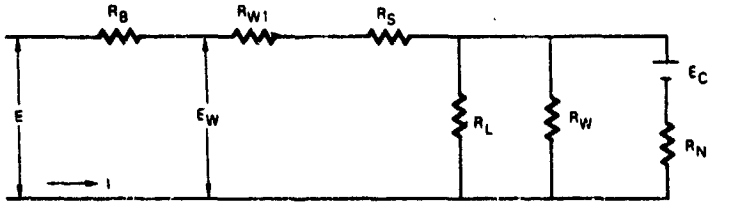

- I = TOTAL CURRENT (amp)
- E = VOLTAGE APPLIED TO BUS (mv)
- E_C = VOLTAGE ACROSS THROAT (mv)
- R_B = BUS RESISTANCE (Ω)
- R_{W_1} = THROAT WALL RESISTANCE PERPENDICULAR TO CURRENT (Ω)
- R_L = BYPASS LEAKAGE CURRENT RESISTANCE OUTSIDE THROAT (Ω)
- R_W = THROAT WALL RESISTANCE PARALLEL TO CURRENT (Ω)
- R_S = SPLITTER PLATE RESISTANCE (Ω)
- R_N = INDUCED BACK emf (mv)
- E_W = THROAT VOLTAGE DROP (mv)
- G = FLUX DENSITY [gauss (gauss × 1.00×10^{-4} = tesla)]
- Q = FLOW RATE [lb/sec (lb/sec x 0.45 = kg/sec)]
- $M_1, M_2, M_3, M_4, M_5, K_{AR}$ = GEOMETRIC FACTORS

6530 5405

Figure 6. dc Pump Equivalent Circuit

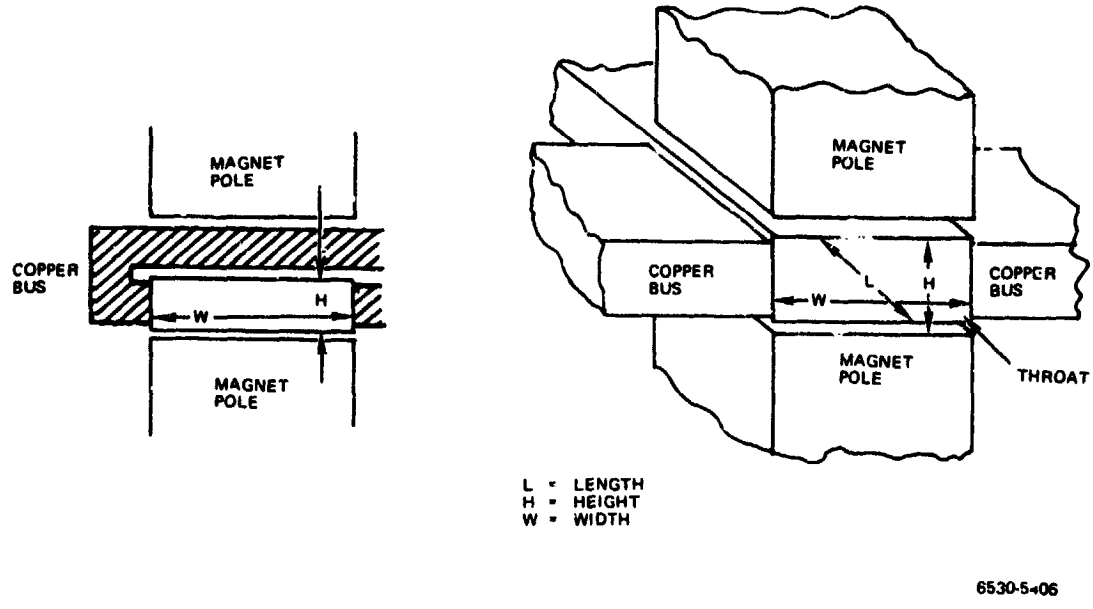

Figure 7. Throat Configuration of Compensated and Uncompensated dc Conduction Pumps

TABLE 3

dc CONDUCTION PLPA DESIGN INPUT AND VARIABLES

Constants	Variables
Flow Rate, 9.1 kg/sec (20 lb/sec)	Throat Length
Pressure, 48.3 kN/m^2 (7 psi)	Throat Width
Throat Wall Thickness, 0.762mm (0.030 in.)	Throat Height
Insulation Thickness, 0.762mm (0.030 in.)	Number of Splitters
Coolant, NaK-78	2 or 3 Pumps in Series
Materials	Compensated or Uncompensated
Permanent Magnet, Alnico V-7	Voltage
Yoke and Pole Piece, Hiperco 27	Current
Bus, Copper-OFHC	Power
Throat, Type 316 Stainless Steel	Efficiency
Magnet	Weight
Flux Density, 1.1250 teslas	Throat Magnetic Flux Density
Field Intensity, 645 oersteds	PLPA Configuration
Temperature, 371°C (700°F)	

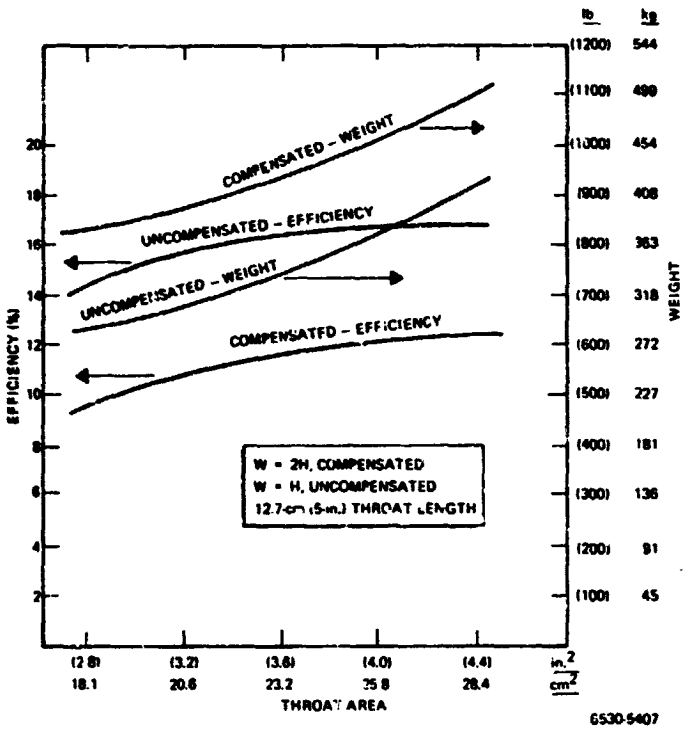

Figure 8.

Efficiency and Pump Weight vs Throat Area for dc PLPA (3-pump PLPA)

Figure 9. ⟶

Efficiency and Pump Weight vs Throat Aspect Ratio for dc PLPA (Uncompensated 3-pump PLPA)

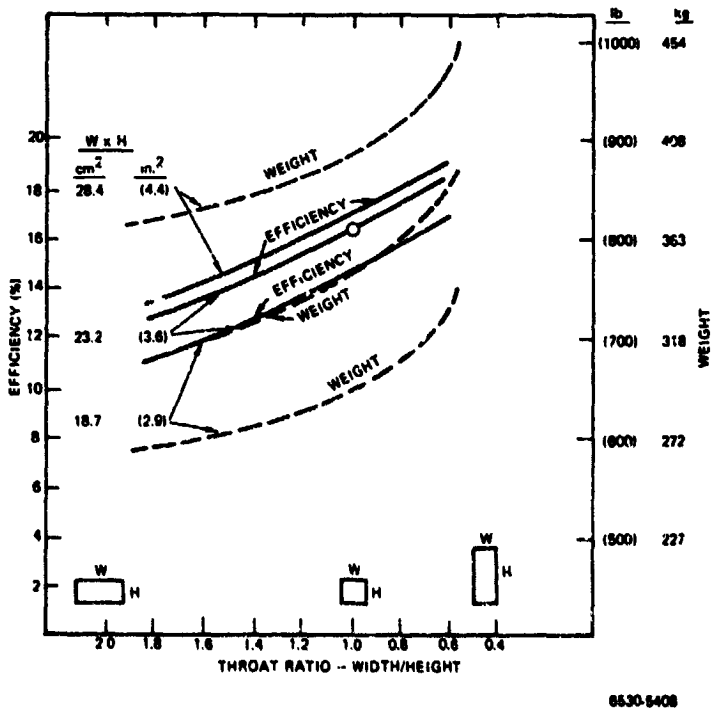

A number of computer design iterations were performed, varying pump throat length, width, and height for both compensated and uncompensated systems. These results showed that there was little difference between the two- and three-pump configurations for shorter throat lengths, but a significant difference between the compensated and uncompensated configurations. This is best shown in Figure 8 for three-pump compensated and uncompensated configurations, both with 13-cm (5-in.) long throats. It was assumed that 80% full compensation could be achieved. On the basis of this analysis, which shows the compensated pump to be ~25% higher in weight and 25% lower in efficiency than the uncompensated pump, the compensated configuration was dropped from further consideration. This results from the fact that the increased air gap of the compensated configuration degrades the performance more than the current compensation increases efficiency.

In the compensated configuration, the optimum throat width was determined to have a width equal to twice the height. For the uncompensated configuration, the optimum throat dimensions show the width equal to the height. As will be shown here, optimum is determined on the basis of both efficiency and weight. In all figures shown in this report for the dc conduction PLPA, the weight shown includes only the magnet, yoke, pole pieces, and copper bus. The efficiency shown includes a copper bus with a cross section equal to the throat length times throat height by 51 cm (20 in.) in length.

Figure 9 shows how effieiency and weight vary as the ratio of throat width to height is varied. Efficiency continually improves as this ratio decreases, but weight increases at a much faster rate, particularly below a square configuration when the width exceeds the height. On this basis, a square throat was selected for the uncompensated pump.

Figures 10 and 11 show the effect of varying throat length and throat cross-sectional area for a square duct for both two- and three-pump uncompensated configurations. The design points in both figures were selected on the basis of obtaining high efficiency-to-weight ratios. Increasing throat length and cross section above the selected points results in little gain in efficiency, and high increases in weight.

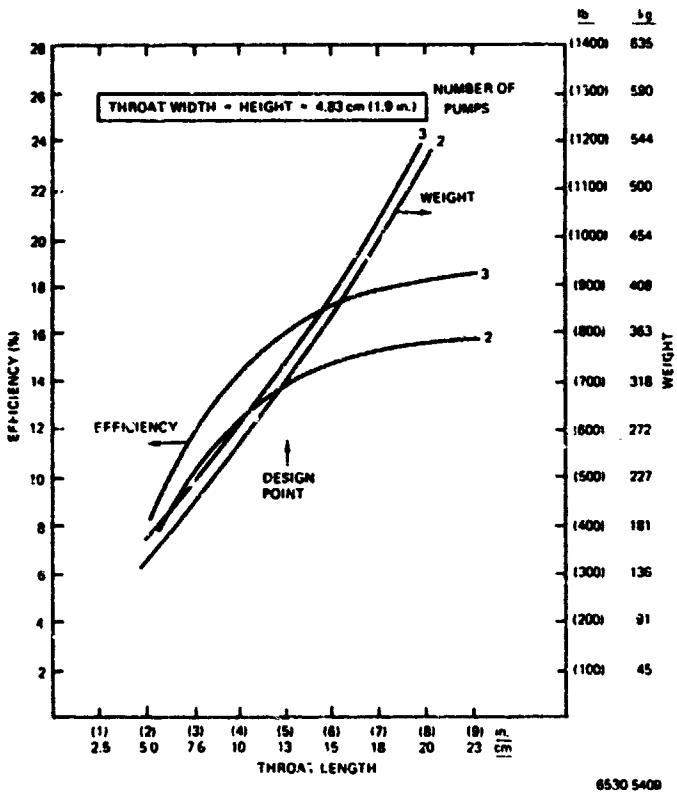

Figure 10.

Efficiency and Pump Weight vs Throat Length for dc PLPA (Uncompensated pump PLPA)

Figure 11.

Efficiency and Pump Weight vs Throat Cross-Sectional Area for PLPA (Uncompensated pump PLPA)

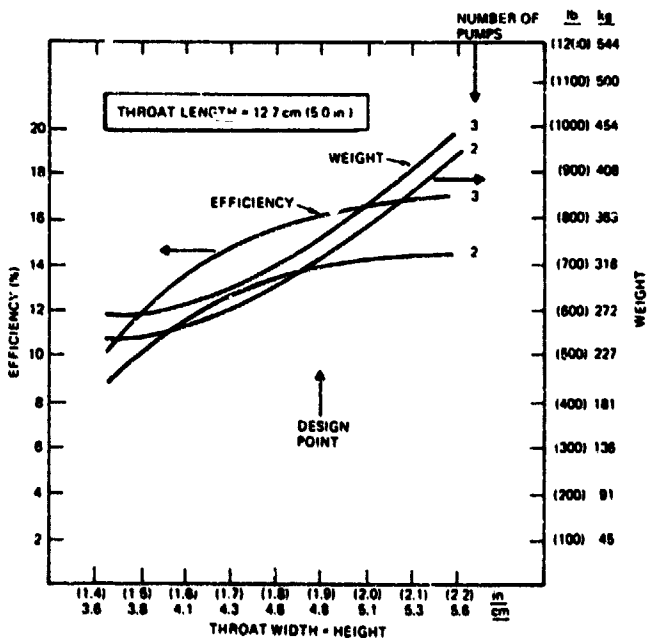

Table 4 summarizes the design performance and configuration for the two- and three-pump uncompensated PLPA's. The three-pump concept appears to be the best configuration for the specified requirements, based upon its higher efficiency. The higher overall efficiency is the result of there being a smaller braking effect associated with the smaller standby pump in the three-pump option, as compared to the larger standby pump in the two-pump option.

TABLE 4

TWO- vs THREE- dc PUMP PLPA COMPARISON

	3-Pump		2-Pump	
Flow [kg/sec (lb/sec)]	9.1	(20)	9.1	(20)
Pressure [kN/m^2 (psi)]	48.3	(7)	48.3	(7)
Power [kw]	3.8		4.4	
Voltage [v]	0.179		0.263	
*Current [amp]	10,530		16,707	
Efficiency [%]	16.1		13.8	
Flux Density				
teslas	0.324		0.4177	
(gauss)		(3,242)		(4,177)
lines/cm^2	3,242		4,178	
(lines/$in.^2$)		(20,916)		(26,953)
*Size				
Width [cm (in.)]	34.3	(13.5)	39.6	(15.6)
Length [cm (in.)]	17.8	(7.0)	17.8	(7.0)
Height [cm (in.)]	29.2	(11.5)	34.5	(13.6)
Throat Dimensions				
Length [cm (in.)]	12.7	(5.0)	12.7	(5.0)
Width [cm (in.)]	4.8	(1.9)	4.8	(1.9)
Height [cm (in.)]	4.8	(1.9)	4.8	(1.9)
*Bus Dimensions				
Length [cm (in.)]	50.8	(20)	50.8	(20)
Area [cm^2 ($in.^2$)]	61.29	(9.5)	61.29	(9.5)
Total PLPA Weight [kg (lb)]	345	(756)	323	(712)

*Per pump

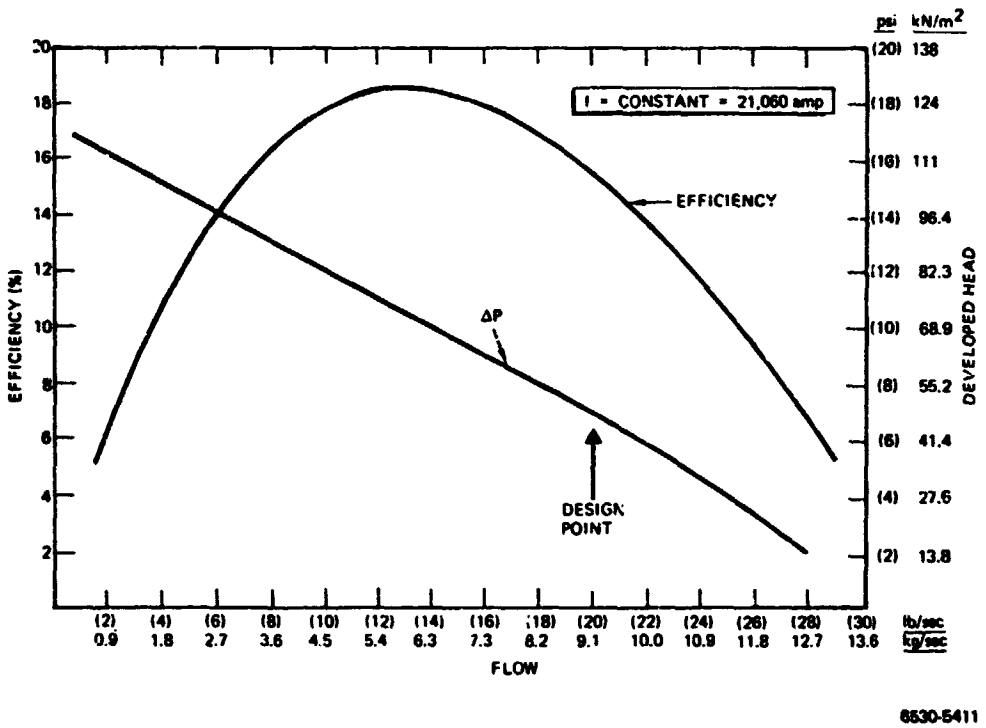

Figure 12. Head Rise and Efficiency vs NaK Flow for dc PLPA (Uncompensated 3-pump PLPA)

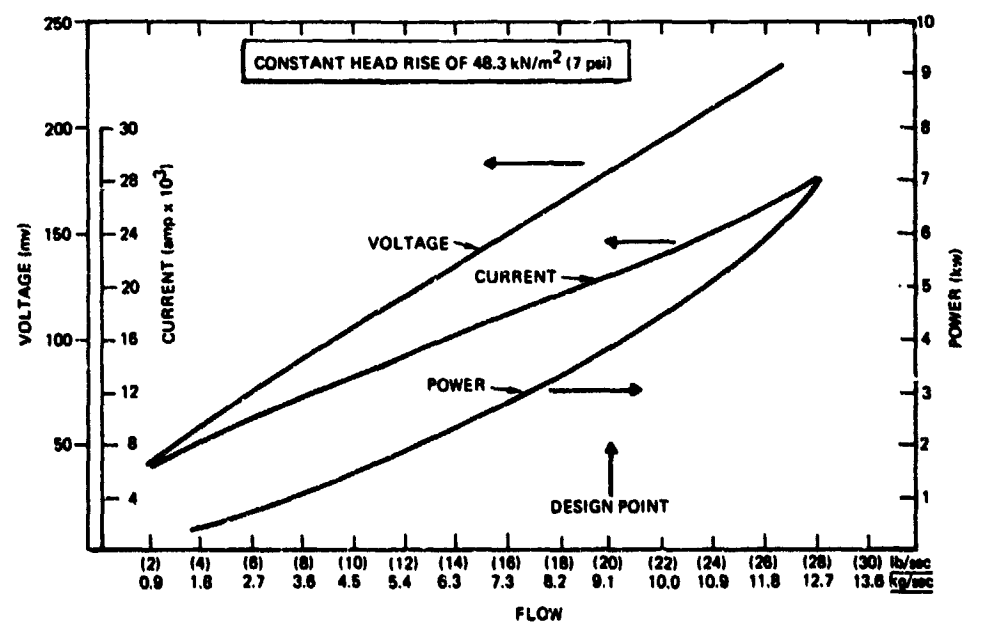

Figure 13. Power vs Flow Rate for dc PLPA (Uncompensated 3-pump PLPA)

Figure 12 shows the developed head and efficiency vs flow at constant current input for the uncompensated design. Peak efficiency for this design is at less than design flow, but this provides good efficiency at both startup and design conditions. Figure 13 shows the voltage, current, and power, plotted as a function of flow at the design pressure head of 48.3 kN/m^2 (7 psi). Since the pressure head would be expected to drop as flow is lowered, a more realistic performance curve is shown in Figure 14, where it is assumed that pressure is related to the square of the flow rate. This figure shows pressure, efficiency, and input power, plotted as a function of flow rate when this assumption is made. It is seen that startup power is minimal (~20 w), at flow rates of <15% of design flow. However, it should be kept in mind that the voltage drop across the diodes used in the power conditioning equipment for the dc pumps is nearly constant with power output, and this will penalize the pumps at low flow conditions.

C. POWER CONDITIONING CONSIDERATIONS

After selecting the dc conduction three-pump option, as defined in Table 4, as the best of the dc pump options, consideration was then given to obtaining the low-voltage (0.179 v), high-amperage (21,000 amp) power required to operate a dc PLPA. A power supply to convert the 440-Hz high-voltage Brayton-produced power to that required for the dc pumps has a conversion efficiency of ~25%,[9] and would have to be packaged in close proximity to the PLPA to avoid excessive I^2R losses in the bus bars. Close coupling to the pump would require that the electrical components in the power supply be radiation hardened, to meet the 8×10^9 rad γ and 8×10^{17} nvt neutron (>1 Mev) radiation.

The dc conduction pump could possibly be powered with compact thermoelectric power conversion modules, operating off the reactor heat, in close proximity to the pumps. However, using current state-of-the-art pump modules, which produce 500 amp at 0.22 load voltage when operating at an average hot junction temperature of 607° C (1125° F) and cold junction of 299° C (570° F), it would require ~35 to 40 modules. These modules are 5.69 cm (2.24 in.) in diameter, 18 cm (7 in.) long, weigh ~3.58 kg (7.9 lb) each, and are ~3.4% efficient. If half as many modules were desired, and further development allowed, the active length of the module might be increased to 35.6 cm (14 in.), while the

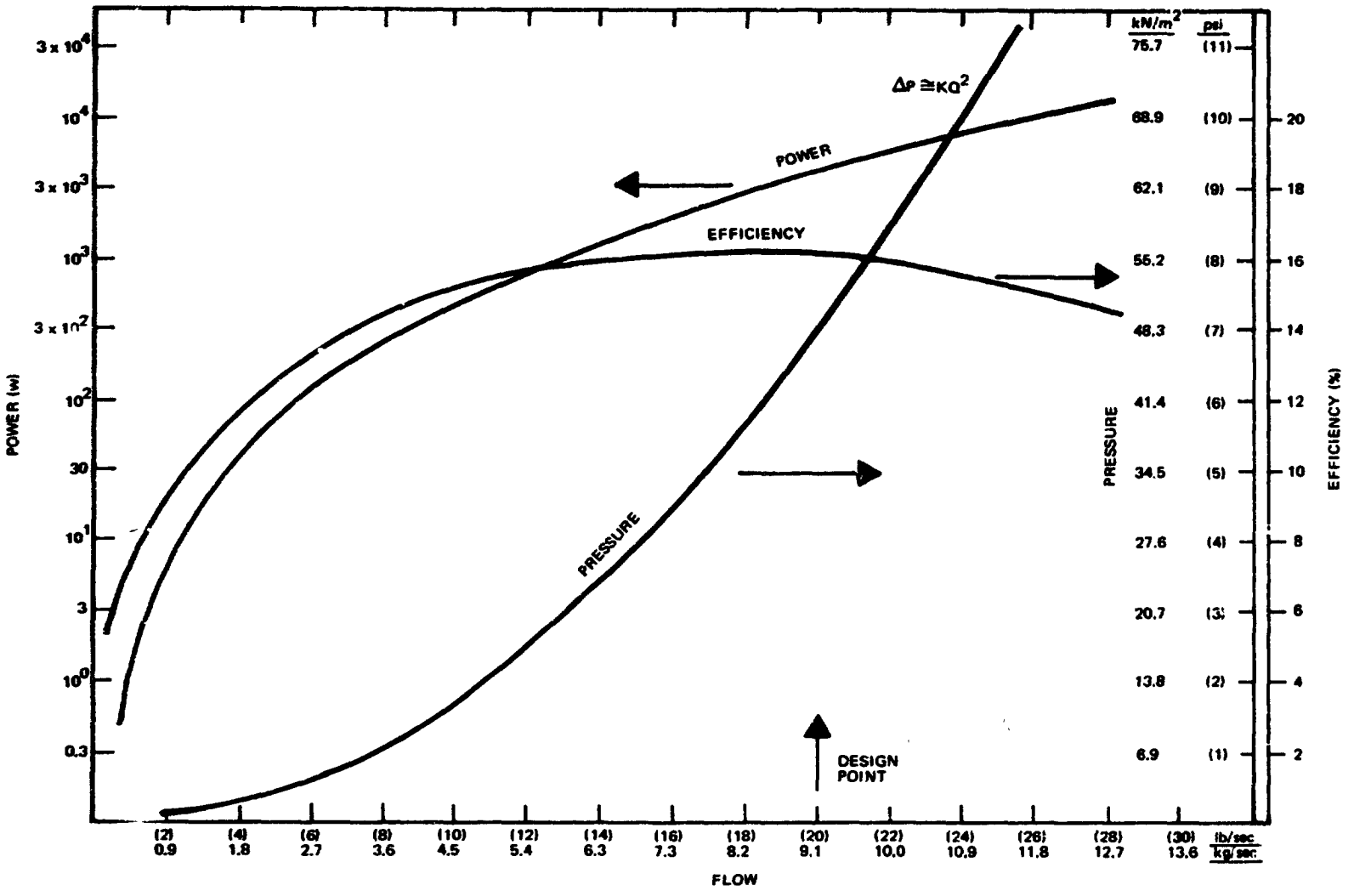

6530-5413

Figure 14. Head Rise, Power, and Efficiency vs NaK Flow Rate for dc PLPA (Uncompensated 3-pump PLPA)

thicknesses of the thermoelectric washers were adjusted to give proper load voltage. Modules to power the PLPA would weight ~127 Kg (280 lb), excluding interconnecting piping and copper buses. Although the pumps and modules would be closely coupled, there would still be an appreciable voltage drop in the interconnecting buses that must be accepted. Considerable difficulty can be anticipated in maintaining hydraulic losses and piping stress low, and in packaging the modules in the confined gallery area.

In lower flow and lower head-rise applications than those specified for the PLPA, the combination of thermoelectric modules with dc conduction pumps in parallel hydraulically has been shown to look attractive. With reduced hydraulic power requirements, the number of thermoelectric modules required can be reduced to a manageable number, and NaK manifolding and copper bus problems are reduced.

The thermoelectric module concept is also not really amenable to powering only two out of three pumps hydraulically in series, and then switching from a failed pump to the third standby. To do so would require the diverting of NaK flows to various standby modules or large electrical switches. Although beyond the scope of the program, a better approach might be to power all pumps simultaneously, and allow for performance degradation by increased initial module and pump capacity.

Also, the control of NaK flow during programmed startup of the Brayton system would be very poor for thermoelectric pumps, since the power available at any given time would be strictly dependent upon the temperature difference across the thermoelectric modules.

D. CONCLUSIONS

A comparison between dc and ac pumps is shown in Table 5, in which most of the preceding comments are summarized. In general, the relatively high-head, high-flow requirements of the combined system test required the dc pumps to be larger than those previously studied for other space power systems. In addition, overall compatibility with the Brayton ac power source was not as great as for the ac pumps, due to the power conditioning losses that would be incurred. As a result of this comparison, the design effort on the dc pump was de-emphasized, in favor of additional effort on the ac pumps.

TABLE 5

dc CONDUCTION vs ac INDUCTION PUMP COMPARISON

dc Pumps	ac Pumps
Brayton Power Source	Brayton Power Source
ac to dc Conversion Efficiency ~25%	Power Conditioning Efficiency ~85%
Pump Efficiency ~16% x 0.25 = 4%	Pump Efficiency ~8.7% x 0.85 = 7.4%
High Bus Losses	Flow Variable with Voltage for Controlled Brayton Start
Electronics Must be Radiation Hardened	
Rapid Drop of Efficiency with Low Flow - Low Voltage	
Thermoelectric Module Power Source	
Requires 35 to 40 Modules in Gallery	
Manifolding and Pressure Drop Problems with NaK Lines	
Boot Strap Startup and Shutdown	

III. ESTIMATED RELIABILITY OF ac INDUCTION PUMP OPTIONS

Following the de-emphasis of the dc pump options, a reliability analysis was conducted on the remaining two- and three-pump ac linear and helical induction options, to determine whether the number of PLPA approaches being considered could be further reduced. The reliability comparison discussed here was performed, using the conceptual layout drawings and estimated winding temperatures of the various ac options as they existed at that time.

The fault trees for two- and three-pump helical PLPA's were generated, and are shown in Figures 15 and 16. Those for the linear pump concepts were very similar. It is seen that the overall reliability of the various pump concepts will be dependent on the individual pump throat, electrical winding, gas containment can, and cooling coil reliabilities. The equations used to calculate the overall PLPA reliabilities are contained in Appendix I. In order to obtain quantitative reliability numbers, it was necessary to obtain individual component reliability factors which can be used in the probability formulas. These reliability factors, in turn, depended on the pump design features and operating conditions. As an example, the throat reliability depended upon wall thickness and length, and the difficulty of welds, braze joints, etc. The winding reliabilities depended upon temperautre, current density, number of splices, difficulty of assembly, etc.

The winding reliability factors were arrived at by considering the effect of hot spot temperatures, current density, number of splices, and fabrication awkwardness. Numerical values for the current density factor, F_C, were obtained, using the following relationship:

$$F_C = 1 - 2.7 \times 10^{-9} \left[I^2(1 + 10^{-7} I^2) - 10^6\right] \quad , \qquad \ldots(8)$$

where F_C approaches 1.0 at 155 amp/cm^2 (1000 amp/in.^{2}) and 0.0 at 1163 amp/cm^2 (7500 amp/in.^{2}). The equation is in the form of watts/unit length of conductor. The 155 amp/cm^2 (1000 amp/in.^{2}) is the current density that will cause a 40° C (104° F) temperature rise in the conductor, above the ambient temperature of 30° C (86° F), for a horizontally positioned wire exposed to a gas. A conductor is normally capable of operating indefinitely under these conditions, and, for this reason, 155 amp/cm^2 (1000 amp/in.^{2}) was selected for the lower current density

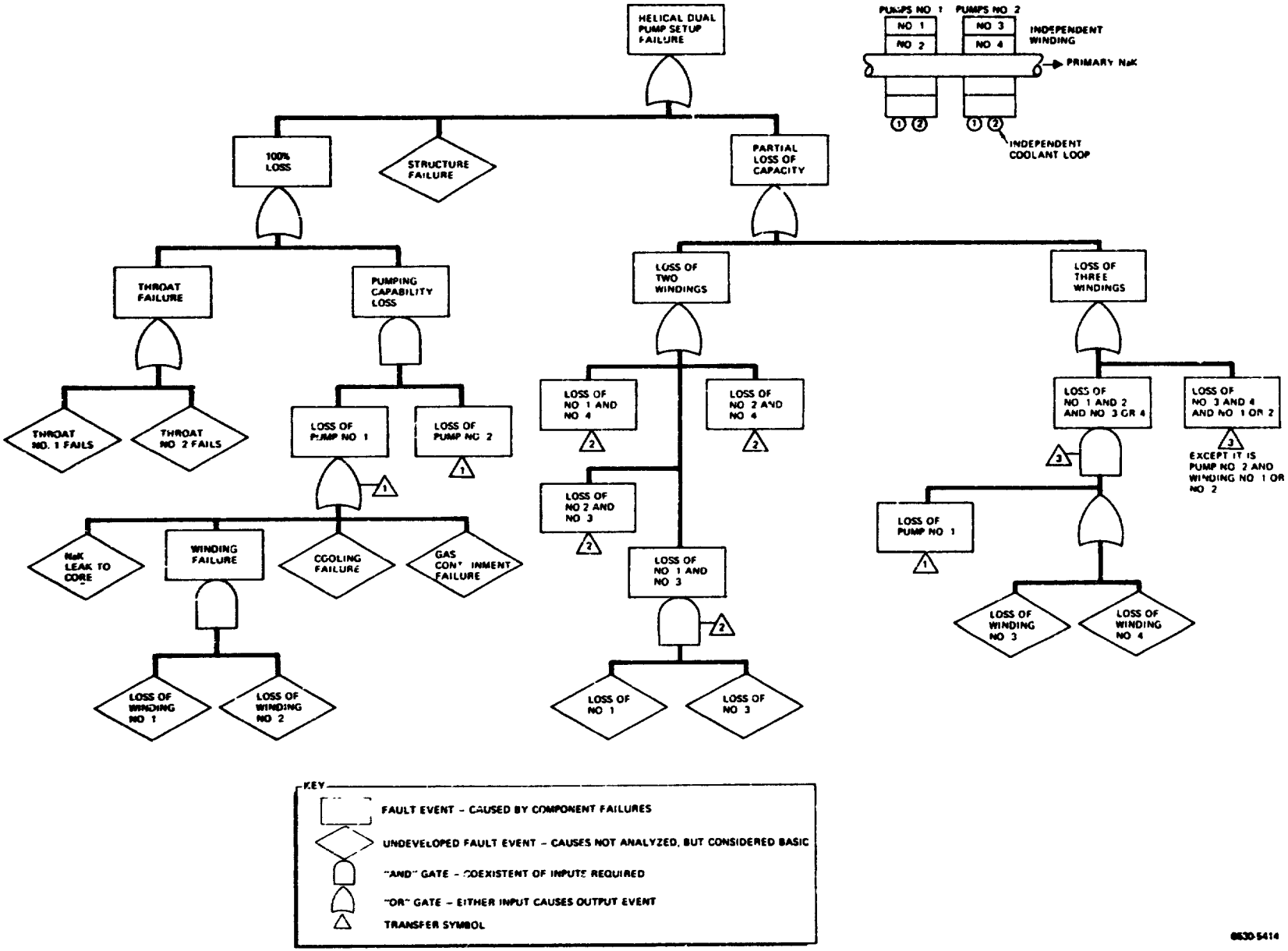

Figure 15. Fault Tree Diagram — Dual Helical PLPA

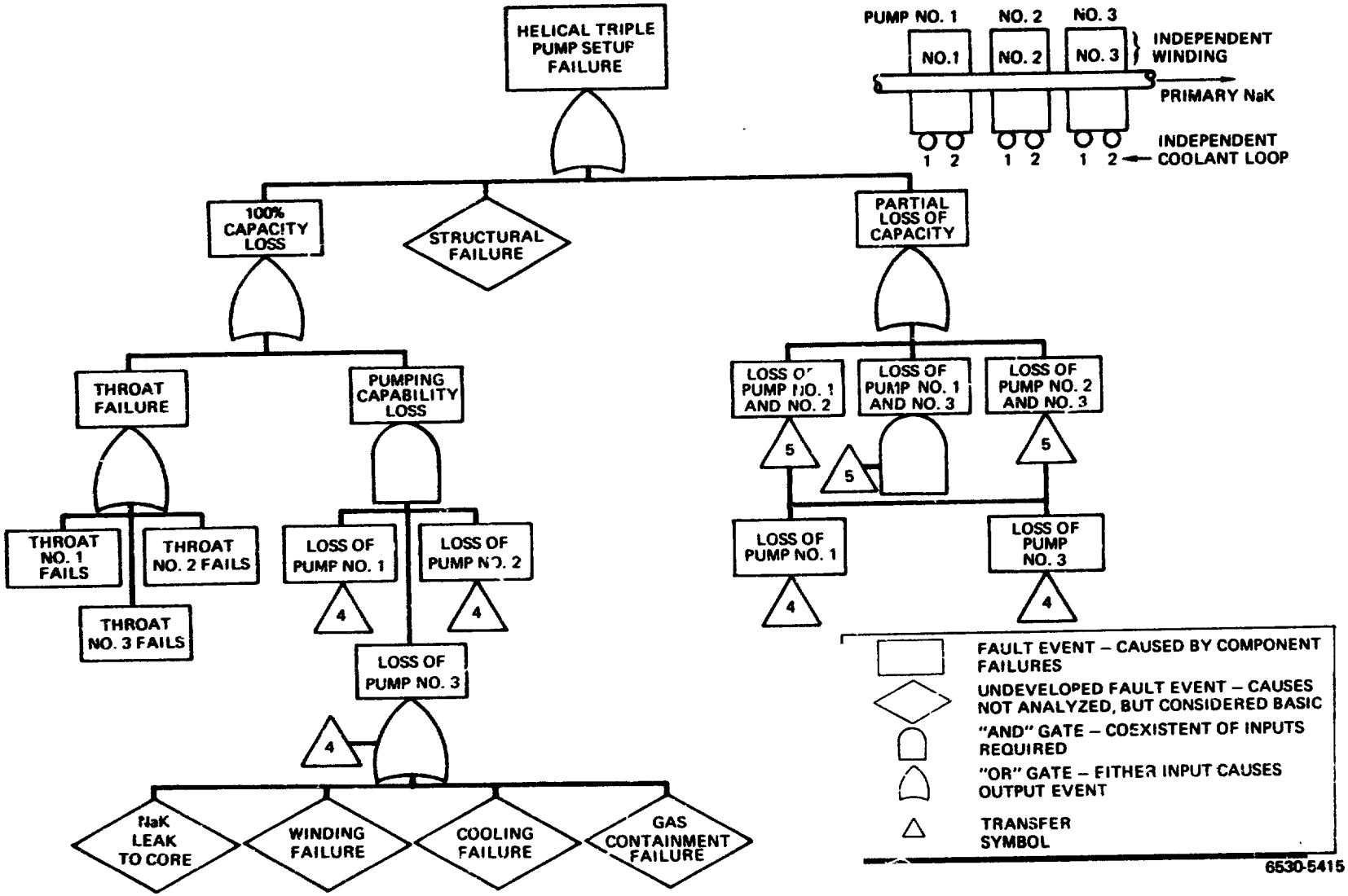

Figure 16. Fault Tree Diagram – Triple Helical PI-PA

TABLE 6

INITIAL WINDING RELIABILITY EVALUATION

Configuration	Current Density I [(amp/in.^{2}) amp/cm^2]	F_C	Estimated Peak Coil Temperature [(°F)°C]	F_T	Number of Splices per Pump	Failure Rate per Pump	F_S	F_F	R_W
Dual Helical									
24.9-cm (9.8-in.) Stack OD	(3050) 473	0.944	(910) 483	0.913	118	118×10^{-9}	0.9948	0.996	0.8540
29.0-cm (11.4-in.) Stack OD	(2320) 360	0.980	(760) 404	0.977	118	118×10^{-9}	0.9948	0.996	0.9487
Triple Helical									
24.9-cm (9.8-in.) Stack OD	(2444) 379	0.977	(775) 413	0.972	226	226×10^{-9}	0.9901	0.998	0.9384
29.0-cm (11.4-in.) Stack OD	(1860) 288	0.990	(700) 371	0.991	226	226×10^{-9}	0.9901	0.998	0.9694
Dual Linear	(1600) 248	0.994	(660) 349	0.997	39	39×10^{-9}	0.9983	0.999	0.9883
Triple Linear	(1100) 171	0.999	(578) 303	1.000	38	38×10^{-9}	0.9983	0.999	0.9963

limit. Limited empirical data indicate that a current density of 1163 amp/cm^2 (7500 amp/in.^{2}) produces long-term winding burnout, and was therefore selected as the upper limit.

The peak coil temperature factor, F_T, was arrived at using the following relationship:

$$F_T = 1 - \frac{(T - 600)^2}{1.11 \times 10^6} \qquad \text{(Capital T is in °F)} \qquad \ldots(9)$$

A temperature factor value of 1.0 is achieved at a temperature of 316°C (600°F), which coincides with the short-time annealing range for pure copper. Below this temperature, the diffusion and grain growth rates should be sufficiently low to preclude failures solely attributable to temperature effects. A zero value of F_T was assumed to occur at a temperature of 899°C (1650°F), which is ~167°C (300°F) below the melting point of copper.

The winding splice factor, F_S, was arrived at by multiplying the number of wiring splices times the number of hours times a failure rate of 1×10^{-9} failures per hour. Fabrication factors, F_F, of 0.996 and 0.998 were arbitrarily assigned to the helical and linear pump windings, respectively. The helical winding was penalized, because access to the stator slots through the bore is restricted, when compared to the flat linear stators.

A total estimated winding reliability (R_W) was arrived at by multiplying the various factors:

$$R_W = F_C \times F_T \times F_S \times F_F \qquad \ldots(10)$$

The results of the initial winding reliability evaluation is shown in Table 6. It is apparent that the larger-size pumps, in a given option, result in higher winding reliabilities, since the individual windings were being driven less hard. Also, the windings of the three-pump option, with their single windings, were more reliable than the two-pump option, where there were two windings in each pump. In this initial comparison, the linear pump windings appeared significantly higher in reliability, because of their lower current density, lower estimated winding temperatures, and small number of splices. Later in the study, when the efficiencies and temperature were better defined for the two-pump linear option, this apparent advantage of the linear pump ceased to exist.

TABLE 7

THROAT WELD RELIABILITY ANALYSIS

No.	Weld Location	Actual Weld Length	Welding Method			Stress			Inspection		Discontinuity		Net Factor K = A-B-C-D-E-F-G H-I-J	Weighted Length = Actual Length x K cm(in.)
			TIG			Primary Bending		Secondary Loading						
		cm (in.)	Machine A	Manual B	EB C	Non-Self-Relieving D	Self-Relieving E	Self-Relieving F	X-ray G	Dye Penetrant Only H	Thickness I	Geometry J		
	Helical Pump		1.10	1.25	1.00	1.30	1.10	1.0	1.0	1.5	1.10	1.30		
1	Inlet Mount Duct Section	27.9 (11)	1.10	-	-	1.30	1.10	1.0	1.0	-	-	-	1.58	44.20 (17.40)
2	Transition – Outer Duct to Throat (Inlet)	41.4 (16.1)	1.0	-	-	1.30	1.10	1.0	-	1.5	1.10	1.30	3.84	158.75 (62.50)
3	Center Body Closure – Left End	30.0 (11.8)	-	1.25	-	1.30	1.10	1.0	-	1.5	1.10	1.30	3.38	101.35 (39.90)
4	Center Body Closure – Right End	30.0 (11.8)	1.10	-	-	1.30	1.10	1.0	-	1.5	1.10	1.30	3.38	101.35 (39.90)
5	Same as 2 (Outlet)	41.4 (16.3)	1.10	-	-	1.30	1.10	1.0	-	1.5	1.10	1.30	3.38	158.75 (62.50)
6	Throat to Duct Transition	19.94 (7.85)	-	1.25	-	1.30	1.10	1.0	-	1.5	1.10	-	1.96	39.12 (15.40)
7	Duct to 180° Bend	19.94 (7.85)	-	1.25	-	1.30	1.10	1.0	-	1.5	-	-	1.79	35.69 (14.05)
8	Longitudinal Throat	17.8 (7.0)	1.10	-	-	1.30	1.10	1.0	1.0	-	-	-	1.58	28.07 (11.05)
													TOTAL	667.26 (262.70)
	Linear													
1	3.5 OD to Transition	27.9 (11.0	1.10	-	-	1.30	1.10	-	1.0	-	-	-	1.515	44.07 (17.35)
2	Transition to Throat	27.9 (11.0)	-	1.25	-	1.30	1.10	-	1.0	-	1.1	1.3	2.56	71.50 (28.15)
3	Four Lengthwise Welds	243.8 (96.0)	-	-	1.00	1.30	1.10	-	-	1.2	1.1	1.3	2.23	543.56 (214.00)
4	Same as 2	27.9 (11.0)	-	1.25	-	1.30	1.10	-	1.0	-	1.1	1.3	2.56	71.50 (28.15)
5	Junction of 2.5 OD and Transition	19.94 (7.85)	1.10	-	-	1.30	1.10	-	1.0	-	-	-	1.575	31.37 (12.35)
													TOTAL	762.00 (300.00)

Throat reliabilities, Table 7, were computed by summing up the weighted weld lengths and applying a failure rate to the total length, in the form of failures per hour per inch of weld. The latter factor, 1×10^{-10} failures/hr/in. of weld, was arrived at on the basis of a review of liquid metal system operating experience, where a reasonable amount of quality assurance was used. Weighting factors were used to multiply the actual weld length, depending on the welding method, estimated stress loading, weld inspectability, and weld geometry. Machine-made welds were considered more reliable than manual welds. The stress-loading factor varied between 1.0 and 1.3, depending upon the stress levels and intensity. Also, a geometry factor, which varied between 1.0 to 1.3, depending upon change in thickness, etc., was used to weight the actual weld lengths. As can be seen in Table 7, both types of pumps had approximately the same length of welds.

A similar approach was used to calculate a reliability for the stator can, which contained a heat transfer cover gas over the electrical windings. Table 8 shows that the larger sized linear pump had considerably more weld length in its stator can than the comparable helical pump.

The results of the initial reliability study, based on early helical and linear ac pump designs, are indicated in Table 9. Probabilities of achieving both 100% flow and some flow (one or more coils functioning) for 5 years are shown for several helical two- and three-pump PLPA's, several linear two-pump PLPA's, and one three-pump PLPA. Reliabilities are also shown for the assumptions that,(1) loss of gas containment is a catastrophic failure, and (2) loss of gas containment has no influence on pump operation.

The significance of the helical two-pump stack OD's is that the larger 28.96 cm (11.4 in.) diameter allows for greater conductor cross-sectional area, and thus a lower current density and lower I^2R losses or copper temperatures. As discussed previously, this results in higher winding reliability. The several two-pump linear PLPA's shown differ, in that the first pump listed has a single containment can enclosing both wound stator halves; while, in the second two-pump PLPA, each stator half is individually canned, and thus a single gas leak will cause only one stator half to fail.

TABLE 8

STATOR CAN WELD RELIABILITY ANALYSIS

No.	Weld Location	Actual Weld Length	Welding Method			Stress Loading			Inspection		Discontinuity		Net Factor K = A-B-C-D-E-F-G-H-I-J	Weighted Length = Actual Length x K
			TIG			Primary Membrane	Primary Bending	Secondary Loading						
		cm (in.)	Machine A	Manual B	EB C	Non-Self-Relieving D	Non-Self-Relieving E	Self-Relieving F	X-ray G	Dye Penetrant Only H	Thickness I	Geometry J		cm (in.)
	Helical													
1	Axial Can Weld	38 (15)	1.10	-	-	1.30	-	-	1.0	-	-	-	1.43	54.4 (21.4)
2	Can to End Bell	84.6 (33.3)	1.10	-	-	1.30	1.10	1.0	-	1.5	-	1.30	3.07	259.6 (102.2)
3	End Bell to Housing	178.8 (70.4)	1.10	-	-	1.30	-	-	-	1.5	1.10	1.30	3.07	548.9 (216.1)
4	Stator Locating Pin	5.1 (2.0)	-	1.25	-	1.30	-	-	-	1.5	1.10	1.30	3.44	17.8 (7.0)
5	Terminal Insulation to Housing	152.4 (60.0)	-	1.25	-	1.30	-	-	-	1.5	1.10	1.30	3.48	530.4 (208.8)
6	Terminal Insulation to Terminal	15.2 (6.0)	-	1.25	-	1.30	-	-	-	1.5	1.10	1.30	3.48	53.1 (20.9)
7	Terminal Construction	38.1 (15.0)	1.10	-	-	1.30	-	-	-	1.5	1.10	1.30	1.57	59.9 (23.6)
												DUAL PUMP UNIT		1524 (600)
	Linear													
1	Weld to Throat	16.0 (6.3)	-	1.25	-	1.30	-	1.0	1.0	-	-	-	1.62	25.9 (10.2)
2	Weld to Bellows	47.8 (18.8)	1.10	-	-	1.30	1.10	-	1.0	-	1.10	1.30	2.25	107.4 (42.3)
3	Bellows Weld (9 Leaves)	343.2 (135.1)	1.10	-	-	1.30	1.10	-	1.0	-	-	-	1.57	538.7 (212.1)
4	Weld to Bellows	37.8 (14.9)	1.10	-	-	1.30	1.10	-	1.0	-	1.10	-	1.73	69.5 (25.8)
5	Bellows to Extension	55.9 (22.0)	-	1.25	-	1.30	-	-	-	1.5	-	1.30	3.17	177.0 (69.7)
6	Extension to End Bell	63.8 (25.1)	-	1.25	-	1.30	-	-	-	-	1.10	1.30	2.32	147.8 (58.2)
7	End Bell to Housing	111.8 (44.0)	-	1.25	-	1.30	-	-	-	1.5	1.10	1.30	3.48	388.9 (153.1)
8	End Bell to Housing	111.8 (44.0)	-	1.25	-	1.30	-	-	-	1.5	1.10	1.30	3.48	388.9 (153.1)
9	Extension to End Bell	32.0 (12.6)	-	1.25	-	1.30	-	-	1.0	-	1.10	1.30	2.32	74.2 (29.2)
10	Weld to Throat	27.9 (11.0)	-	1.25	-	1.30	-	1.0	1.0	-	-	1.30	1.62	45.2 (17.8)
11	Terminal to Housing	152.4 (60.0)	-	1.25	-	1.30	-	-	-	1.5	1.10	1.30	3.48	530.4 (208.8)
12	Terminal Insulation to Terminal	15.2 (6.0)	-	1.25	-	1.30	-	-	-	1.5	1.10	1.30	3.48	53.1 (20.9)
13	Terminal Construction	38.1 (15.0)	1.10	-	-	1.30	-	-	1.0	-	1.10	1.30	1.57	59.9 (23.6)
												DUAL PUMP UNIT		2604 (1025)

TABLE 9

INITIAL ESTIMATED RELIABILITIES OF ac PLPA's

System	Pump System 5-yr Reliability Estimates				Individual Components 5-yr Reliability Estimates			
	Loss of Stator Gas Catastrophic		Loss of Stator Gas no Effect					
	Partial Flow	100% Flow	Partial Flow	100% Flow	Throat	Winding	Cooling Coil	Gas Containment
Helical-Dual								
Stack OD (9.8 in.) 24.9 cm	0.9972	0.9236	0.9973	0.9246	0.9989	0.8540	0.9910	0.9974
Stack OD (11.4 in.) 29.0 cm	0.9977	0.9873	0.9977	0.9877	0.9989	0.9487	0.9910	0.9974
Helical-Triple								
Stack OD (9.8 in.) 24.9 cm	0.9963	0.9849	0.9963	0.9856	0.9989	0.9384	0.9864	0.9979
Stack OD (11.4 in.) 29.0 cm	0.9965	0.9934	0.9965	0.9938	0.9989	0.9694	0.9864	0.9979
Linear								
Dual-Single Can	0.9973	0.9966	0.9973	0.9968	0.9987	0.9883	0.9910	0.9957
Triple	0.9955	0.9955	0.9958	0.9958	0.9987	0.9963	0.9864	0.9957
Dual-Double Can	0.9969	0.9963	0.9973	0.9968	0.9987	0.9883	0.9910	0.9957

The conclusions to be drawn from Table 9 are as follows:

1) In terms of achieving some flow for 5 years, the three-pump PLPA's show a slight advantage over the two-pump options.

2) With regard to achieving 100% flow, the small-diameter helical three-pump PLPA shows a significant advantage over the small-diameter helical two-pump PLPA. When the larger-diameter helical two- and three-pump PLPA reliabilities are compared, the three-pump PLPA advantage is considerably reduced. This occurs because, for the large-diameter pumps, both the three- and two-pump PLPA's have relatively low current densities.

   In the case of the linear pumps, largely because the current densities are low in all cases, there is no significant difference in reliability among any of the pumps.

3) The loss of gas containment failure mode does not significantly reduce the reliability figures, over the case where loss of gas containment does not fail the pump.

4) The linear pumps generally show higher reliability than the helical pumps. However, when low-current-density pumps are compared [e.g., the 29.0-cm (11.4-in.) diameter triple helical and the triple linear pump PLPA], the difference is rather small. Comparison of the two-pump PLPA's would show a slightly greater margin in favor of the linear pump.

Subsequent to the reliability studies, it was determined, from coil configuration layouts, that the linear pump conductor area had to be reduced and the mean length of turn increased, both tending to increase the stator I^2R losses. A thermal analysis, based on the revised coil and slot configuration, showed a substantial increase in coil temperature over these earlier estimates. Since both the winding hot spot temperature and current density enter into the calculated winding reliability, as discussed previously, the reference design linear pump ultimately had a lower calculated reliability than that shown previously, and a revised estimate is shown later in the report.

The preceding reliability estimates were combined with efficiency, weight, and size of the various options, as they existed at that time from the parametric studies, and the interim comparison shown in Table 10 was made. For the reactor Brayton space power system, the ability to produce some power over the 5-year mission was considered more important than the ability to produce full power. Therefore, more weight was placed on the reliability of the PLPA producing some flow over the expected mission life. Efficiencies of the two-pump PLPA's were significantly higher than for the three-pump option, because of their shorter NaK flow passages and lower hydraulic losses. The dual units were ~30% higher in efficiency than their triple-pump counterpart. Also, the triple-pump options were >60% larger in volume, and weighed 181 to 318 kg (400 to 700 lb) more than the comparable dual units. Since the difference in estimated reliabilities between the two- and three-pump options were considered insignificant, when compared to the dual unit's higher efficiency, lower weight, and smaller envelope, the three-pump options of the PLPA were de-emphasized midway in the program.

TABLE 10

INTERIM PLPA COMPARISON

Characteristics	ac Helical Induction Option		ac Linear Induction Option	
	2-Pump PLPA	3-Pump PLPA	2-Pump PLPA	3-Pump PLPA
Efficiency/PLPA [%]	9.1	7.2	8.6	6.8
PLPA Envelope [(in.) cm]	(41 x 25 x 15) 104 x 64 x 38	(47 x 38 x 16) 119 x 97 x 41)	(52 x 40 x 15) 132 x 102 x 38	(58 x 60 x 15) 147 x 152 x 38
PLPA Weight [kg (lb)]	399 (880)	590 (1300)	630 (1390)	948 (2090)
Some Flow 5-yr Reliability	0.998	0.996	0.997	0.996
Full Flow 5-yr Reliability	0.987	0.993	0.997	0.996

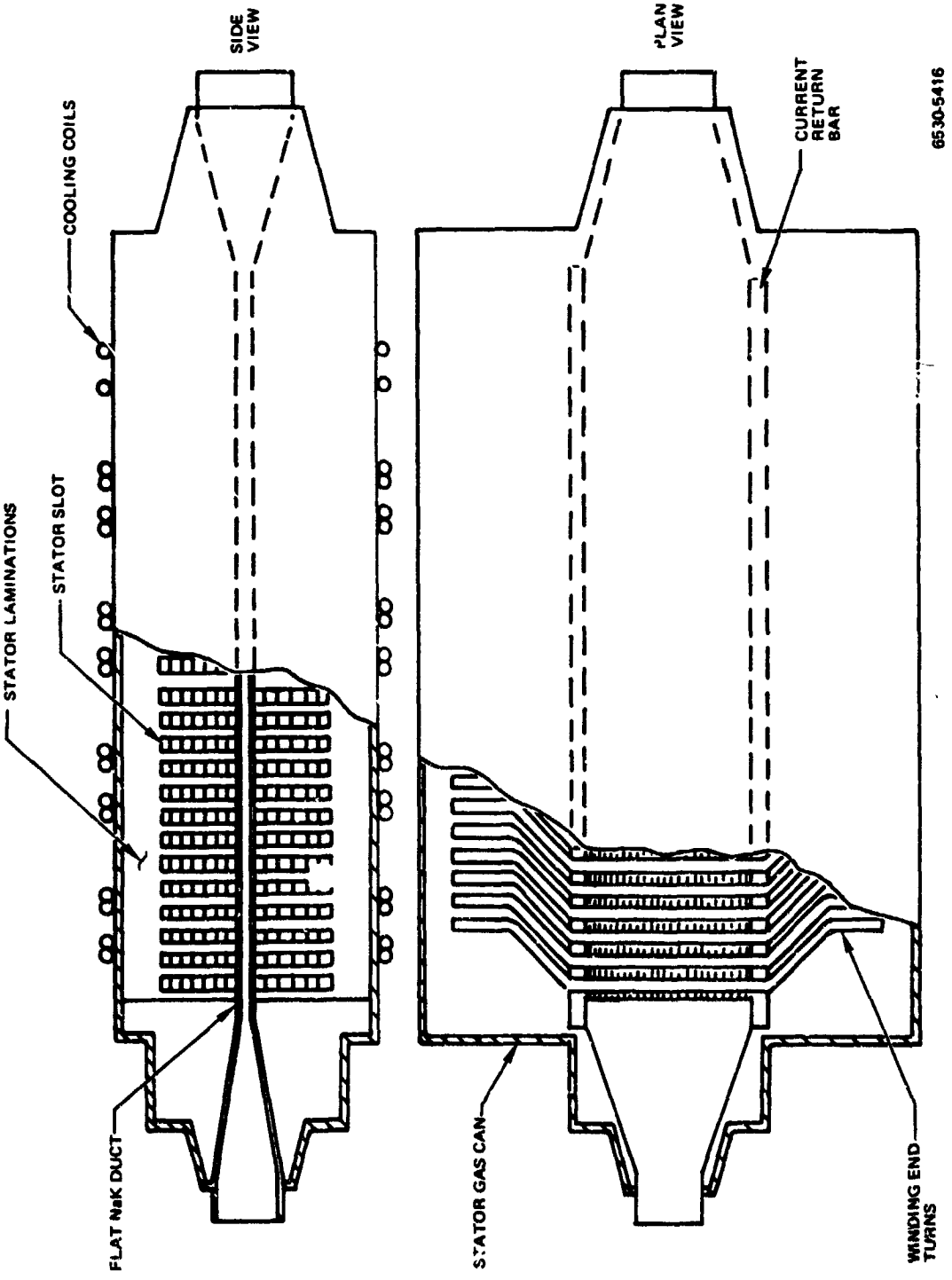

Figure 17. ac Linear Induction Pump

IV. ac LINEAR INDUCTION PUMP

A. PRINCIPLE OF OPERATION

The principle of operation of a linear induction pump is similar to that of the later-discussed helical induction pump, although the actual configuration is quite different. In the linear induction pump, the flow channel is a cylinder of rectangular cross section. The axial component of force and pressure is developed directly by the interaction of a magnetic field perpendicular to the direction of flow and a current induced in the fluid mutually perpendicular to the magnetic field and the direction of flow. The current is induced by the axial motion of a linearly travelling ac field relative to the motion of the fluid.

B. BASIC DESIGN CONFIGURATION

For purposes of calculation, the linear induction pump may be represented by the model shown in Figure 17. The flat rectangular duct, with current return bars brazed to either side, is centered and supported within the properly spaced stator halves. The current return bars serve to reduce the resistance of the current loop. Space within the air gap must be provided between the duct and the stator halves for thermal insulation, to reduce heat being conducted from the hot NaK into the electrical windings. The assembly of duct and stators is enclosed in an outer gas containment can provided with cooling coils. Inert gas within the can protects the copper from oxidation during ground testing, and also provides heat transfer between the end turns and the cooling coils. The electrical windings are fed through hermetically sealed terminals, not shown.

The stator laminations are stacked tightly together to form a block. Each stator consists of a number of slots and teeth, held together by the "backiron." The slots contain coils arranged in a standard diamond distributed winding (see Figure 18 for a typical connection). In the center of the machine the slots are filled; while, at the ends of the machine, only one coil side lies in a slot. The effect of this on machine performance will be discussed later. When energized, the windings produce a sinusoidal magnetic flux pattern that moves in a translatory manner in the direction of fluid flow. On the two-pump PLPA, isolation of the two separate windings is accomplished by bringing out the three 3-phase leads from each stator half to separate feed throughs (six total) in the gas containment

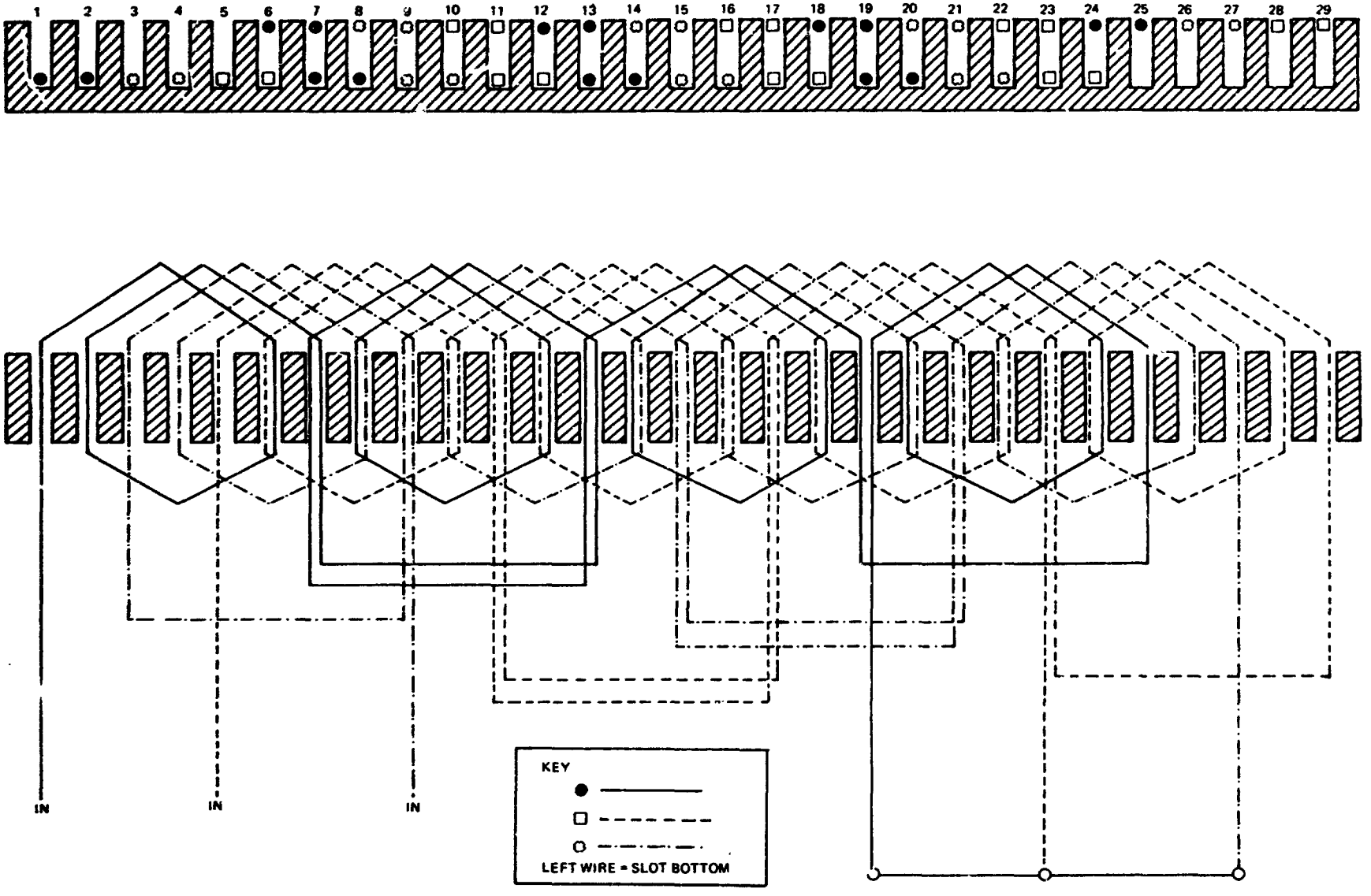

Figure 18. Coil Winding for ac Linear Induction Pump

can. In the single-winding 3-pump PLPA's, the 2-stator half windings are paralleled internally in the gas containment can, and only three leads are brought out.

The windings in the slots are energized by 3-phase power. Each turn of the stator winding is insulated from the adjacent turn and the slot walls by ceramic strip insulation. In the end turn section of the winding, "S" glass, in tape form, is used in place of strip insulation, due to the curvature of the end turns. All connections between coils are made by welding.

Fluid transition sections (circular to flat duct) complete the flow path connection between the duct and the attached circular pipe.

C. CALCULATION METHOD

1. Electromagnetic

Except for the treatment of discontinuity losses, the method of calculating developed head and machine losses is identical to that used for the helical pump, described in Section V. The discontinuity losses arise in the linear induction pump because, in the flat stator, unlike the cylindrical stator, a discontinuity must exist in the instantaneous value of the air gap field at each end of the stator laminations. A detailed Fourier analysis of the flux and MMF wave will reveal the existence of standing waves at the discontinuities, and the presence of forward- and backward-moving harmonics. The standing waves will produce losses without producing a pressure rise. The harmonics waves will produce losses and, in addition, negative pressures. These effects can be minimized by making the discontinuity less abrupt. This has been done in the calculational model by providing only one coil in the last group of slots on each end of the stators. As can be expected, a precise calculation of the influence of the discontinuous field is difficult to perform, and is subject to major inaccuracies. Accordingly, for purposes of the computer studies, empirically derived factors were applied to the theoretically computed pressure to account for the discontinuity effects. These factors were based on a comparison of experimental vs analytical performance data previously obtained in other programs with equipment of similar physical size.

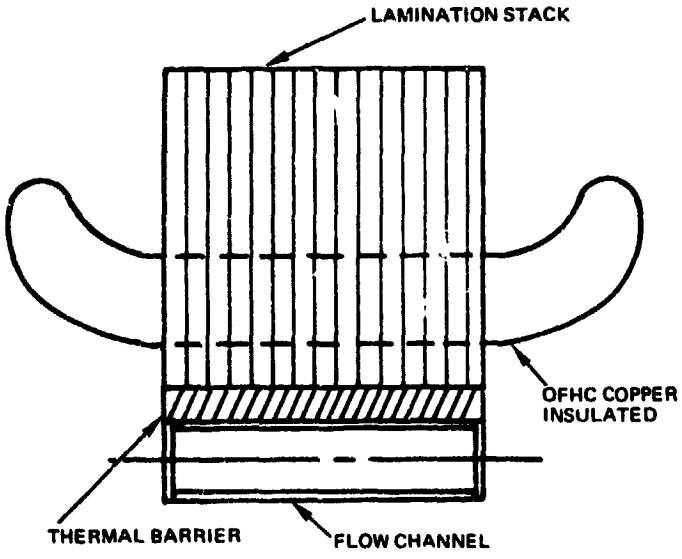

SECTIONAL VIEW

CALCULATIONAL VARIABLES

- CORE LENGTH
- MAGNETIC GAP
- FLUID THICKNESS
- NUMBER OF SLOTS
- SLOT WIDTH
- SLOT DEPTH
- TYPE OF SLOT
- CONDUCTOR AREA
- TURNS/COIL
- COIL THROW
- VOLTAGE
- FREQUENCY
- FLUID VELOCITY
- FLUX DENSITY

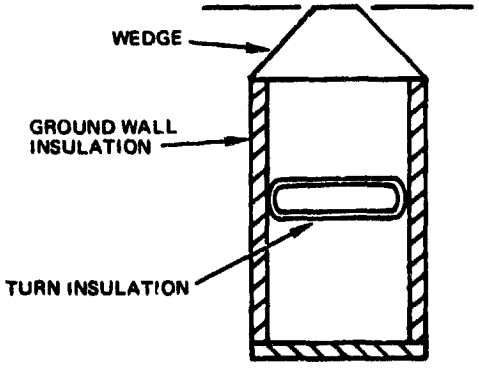

SLOT DETAIL

ORIGINAL CALCULATIONAL CONSTANTS

TYPE 316 STAINLESS STEEL DUCT – 0.076 cm (0.030 in.)
610°C (1130°F) DUCT TEMPERATURE
610°C (1130°F) NaK TEMPERATURE

THERMAL INSULATION – 0.076 cm (0.030 in.)
ELECTRICAL INSULATION GROUND WALL AND TURN TO TURN – 0.114 cm (0.045 in.)

OTHER ASSUMPTIONS

END EFFECT LOSS
- 2-POLE – 66%
- 4-POLE – 40%
- 6-POLE – 28%

TWO-LAYER LAP WINDING
NEGLIGIBLE END RING RESISTANCE

6530-5418

Figure 19. ac Linear Induction Pump Design Assumptions

2. Hydraulic Loss

The hydraulic loss calculation for the linear pump differs from the helical loss calculation, only by virtue of the duct section being linear. The formulae described in the helical pump section for entrance loss, exit loss, straight pipe loss, and 180° bend loss, were applied. Due to the nature of the flat duct and the requirement for numerous stiffeners across the duct, the flow passages are relatively small, and the head drop in the channel or duct is quite high, for the moderate flow rates of the linear pumps.

3. Calculational Logic

As with the helical pump, the electromagnetic and approximate hydraulic calculations were performed for the two- and three-pump PLPA. The typical input used in the calculations is shown in Figure 19.

The logic used to calculate electrical and magnetic circuit parameters, and the equivalent circuit, is shown in the block diagram of Figure 20. A set of input data is required initially. This consists of trial dimensions of the pump and the basic operating parameters, such as voltage, frequency, etc. The performance is calculated at the rated point. Output is then checked for agreement with the desired rating. If the output does not agree, the voltage is changed and the results again are compared. This is repeated until agreement is reached. The performance of the design is then calculated at rated conditions and over a range of operating conditions.

By changing the input data, the effect of such changes on the output can be determined. Using this method, each element of the linear pump was optimized, to obtain the optimum design for mechanical evaluation. In turn, the effect of mechanical changes on the performance was determined.

D. PARAMETRIC STUDY RESULTS

1. Initial Optimization Study

In the optimization of the linear pump, an initial pump size matrix calculation was performed for both two- and three-pump PLPA machines, to determine "ball-park" values of optimum machine parameters. This initial matrix for the dual PLPA, based on a 4-pole design, is shown as Figure 21. Typical performance curves for a 4-pole, 56-cm (22-in.) long, 2-pump machine are shown in

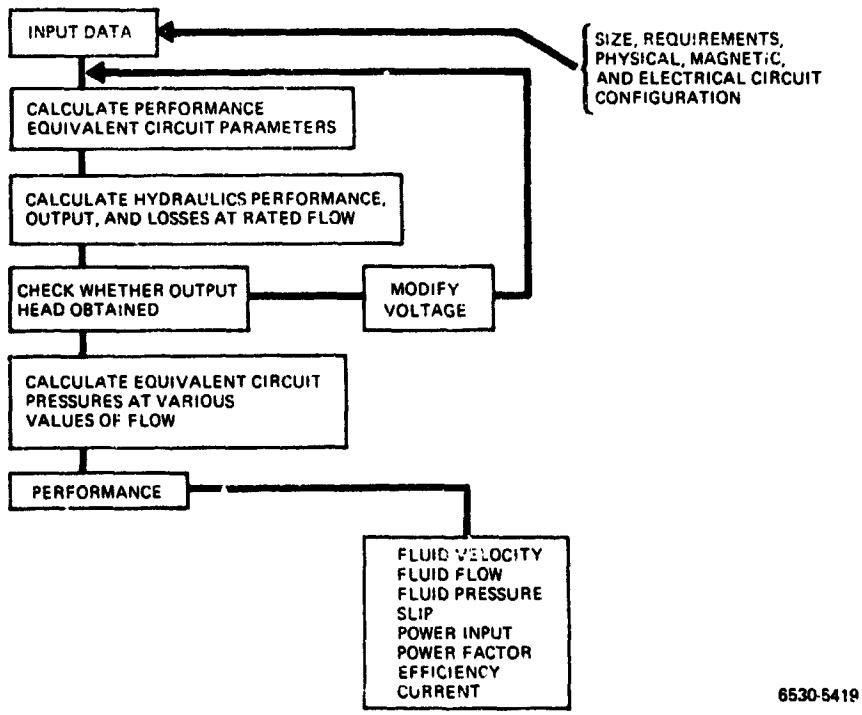

Figure 20. Calculational Logic for ac Linear Induction Pump

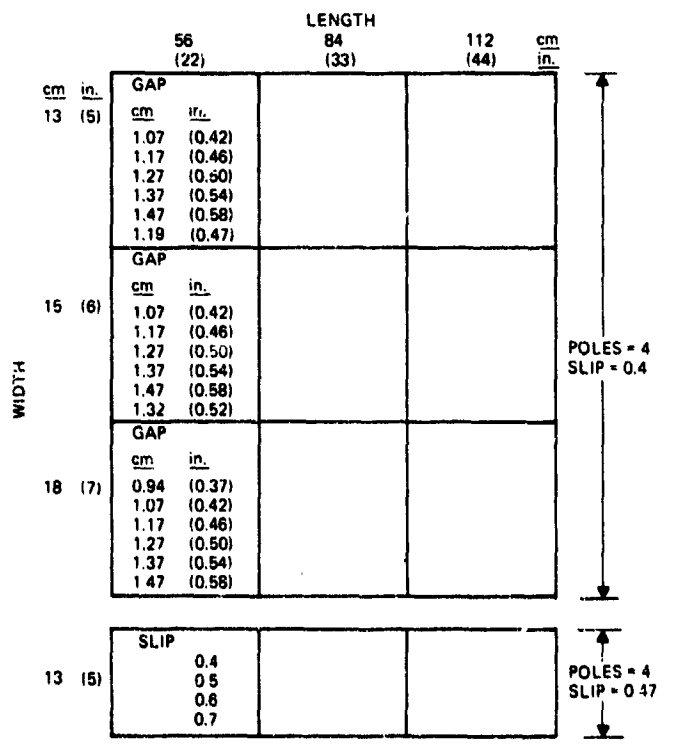

Figure 21. Initial Design Matrix for ac Linear Induction Two-Pump PLPA

Figures 22a, b, and c. Expanding this matrix to include 6- and 8-pole machines, as shown in Figure 23, produced the consolidation curve of Figure 24, where the two best 2-pump machines in each length were plotted. As can be seen, the machine favors a longer length, but concurrent layout design of the linear pump indicated that machines with a stack length >61 to 64 cm (24 to 25 in.) could not be accommodated in the available space. Calculations had previously shown that increasing the number of poles by reducing the number of slots/phase/pole from two to one very seriously degraded performance. Therefore, a 4-pole machine was selected.

A detailed winding layout of this pump design revealed several problems. It was found that it was extremely difficult to make the phase connections, due to lack of available space. As a result, it was necessary to change the pump configuration to accommodate the winding connections. This was done by increasing the pump length to 62.81 cm (24.73 in.). However, the only internal change made was to increase the tooth width. This made it possible to accommodate the winding with the least number of internal changes.

Due to the increased stack length, the winding length also changed. This necessitated recalculation, and the plotting of a series of trend curves, for optimization. The revised matrix is shown in Figure 25. Calculations and curves, based on the design matrix demonstrated, as seen in Figure 26a, shows that maximum efficiency could be obtained with a machine having a duct width of 17.8 cm (7 in.) and a magnetic gap of 1.19 cm (0.47 in.), when operated at a slip of 0.5. However, a pump with a duct width of 15 cm (6 in.), as seen in Figure 26b, would require only a small additional amount of power, as shown in Figure 26c, and duct stresses and fabrication would not be as severe. Further reduction of duct width increases input power substantially.

For the reasons discussed previously, a 4-pole pump with a duct width of 15 cm (6 in.), a duct height of 1.0 cm (0.4 in.), and a magnetic gap of ~1.32 cm (0.52 in.) was selected as the reference linear dual pump design.

2. Detailed Hydraulic Calculations for Dual Linear PLPA

a. Main NaK Flow

As previously mentioned, the initial pump design used approximated hydraulic losses, with allowance to accommodate the PLPA inner connecting

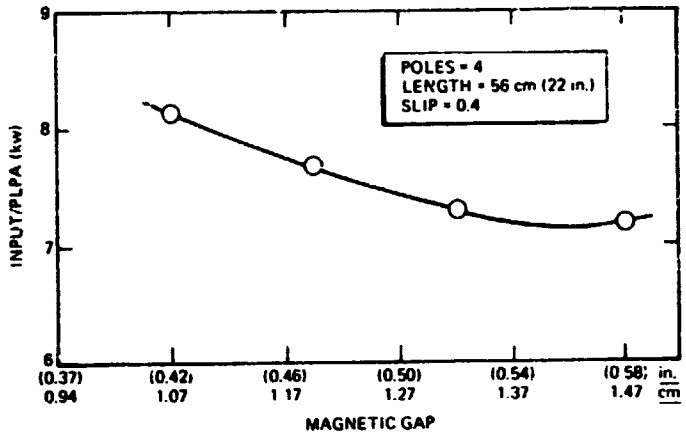

← a. Width = 13 cm (5 in.)

b. Width = 15 cm (6 in.) →

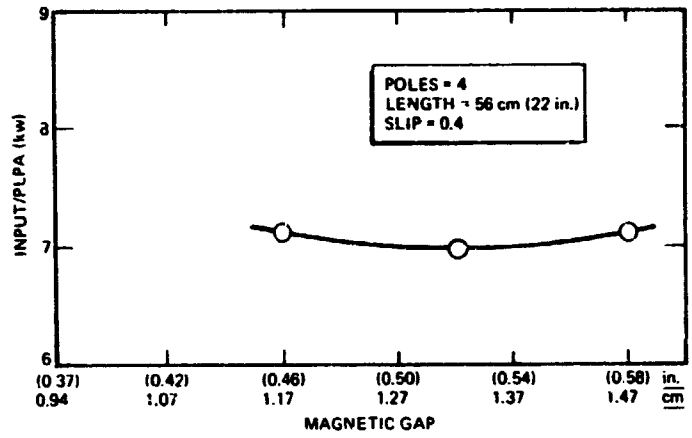

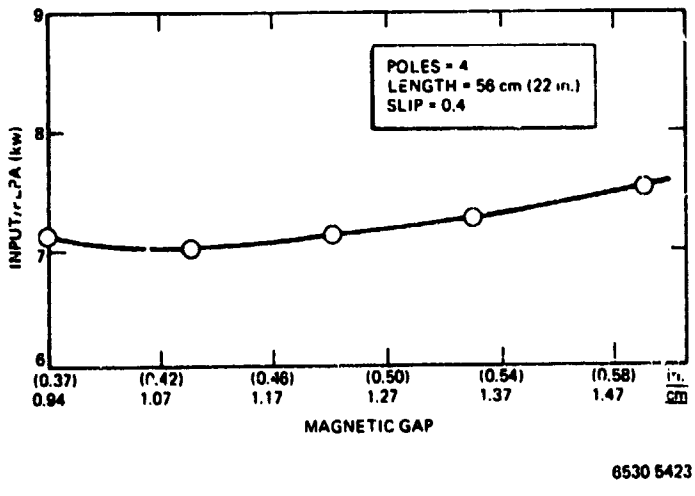

c. Width = 18 cm (7 in.) ←

Figure 22. Power Input vs Gap Height for ac Linear Induction Two-Pump PLPA

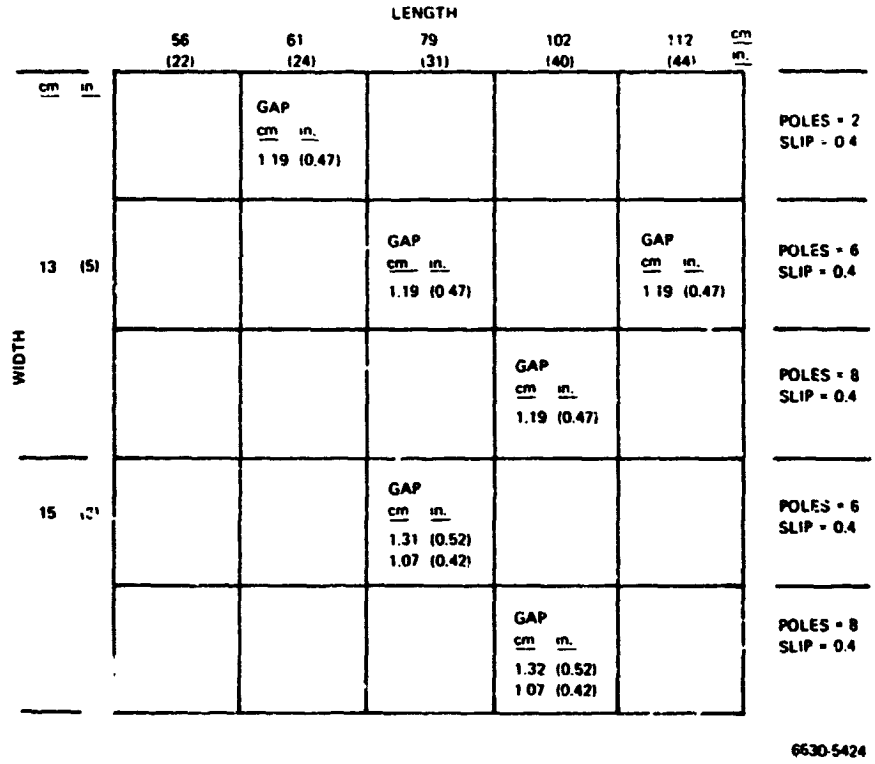

Figure 23. Expansion of Initial Design Matrix for ac Linear Induction Two-Pump PLPA

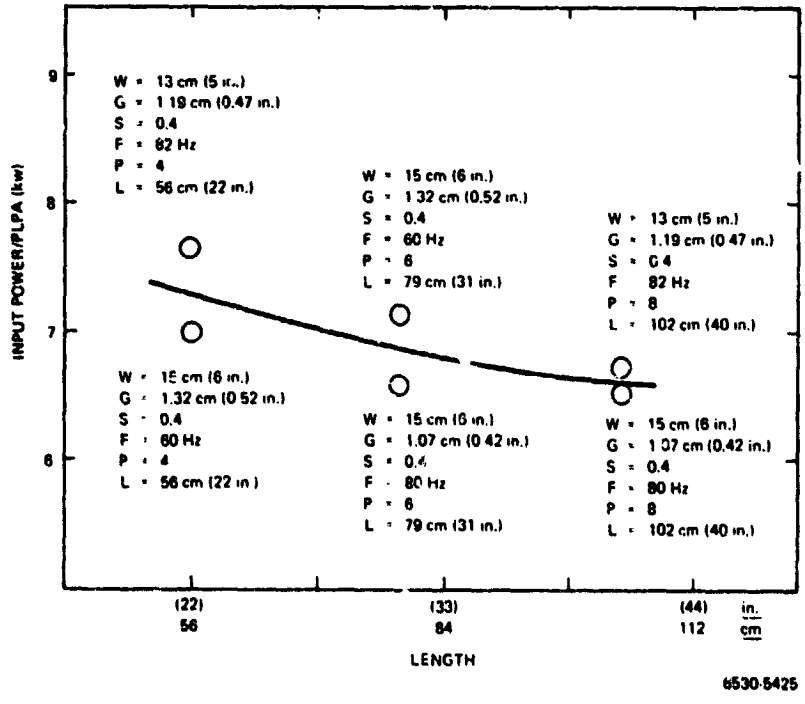

Figure 24. Input Power vs Length for ac Linear Induction Two-Pump PLPA

WIDTH	SLIP		
	0.4	0.5	0.6
13 cm (5 in.)	GAP cm / in. 1.07 (0.42) 1.19 (0.47) 1.32 (0.52) 1.45 (0.57)	GAP cm / in. 0.94 (0.37) 1.07 (0.42) 1.19 (0.47) 1.32 (0.52) 1.45 (0.57) 1.55 (0.61)	GAP cm / in. 0.94 (0.37) 1.07 (0.42) 1.19 (0.47) 1.32 (0.32) 1.45 (0.57) 1.55 (0.61)
15 cm (6 in.)	GAP cm / in. 1.07 (0.42) 1.19 (0.47) 1.24 (0.49) 1.32 (0.52) 1.45 (0.57)	GAP cm / in. 1.07 (0.42) 1.19 (0.47) 1.32 (0.52) 1.45 (0.57) DESIGN NO. 86	GAP cm / in. 1.07 (0.42) 1.24 (0.49) 1.45 (0.57)
18 cm (7 in.)	GAP cm / in. 0.94 (0.37) 1.07 (0.42) 1.19 (0.47) 1.32 (0.52) 1.45 (0.57)	GAP cm / in. 0.94 (0.37) 1.07 (0.42) 1.19 (0.47) 1.45 (0.57) 1.45 (0.57) 1.57 (0.62)	GAP cm / in. 0.94 (0.37) 1.07 (0.42) 1.19 (0.47) 1.45 (0.57) 1.45 (0.57) 1.57 (0.62)

6530-5426

Figure 25. Design Matrix for ac Linear Induction Two-Pump PLPA, Modified for Slot Geometry [Length = 63 cm (24.7 in.), poles = 4]

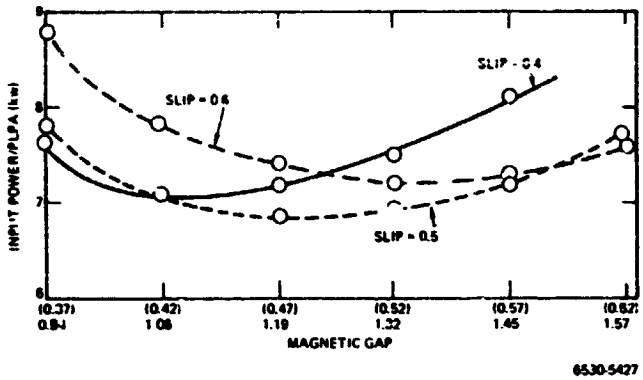

a. Width = 18 cm (7 in.)

b. Width = 15 cm (6 in.)

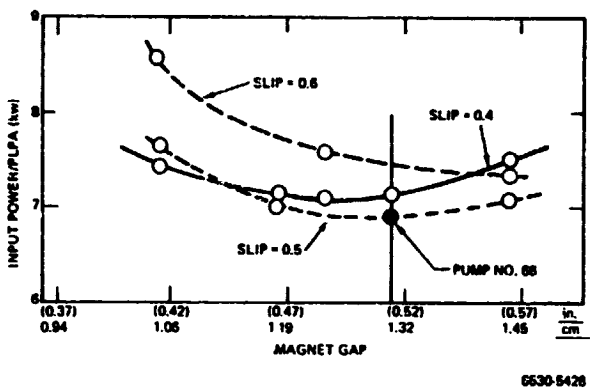

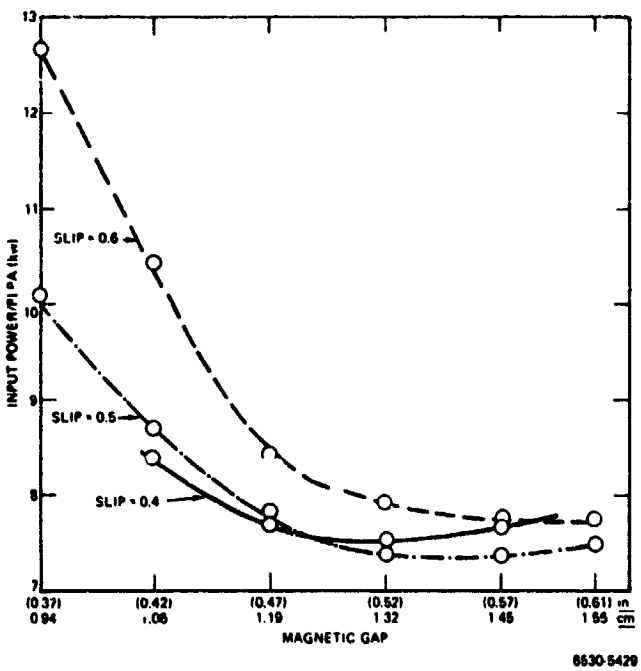

c. Width = 13 cm (5 in.)

Figure 26. Input Power vs Gap Height, as a Function of Slip, for ac Linear Inductior Two-Pump PLPA [Length = 62.7 cm (24.7 in.), poles = 4]

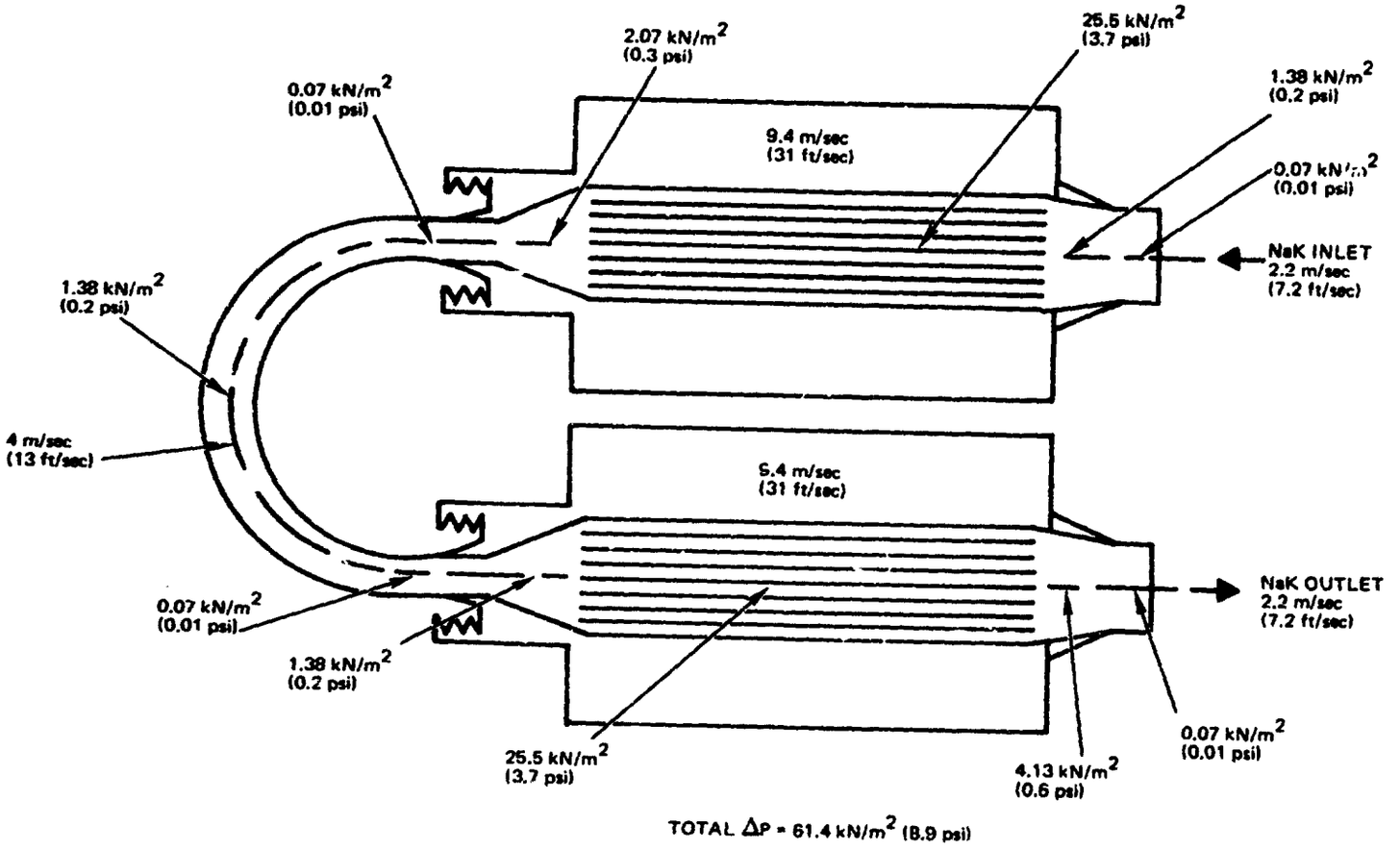

Figure 27. Hydraulic Pressure Loss for ac Linear Induction Two-Pump PLPA

piping. Using the hydraulic formulas discussed under the helical pump section, more detailed calculations were performed to determine the adequacy of the original allowance. For pressure drops, it was anticipated that the original allowance would be low, since the effect of splitter plates was not considered. Later in the program, it was determined that seven splitter plates would be required in the flow channel to supply the necessary mechanical strength. The total head drop allowed in the early calculations, shown in the previous electrical performance curves, was 5.8 m (19 ft), or 41.02 kN/m^2 (5.95 psi).

Refined pressure drop calculations with various ID's of connecting pipe were performed, and the results are as follows:

Connecting Pipe Diameter		Hydraulic Loss in 2-Pump PLPA	
cm	in.	kN/m^2	psi
2.5	(1)	184.1	(26.7)
3.8	(1-1/2)	80.0	(11.6)
5.1	(2)	61.4	(8.9)
6.4	(2-1/2)	61.4	(8.9)
7.6	(3)	61.4	(8.9)

Based upon the preceding calculations, there was no advantage in using a connecting pipe with an ID >5.1 cm (2 in.). The loss for larger pipe remains constant, due to the fact that the decrease in pipe loss is balanced by an increase in diffuser loss. The loss distribution for the selected 6.4 cm (2-1/2 in.) ID connection was 20.34 kN/m^2 (2.95 psi) higher than originally allocated. With this discrepancy in loss, the required power was increased for the rated operation point. A breakdown of the various pressure losses for the dual linear pump is shown in Figure 27. Better than 80% of the pressure loss occurs in the flat pump ducts, where the fluid velocity is highest. The majority of the remaining pressure loss is associated with the transition sections of the PLPA.

b. Electrical - Hydraulic Performance Summary

As can be seen in the Performance Summary (Table 11), the input power required to produce rated conditions has increased from ~7 to 8.6 kwe, as a result of the higher hydraulic losses. Therefore, the efficiency of the dual ac

TABLE 11

DESIGN AND PERFORMANCE SUMMARY OF ac LINEAR INDUCTION TWO-PUMP PLPA– DESIGN NO. 66

NaK Flow Rate [kg/sec (lb/sec)]	9.1 (20)
NaK Head Rise [kN/m^2 (psi)]	48.3 (7)
Stack Length [cm (in.)]	62.7 (24.7)
Stack Width [cm (in.)]	15.2 (6.0)
Stack Height [cm (in.)]	11.4 (4.5)
Magnetic Gap [cm (in.)]	1.32 (0.52)
Channel Height [cm (in.)]	1.02 (0.40)
Channel Width [cm (in.)]	15.2 (6.0)
Number of Poles	4
Number of Stator Slots	29
Power Input (kw/PLPA)	8.6
Current (amp/phase/winding)	80.5
Line to Line Voltage (v)	66
Power Factor	0.47
Frequency (Hz)	65
PLPA Efficiency (%)	7.0
Slip	0.5

linear PLPA dropped from the earlier 8.6% used in the reliability comparisons to 7.0%, significantly reducing the attractiveness of the linear option. A line to line voltage of 66 v at 65 Hz was required to produce rated conditions.

Electrical requirements needed to produce 10% flow, as would be required during startup of the nuclear Brayton system, are shown in Table 12. Approximately 1% of rated input power would be required to produce the 10% NaK flow, since the pressure drop of the system varies as the square of the flow rate. For this application, the frequency would be held constant at 65 Hz, and flow control would be achieved by varying the input voltage. The effect of varying voltage on the NaK head rise and flow rate is shown in Figure 28. The NaK flow displays a good degree of sensitivity to the voltage; therefore, adequate flow control is achieved by this means.

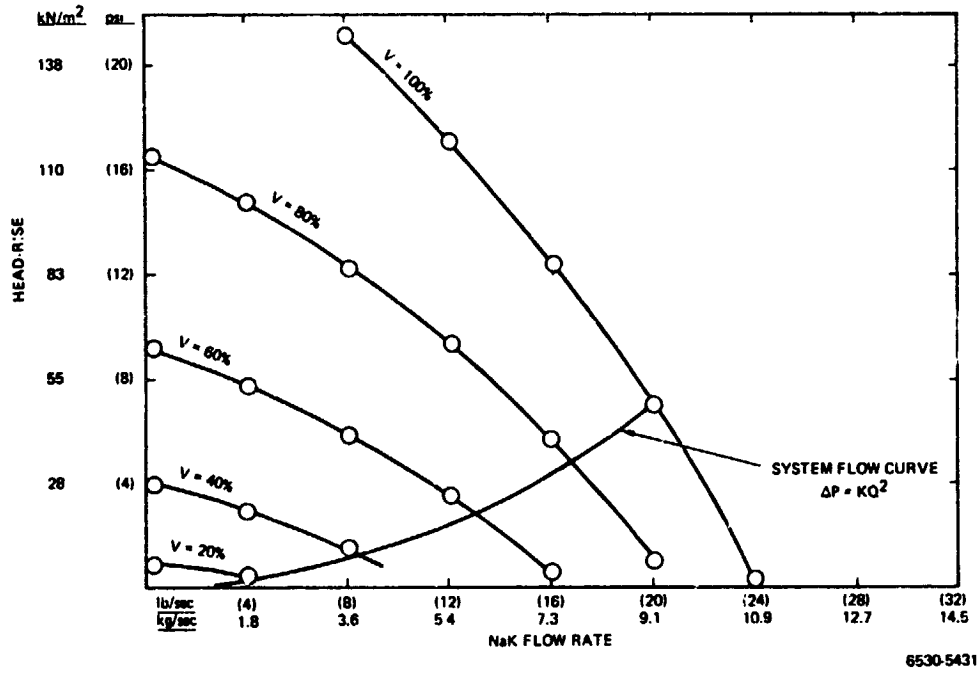

Figure 28. Head Rise vs NaK Flow Rate for ac Linear Induction Two-Pump PLPA – Design No. 66

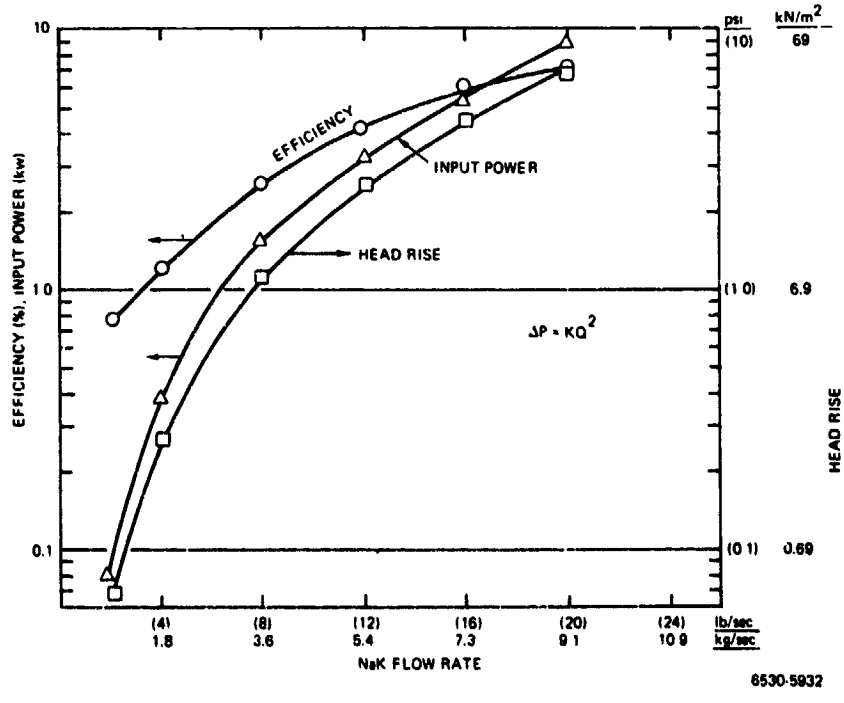

Figure 29. Performance vs Flow Rate for ac Linear Induction Two-Pump PLPA – Design No. 66

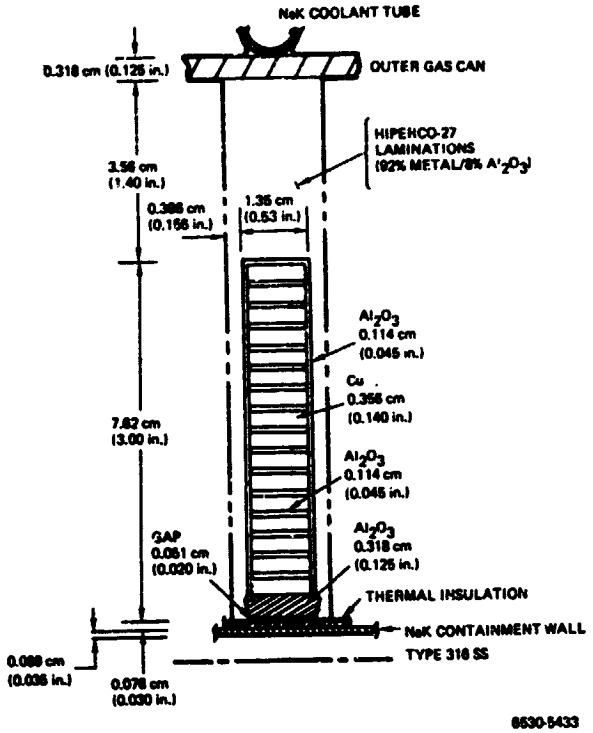

Figure 30.

Design No. 66 – Winding Slot [Width = 15 cm (6 in.)]

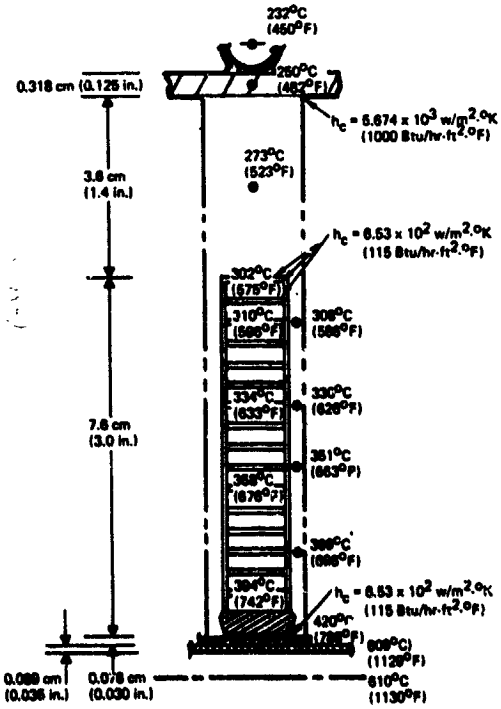

Figure 31.

Thermal Map – Design No. 66 Width Argon Containment Gas and Mica Thermal Insulation

TABLE 12

STARTUP CONDITIONS (10% Flow) FOR
ac LINEAR INDUCTION TWO-PUMP
PLPA – DESIGN No. 66

Current (amp/phase/winding)	7.2
Line to Line Voltage (v)	5.4
Power Input (w)	76
Power Factor	0.57
Frequency (Hz)	65

Head rise, efficiency, and input power for low flow rates are shown in Figure 29. The efficiency of the unit drops to below 1% when the flow is reduced to 10%. Again, the loop pressure drop was assumed to vary as the square of the mass flow.

c. Thermal Analysis

A cross section of the reference linear pump winding slot is shown in Figure 30. The slot is 7.6 cm (3 in.) deep by 1.34 cm (0.53 in.) wide, and contains 16 copper straps when full. Each of the 1.161-cm (0.457-in.) by 0.356-cm (0.140-in.) copper straps is separated from each other and from the Hiperco-27 stator laminations with high-purity ceramic alumina. The winding is held and compressed within the slot with an alumina wedge. End turn insulation consists of "S" glass tape, wound around each of the straps as they are laid into the slots. Thermal insulation separates the stator stack from the hot NaK duct, and cooling coils are brazed to the outer gas containment can.

Detailed thermal analysis was performed on dual PLPA Design No. 66, which was the selected design, based upon the results of the parametric study.

The basic approach, constants, matrix, and computer code, as referred to in the helical pump section, were used in this study. The results of the analysis, in which argon containment gas and mica throat insulation were used, is shown in Figures 31, 32, and 33. Comparing this data with similar helical pump data, it can be seen that these temperatures are ~38°C (100°F) hotter than the temperatures shown for the helical pump. The reason for the higher temperatures, in spite of the fact that the linear pump operates with a lower current density, is

Figure 32. ⟶

End Turn Temperatures — Design No. 66 With Argon Containment Gas and Mica Thermal Insulation

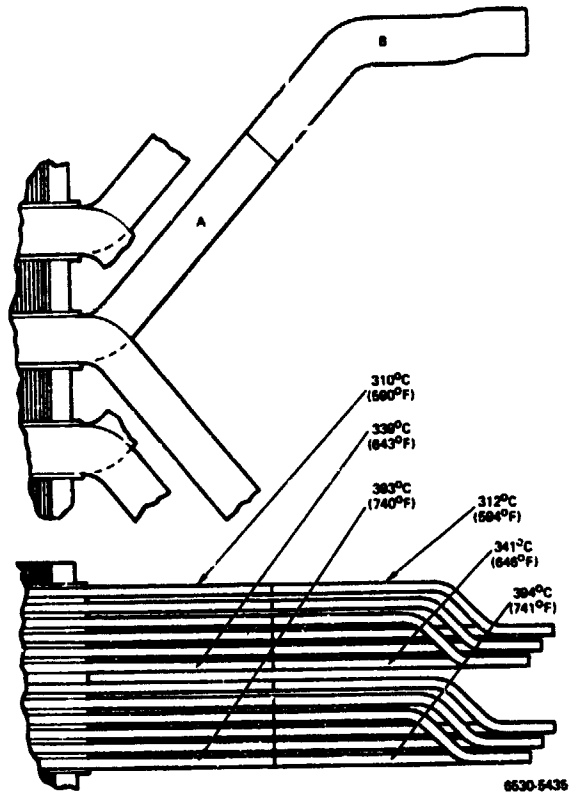

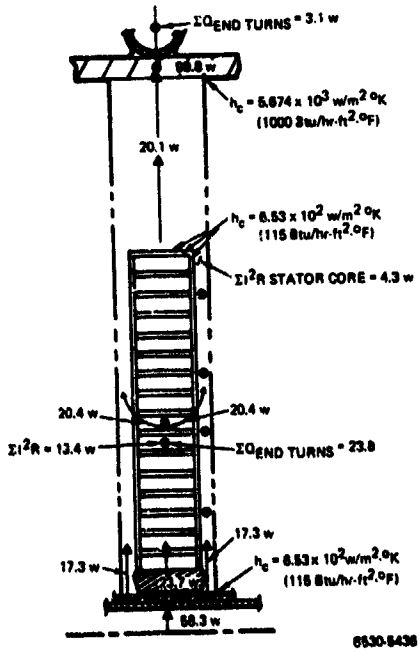

⟵ Figure 33.

Heat Flow Map — Design No. 66 With Argon Containment Gas and Mica Thermal Insulation

the reduced tooth area through which the I^2R and conducted heat must flow to be rejected, and the increased area in contact with the hot NaK channel. The temperatures shown are, however, acceptable.

As shown in the heat flow map, the heat generated in the slot and end turn copper must be conducted primarily up through the stator iron to the cooling coils. Heat transfer through the copper to the cooling coils is limited, because of the numerous interfaces across which it must be radiated. The depth of the slot and the small thickness of the tooth offer considerable resistance to the primary heat rejection path. To achieve the temperatures shown, it is imperative that good mechanical contact be maintained between the stator iron and the outer gas jacket. This would be difficult to achieve, for the flat geometry of this pump, considering temperature differential across the back iron. For this reason, numerous holding lugs were used, and it is probable that copper shims would be required between the laminated stack and gas can to maintain a low thermal resistance. The highest winding temperature, 394°C (742°F), was found in the stator slot, close to the hot NaK duct.

3. Stress Analysis

As with the helical pump, the basic stress criteria was conformance to the intent of Section III, Case 1331-5, of the ASME Boiler and Pressure Code for all main NaK coolant containment parts, and conformance to Section VIII of the Boiler Code for all other parts. Because of the configuration of the linear pump, the main areas of concern were the flattened duct and transition pieces and the gas containment can. The loading conditions are the same as those which were used for the helical pump. The throat loading arises either from the internal pressurization of the channel by the NaK [345 kN/m^2 (50 psid) maximum, 621°C (1150°F)] or by the evacuation of the channel during system filling [-103 kN/m^2 (-15 psid) maximum, 260°C (500°F)]

Since allowing the stator assembly to resist internal throat loading would stress the thermal insulation, complicate the stator structure design, and make analysis per the Code extremely difficult, a decision was made that the throat had to be designed to self-limit deflection to prevent contact with the stators, and be designed to accommodate all resultant stresses. An analysis of the throat stresses clearly indicated that the internal pressure case was the most severe, and that, with the wall thickness of interest, 0.076 cm (0.030 in.), internal

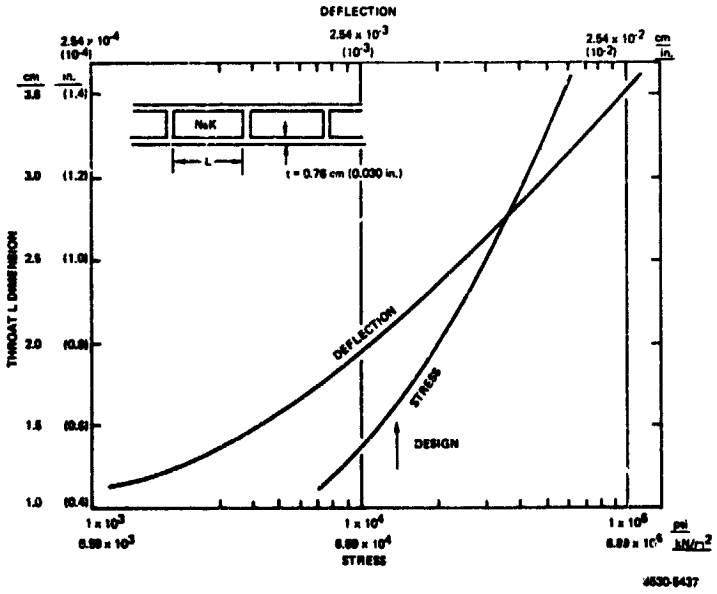

Figure 34.

Linear Pump Throat Deflection and Stress

Figure 35.

Linear Pump Stator Stack Deflection (Loads for full restraint)

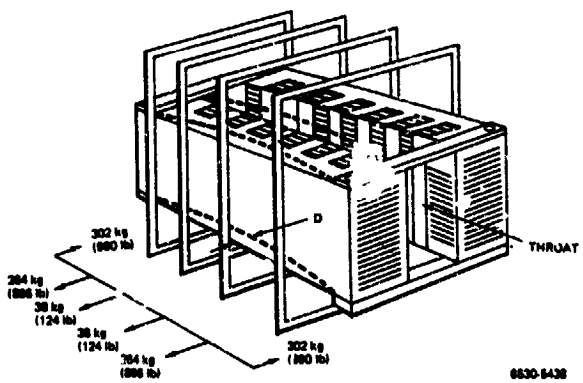

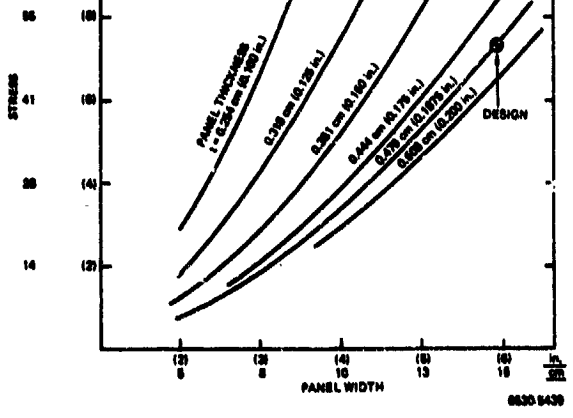

Figure 36.

Outer Gas Shell Stress for Linear Pump [103 kN/m^2 (15 psi) internal pressure]

stiffeners would be required. From Figure 34, it can be seen that, for the required allowables, the maximum stiffener spacing is ~1.8 cm (0.7 in.), dictating seven spacers for a 15-cm (6-in.) wide duct. Since the throat transition pieces are not within the magnetic field, the thickness of those units can be increased to meet stress requirements, and internal stringers are not required.

A second major concern in the linear pump is maintaining a constant magnetic gap between the stator halves. If the gap increases, the magnetic flux will be decreased. If the gap decreases, interference with the throat insulation is possible. Since the backs of the lamination stacks are cooled, while the front surfaces of the teeth are exposed to the effect of the hot throat, a temperature gradient will exist through the lamination back iron. This gradient will cause the laminations, if unrestrained, to bow outward at the ends, as shown in Figure 35. An analysis of the magnitude of the unrestrained bowing [~0.15 cm (0.060 in.) total deflection for each 38°C (100°F) ΔT] indicated the desirability of providing external restraints ("belly bands") to the lamination stacks. The force values shown (Figure 35) are those forces at four equally spaced locations required to maintain the lamination stacks flat. Calculations were also made of the cross-sectional dimensions of the belly bands required to limit deflection to 0.013 cm (0.005 in.). Those dimensions were used in the final layout of Design No. 66.

A third area of concern was the ability of the rectangular containment can to resist the forces resulting from internal pressurization. An analysis was performed which demonstrated that, with a maximum panel width of ~15 cm (6 in.), as established by the belly band spacing, a panel thickness of 0.4763 cm (0.1875 in.) would result in a stress of <551.6 kN/m^2 (8000 psi), well below allowables. Variation of stress with panel width and thickness is shown in Figure 36.

4. Design Details

a. Pump Configuration

The configuration of the reference design linear induction pump is shown in Figures 37 and 38. It is seen that the basic configuration of the analysis model has been retained; however, the overall size has increased substantially. The

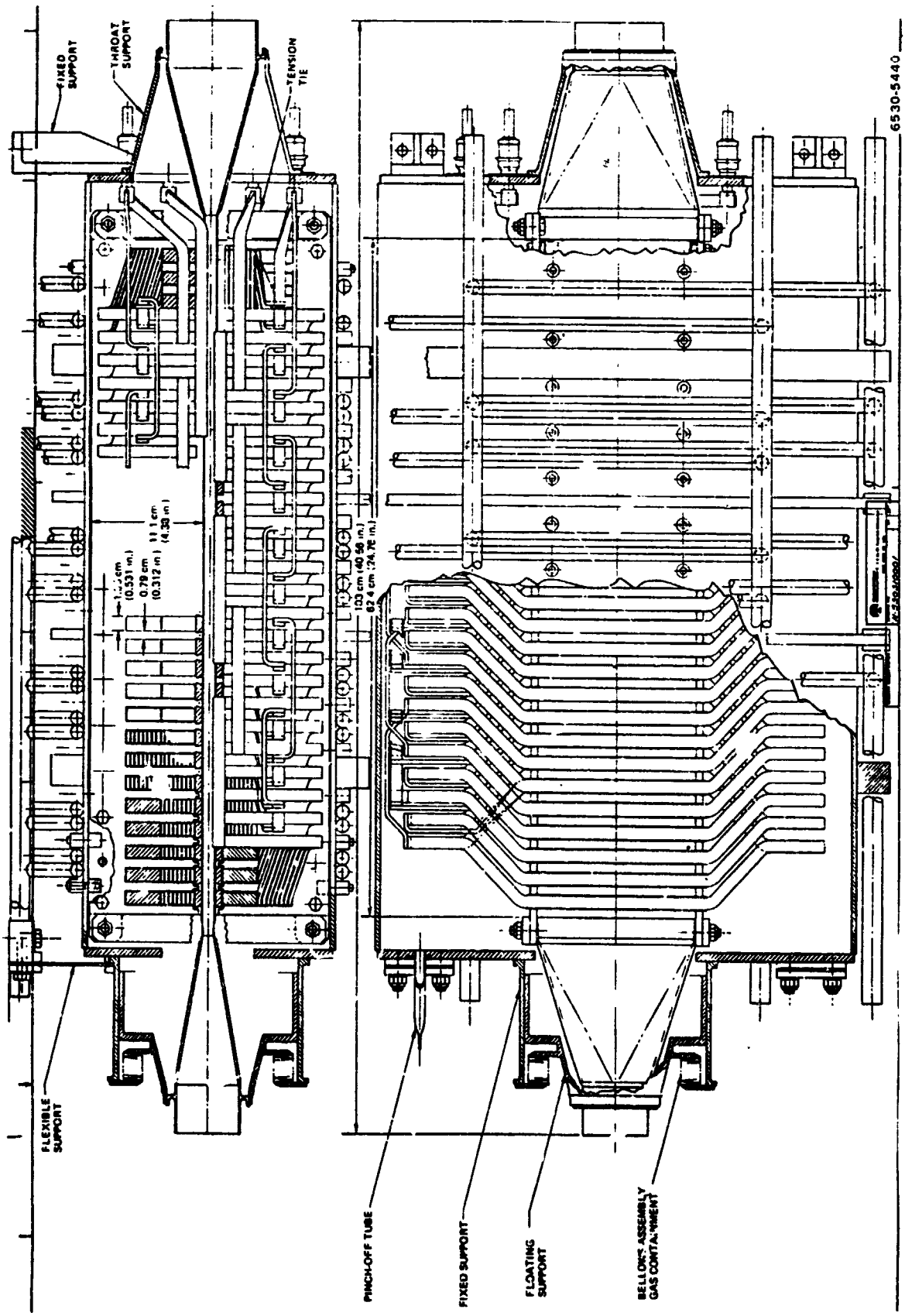

Figure 37. Plan and Side View of Linear Pump (Dwg. N530310001)

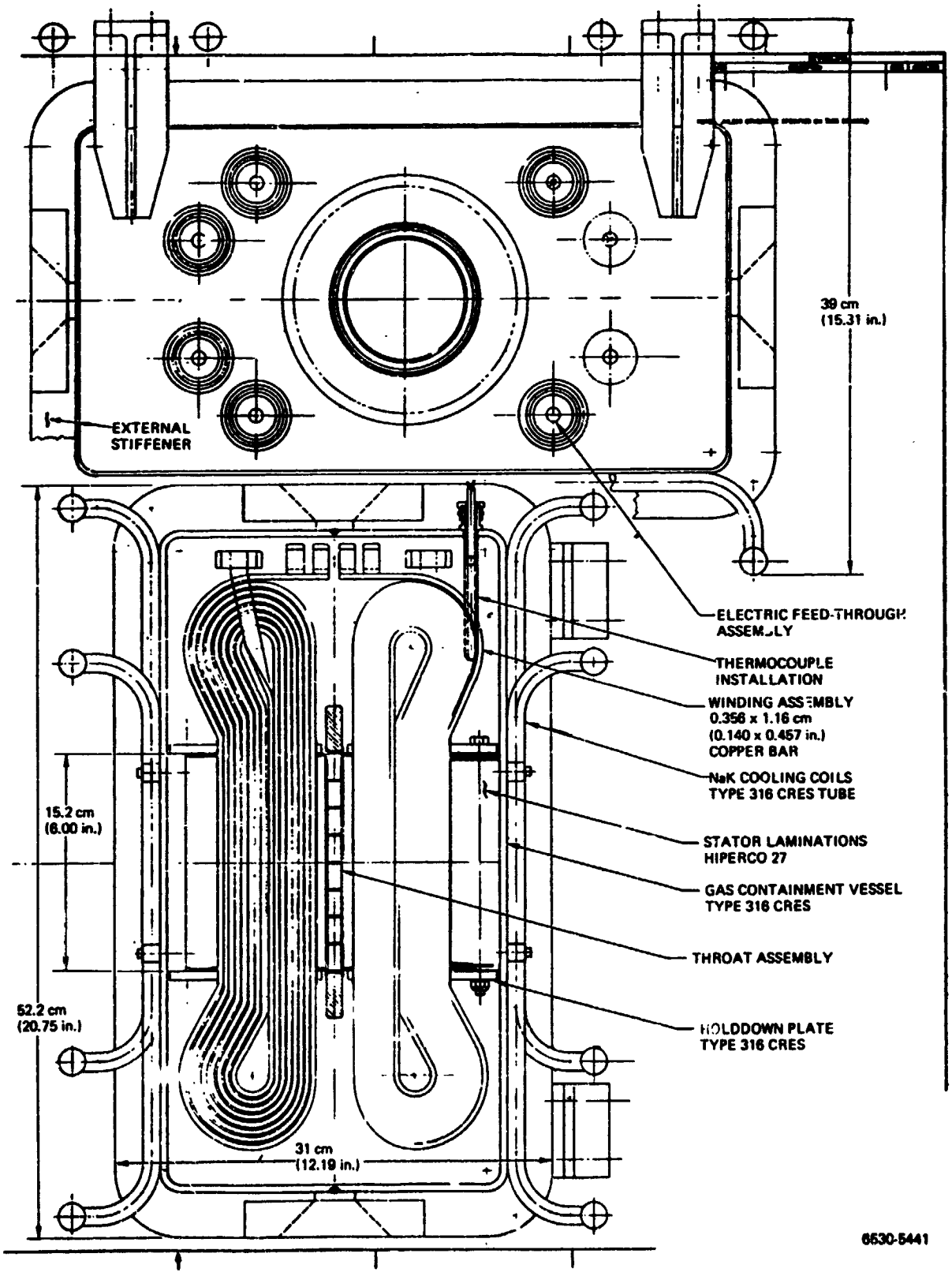

Figure 38. End Views of Linear Pump (Dwg. N530310001)

assembly consists of a flattened throat, internally supported with seven stiffener plates. Rectangular to circular transition pieces are welded to each end of the throat. The configuration incorporates a single gas containment enclosure housing both stator halves, and through which the flow channel must penetrate. To accommodate differential expansion between the flow channel and the containment enclosure, the transition piece at one end of the pump is attached to the containment enclosure, using a guided bellows assembly. The pump inlet end of the flow section is welded to an extension of the containment enclosure for throat support.

The stator halves are made up of an assembly of insulated lamination punchings sandwiched between finger plates which are first compressed, and then held in place by rectangular building bars, welded at the edges, and with through bolts further inboard. The stator halves are spaced and strapped together at the ends. Thermal insulation is provided between the throat and the stator halves. Attachment of the stator halves to the containment enclosure, which is made up in two halves, is by the use of studs threaded into holes tapped into the building bars. To provide containment, the studs are back welded to bushings in the gas can. To prevent bowing of the stator halves, four equally spaced belly bands are welded to the outside of the outer gas containment enclosure.

Manifolds are provided on either side of the pump to feed two independent NaK cooling circuits, the tubes of which are brazed to the containment enclosure. Four supports are provided for attachment to the vehicle mounting structure.

The windings are made up of coils of rectangular copper bars, loosely wound, and formed into a diamond shape to fit the pole pitch. Ceramic strip is used for slot and turn insulation in the slot. Glass tape is used to insulate the windings in the end turn area. The coils are individually formed, and then the joints are welded to make up the winding and phase connections. The windings are held in place by ceramic slot wedges. The phase leads are brought out of the containment enclosure, using glass-to-metal seals.

The more difficult pump fabrication problems will be associated with: (1) the forming of the linear throat and the brazing of the current return bars, (2) the attachment of the stator halves to the containment enclosure to minimize thermal contact resistance, and (3) the forming, stiffening, and final closure of the

containment enclosure to avoid distortion. Forming of the coils and making the inter-coil terminations will require process development. From preliminary fabrication studies, based on AI past experience and industry state of the art, it was concluded that several practical methods exist for fabricating the throat, including electrochemical machining of the complete unit, a technique which minimizes thermal distortion. The copper current return buses would be furnace brazed to either side of the throat, using previously developed processes. It is expected that the other design and fabrication problems could be worked out in the detail design phase.

b. Materials

The tentative selection of materials is as follows:

Throat and transition pieces	Type 316 stainless steel
Thermal insulation	Mica - 316 stainless steel sandwich
Laminations	Alumina-insulated Hiperco
Finger plates and building bars	Type 316 stainless steel
Cooling coils	Type 316 stainless steel
Containment enclosure	Type 316 stainless steel
Support legs	Type 316 stainless steel
Current return bars	OFHC copper
Coil conductor	OFHC copper
Turn and slot insulation	Alumina
End turn insulation	"S" glass tape
Slot wedges	Alumina

c. PLPA Configuration

The arrangement of the reference design pump to form a two-pump PLPA is shown in Figure 39. Because the pumps had become so wide, in order to accommodate the end turn knuckle joints and splices, it was necessary to orient the pumps with the smaller sides adjacent, so that the PLPA would fit within the 41-cm (16-in.) available height. In this configuration, assuming that the pumps could be strapped together and mounted directly to the vehicle structure, and based upon a 6.4-cm (2-1/2-in.) interconnecting pipe, the overall dimensions of the PLPA would be 107 by 143.0 by 38.89 cm (42 by 56.31 by 15.31 in.). Total weight was estimated at 630.5 kg (1390 lb).

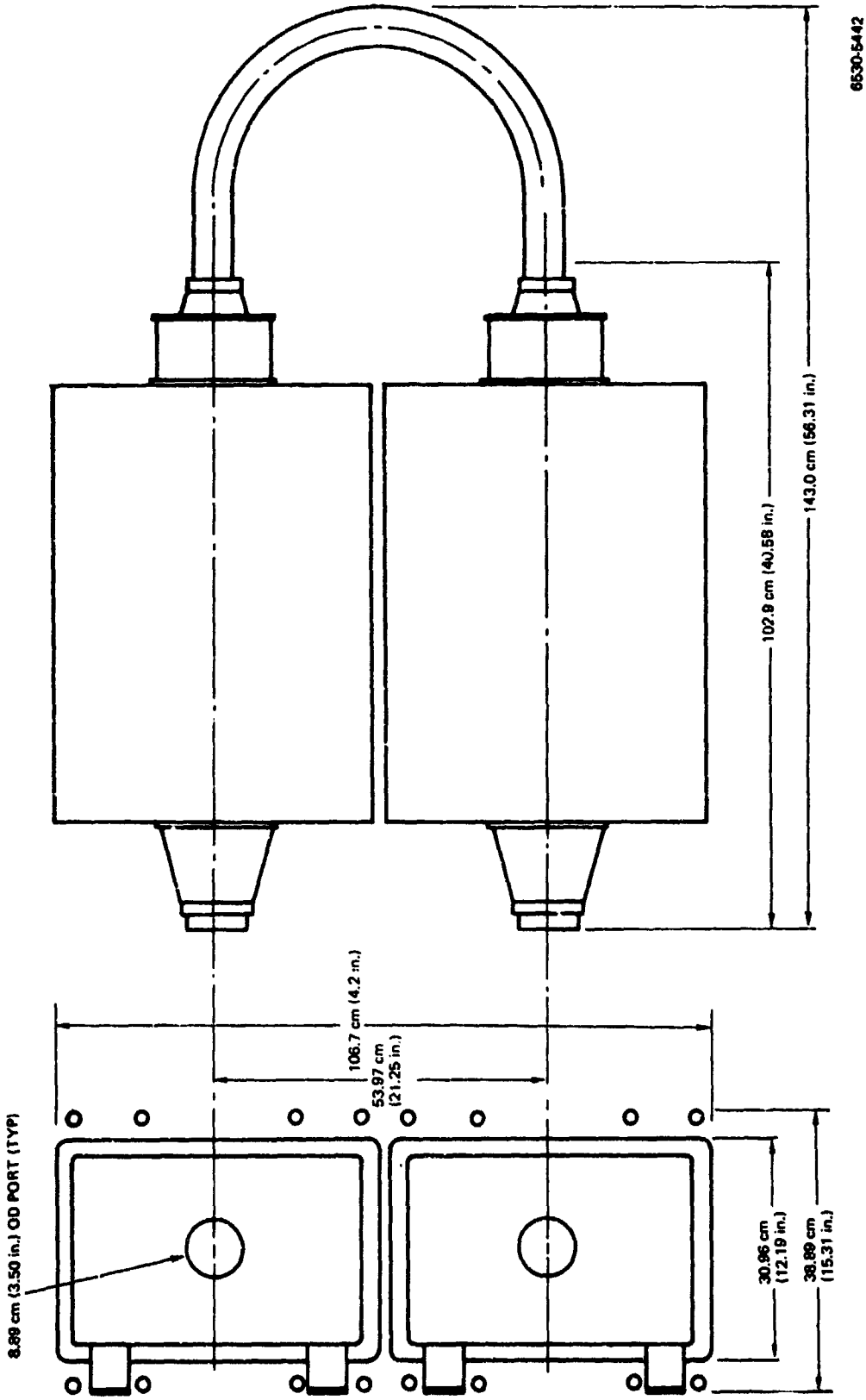

Figure 39. Design No. 66 ac Linear Induction Pump

5. Conclusions

It was concluded, in the study, that an ac linear induction pump PLPA could be designed and fabricated to meet the program requirements. Because of the influence of field discontinuity at the throat extremes, and the relatively high hydraulic losses resulting from the requirement of internal throat stiffeners, the efficiency of the PLPA will be somewhat less than that of the helical induction PLPA. The requirements of internal pressurization of the outer housing, the tendency of the stator halves to bow due to differential thermal expansion, and the space required for the end turns, dictate a large, bulky, and heavy outer containment housing. This, added to the fact that, whatever straight sections of pipe connecting the pumps must be outboard of the pumps, makes for a very large PLPA envelope and high total weight. The general rectangular shape of the linear induction pump complicates fabrication problems, and generally aggravates problems of obtaining low thermal contact resistances.

A low winding current density can be obtained, which improves reliability; however, ideal tooth widths, from electromagnetic and overall size considerations, dictate relatively thin teeth (of constant cross section, as opposed to increasing cross section of the helical pump), which results in poor heat transfer in the laminations and relatively high winding temperatures.

Perhaps the most important advantage of the linear induction pump is the ease of installing the windings and providing separate windings for the two-pump PLPA concept.

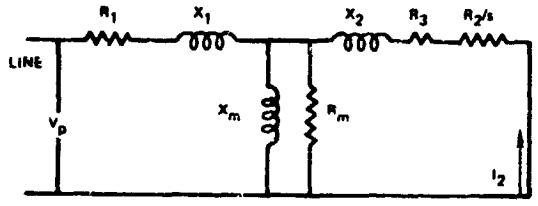

CIRCUIT A

V_p = VOLTAGE APPLIED TO A PHASE
R_1 = WINDING RESISTANCE IN THE STATOR
X_1 = WINDING REACTANCE IN THE STATOR
X_2 = REACTANCE IN THE FLUID, REFLECTED IN STATOR UNITS (TURNS RATIO CORRECTION)
R_3 = SPLITTER RESISTANCE (TURNS RATIO CORRECTION)
R_2 = RESISTANCE IN THE FLUID, REFLECTED IN STATOR UNITS (TURNS RATIO CORRECTION)
X_m = MAGNETIZING REACTANCE (TO SUPPLY NECESSARY CURRENT MAGNETIZE THE PUMP)
R_m = RESISTANCE VALUE TO ACCOUNT FOR THE MAGNETIZING LOSSES ASSOCIATED WITH THE ESTABLISHING OF THE FLUX (CORE, CAN, AND DUCT LOSSES)
s = SLIP FACTOR, TO ACCOUNT FOR DIFFERENCE BETWEEN SPEED OF THE FLUID AND STATOR ((FIELD SPEED - FLUID SPEED)/(FIELD SPEED))
I_2 = CURRENT IN FLUID

6530-5443

Figure 40.

Basic Equivalent Circuit for Induction Machine

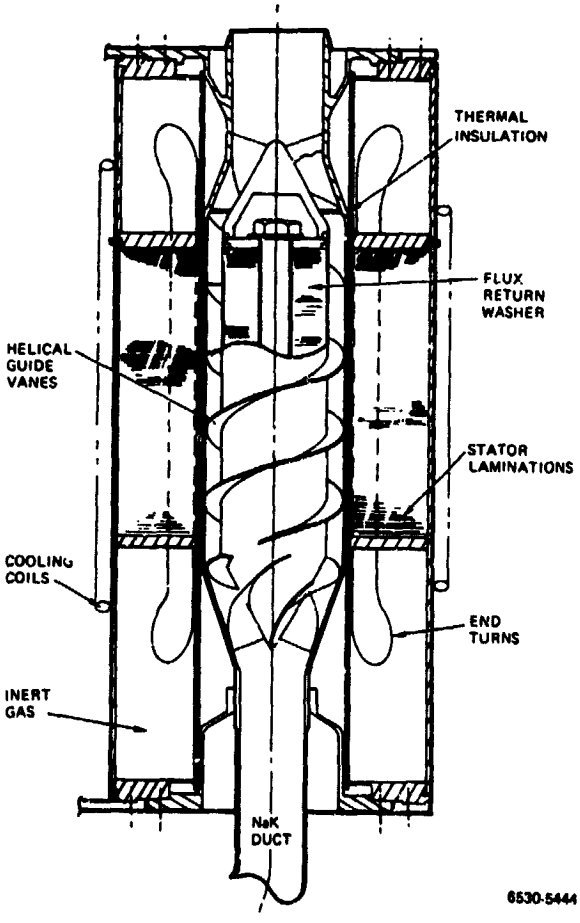

6530-5444

Figure 41.

ac Helical Induction Pump

V. ac HELICAL INDUCTION PLPA

A. GENERAL DESIGN DESCRIPTION

In all electromagnetic pumps, a conducting fluid carrying current is located within a magnetic field. In an ac electromagnetic pump, the current is established by a voltage induced in the fluid, resulting from the relative motion of the fluid and the magnetic field. The resultant current and magnetic field produces a body force within the fluid. As the fluid passes from the pump inlet to the outlet, the body force results in a pressure rise within the field.

B. PRINCIPLE OF OPERATION

The principle of operation of a helical induction pump is similar to that of an induction motor in many respects. The pump is built with a wound stator, the function of which is identical to the induction motor stator (i.e., to convert alternating current into a rotating magnetic field). In an induction motor, this rotating field interacts with conducting bars in a rotor, generating torque from which rotational energy may be removed. In a helical induction pump, the rotor is replaced with an annular duct and a magnetic flux return washer assembly. When a liquid metal is present in the duct, the rotating magnetic field will interact with the liquid metal, causing it to rotate. Rotating the fluid itself in the annulus is of little value for pumping; therefore, helical guide vanes are installed in the annulus to direct the fluid in the desired path. As energy is transferred to the fluid by the rotating magnetic field, a pressure rise occurs in the fluid, which causes the fluid to travel through the pump. This pressure increase is analogous to the developed torque in the induction motor rotor.

The basic method of calculating the performance of inductance machines is to establish numerical values of circuit elements to be inserted into the machine equivalent electrical circuit, and by calculating the voltages and currents to obtain a description of the machine's performance. The end product of a calculation of the equivalent circuit is a determination of the energy delivered to the moving member, and that portion available as mechanical energy (viz., the determination of the energy delivered to the fluid and that portion available to pump the fluid). The basic equivalent circuit for an induction machine is as shown in Figure 40.

C. BASIC DESIGN CONFIGURATION

In order to calculate the numerical values of the equivalent circuit elements, it is necessary to establish a basic pump configuration and select initial dimensions. The dimensions can then be varied to obtain optimum machine performance.

The helical pump shown in Figure 41 was used as a model for the optimization studies. It consists of a pumping section, composed of the center body and pump annulus, and a stator section with mounting provisions. The center body consists of the flux return washers, held together by a through bolt. Centered over the washers, and welded to the end sections or cones, is the inner fluid containment duct, with integrally machined helical guide vanes as a part of its construction. The cone sections also contain guide vanes, to direct the fluid into and out of the helical duct, and to impart or remove the tangential component of motion of the fluid when it enters or leaves the helical duct. The outer containment duct and conical reducers complete the containment of the fluid, and the latter elements serve to match the flow section with the connecting piping. The pump annulus is separated from the stator section by thermal insulation.

The stator section consists of the laminations and windings that produce the rotating field when excited by a three-phase electrical power supply. The stator laminations are held together by building bars, welded into slots around the outside of the stator, while the windings are held in place in the stator slots by ceramic slot wedges. Each turn of the stator winding is insulated from the adjacent turns, and from the slot walls, by ceramic strip insulation. In the end turn section of the winding, the use of ceramic strips is not practical, due to the compound curved shape. In this location, turn insulation is composed of "S" glass in tape form. The turns are connected to each other, and interconnections are made, by welding.

The wound stator is mounted to an outer containment shell using an interference fit, with dowel pins welded in place to assure absence of movement. The outside of the shell contains the coolant circuit. End bells are located and welded to each end of the stator shell. When a stator inner containment can is installed and welded to each end bell, the windings are completely enclosed in a volume which may be pressurized with an inert gas.

In the design, as shown, the thermal insulation, as previously described, is exposed to the operating environment (i.e., either a ground test environment or a space vacuum).

Sealed, insulated power terminations are placed radially on the pump containment shell. These ceramic-insulated feed-through terminals are connected via flexible cable to auxiliary hard-mounted terminals, to which the incoming power cables would be attached.

D. CALCULATION METHOD AND LOGIC

The method of pump electromagnetic calculation used was to establish the values of the various circuit elements in an equivalent circuit, and to solve the equivalent circuit for various values of slip, determining the power flow among the various elements. The useful output power is delivered to the fluid in the form of a body force; and this force, applied to the fluid, produces the pressure rise. Hydraulic calculations must be performed to determine the hydraulic pressure loss which must be subtracted from the developed pressure to produce the net head rise of the PLPA. Since a PLPA will consist of either two or three pumps, hydraulically in series, all the throat and interconnected piping section hydraulic losses must be subtracted from the gross total pump head to determine the output pressure of the PLPA.

For each pump configuration, the value R_2/s was calculated for various values of slip. The energy delivered to the fluid can be calculated from the expression:

$$E = mI_2^2 R_2/s \quad , \qquad \ldots(11)$$

where:

E = energy to the fluid

m = number of phases

I_2 = current flowing through the value, R_2/s

R_2 = fluid resistance

s = slip, in decimal units.

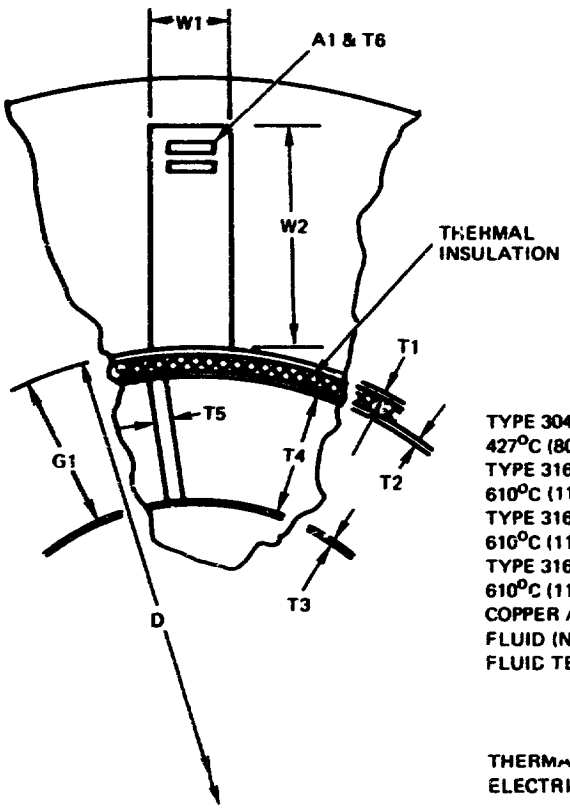

CALCULATION VARIABLES

STATOR ID	D
CORE LENGTH	CL
MAGNETIC GAP	G1
FLUID THICKNESS	T4
HELIX TURNS	F2
NUMBER OF SLOTS	S1
SLOT WIDTH	W1
SLOT DEPTH	W2
TYPE OF SLOT	W3
CONDUCTOR AREA	A1
TURNS/COIL	T6
COIL THROW	T7
VOLTAGE	V1
FREQUENCY	F1

ORIGINAL CALCULATION CONSTANTS

TYPE 304 SS CAN THICKNESS – 0.051 cm (0.020 in.)	T1
427°C (800°F) CAN RESISTANCE – $40.9 \times 10^{-6}\ \Omega$	R1
TYPE 316 SS OUTER DUCT THICKNESS – 0.076 cm (0.030 in.)	T2
610°C (1130°F) OUTER DUCT RESISTANCE – $45 \times 10^{-6}\ \Omega$	R2
TYPE 316 SS INNER DUCT THICKNESS – 0.076 cm (0.030 in.)	T3
610°C (1130°F) INNER DUCT RESISTANCE – $45 \times 10^{-6}\ \Omega$	R3
TYPE 316 SS SPLITTER THICKNESS – 0.152 cm (0.060 in.)	T5
610°C (1130°F) SPLITTER RESISTANCE – $45 \times 10^{-6}\ \Omega$	R4
COPPER AT 604°C (1120°F) CONDUCTOR RESISTANCE – $2.12 \times 10^{-6}\ \Omega$	R5
FLUID (NaK)	FL
FLUID TEMPERATURE – 610°C (1130°F)	FLT

INSULATION

THERMAL – 0.076 TO 0.089 cm (0.030 TO 0.035 in.)
ELECTRICAL, ALUMINA – 0.114 cm (0.045 in.)

6530-5445

Figure 42. ac Helical Induction Pump Design Assumptions

The loss in the fluid is numerically equal to:

$$E_1 = mI_2^2 R_2 \quad , \qquad \ldots(12)$$

and the output energy to the fluid is:

$$E_2 = mI_2^2 R_2\left(\frac{1 - s}{s}\right) \quad . \qquad \ldots(13)$$

Equating the preceding expression to the hydraulic energy delivered to the fluid results in the following expression for the gross pressure rise:

$$P = \frac{2.3 I_2^2 R_2(1 - s)}{Fs} \quad , \qquad \ldots(14)$$

where:

P = pressure (psi) (psi x 6.8947572 = kN/m^2)

F = flow (gpm) (gpm x 0.06309 = ℓ/sec)

The pressure developed is the gross pressure, from which the hydraulic losses must be subtracted, which is discussed later in the report.

The preceding calculations were used in determining the performance of both 2-pump and 3-pump PLPA's. Data used in the calculations included the pump detailed dimensions, material characteristics, the selected PLPA fluid head output (in psi), NaK flow (in lb/sec), and the desired slip at rated point. An example of the size and material characteristics used in the initial designs is shown in Figure 42.

The resistance and reactances of the equivalent circuit, and the electromagnetic performance of the pump(s), based upon the equivalent circuit, were then calculated. From this, the calculated hydraulic loss, including an allowance for the interconnecting piping, was subtracted, and the net pump output was calculated.

To allow an approximate calculation of PLPA head loss over a wide variation of throat geometries and PLPA configurations, a simplified method of calculating hydraulic loss was used. The helix loss was calculated as a rectangular cross-section length of pipe with a friction factor (f) value of 0.015. Other losses

Figure 43.

Beginning Electromagnetic-Hydraulic Calculation Logic

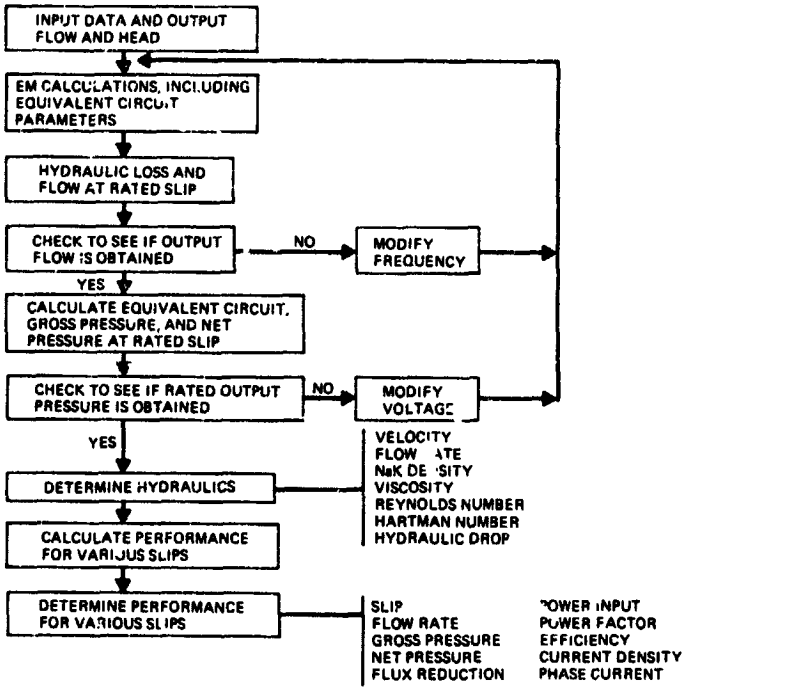

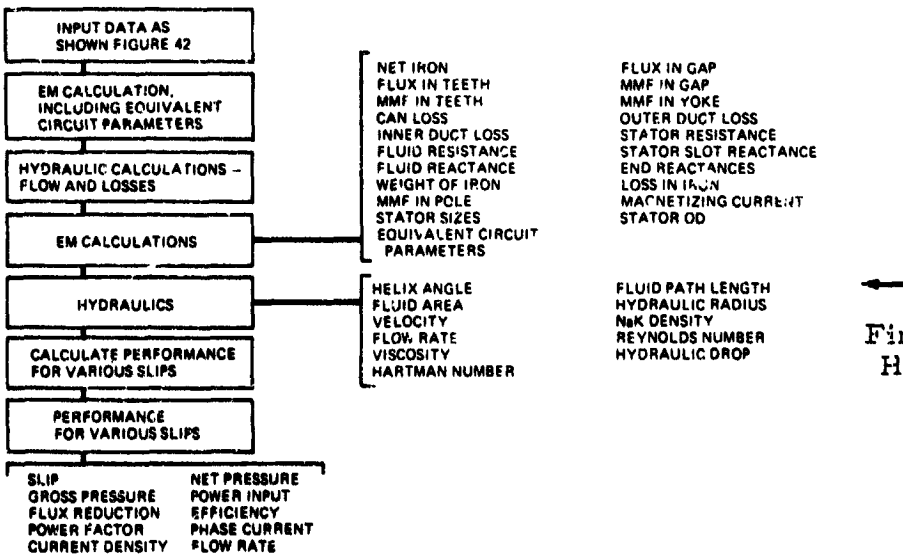

Figure 44.

Final Electromagnetic-Hydraulic Calculation Logic

were calculated as one velocity head per pump. As discussed later, a more rigorous analysis was made on the reference design pumps after completion of the parametric studies.

The voltage and frequency were adjusted to obtain the rated head and rated flow at the rated slip. By systematically changing the input data, the trend of such changes on the PLPA performance could be determined. Using this method, each element of the machine was optimized from a performance standpoint. Final design point selection, however, required an iterative process, factoring in other data resulting from stress, thermal, and reliability studies, as discussed subsequently.

Figures 43 and 44 illustrate the design logic used to determine the performance of a given pump. Figure 43 describes the logic used for evaluation of trends, and Figure 44 relates to the logic used for providing data for detailed engineering evaluation of the operating conditions of the pumps.

E. PARAMETRIC STUDY RESULTS

By the preceding system, with the correction of voltage and frequency, trend curves are obtained readily by successive calculations with the change of a single variable. Using the detail of the slot geometry shown in Figure 45, an initial pump size calculation matrix was performed to determine "ball park" values of optimum machine parameters. The design matrix is shown in Figure 46. Calculations at each value of diameter, core length, and magnetic gap, shown in Figure 46, provided the information for plotting trend curves.

Figure 47 is such a curve, showing the variation of input power to the PLPA for various core lengths. Based on performance alone, the most desirable core length for the two-pump PLPA is 27.9 to 30.5 cm (11 to 12 in.). Due to expected fabrication difficulties, the stack length was limited to 25.4 cm (10 in.) for the 12.7 to 15.2 cm (5 to 6 in.) bore diameter.

Figure 48 shows that the effect of various bore diameters within the range of 12.7 to 14 cm (5 to 5.5 in.) is negligible, but the magnetic gap is critical. This is replotted in Figure 49. As can be observed, a gap of 2.03 cm (0.8 in.) is optimum for the 2-pump PLPA. All calculation runs allowed for 0.076 cm (0.03 in.) of thermal insulation between the outer duct and the gas containment can.

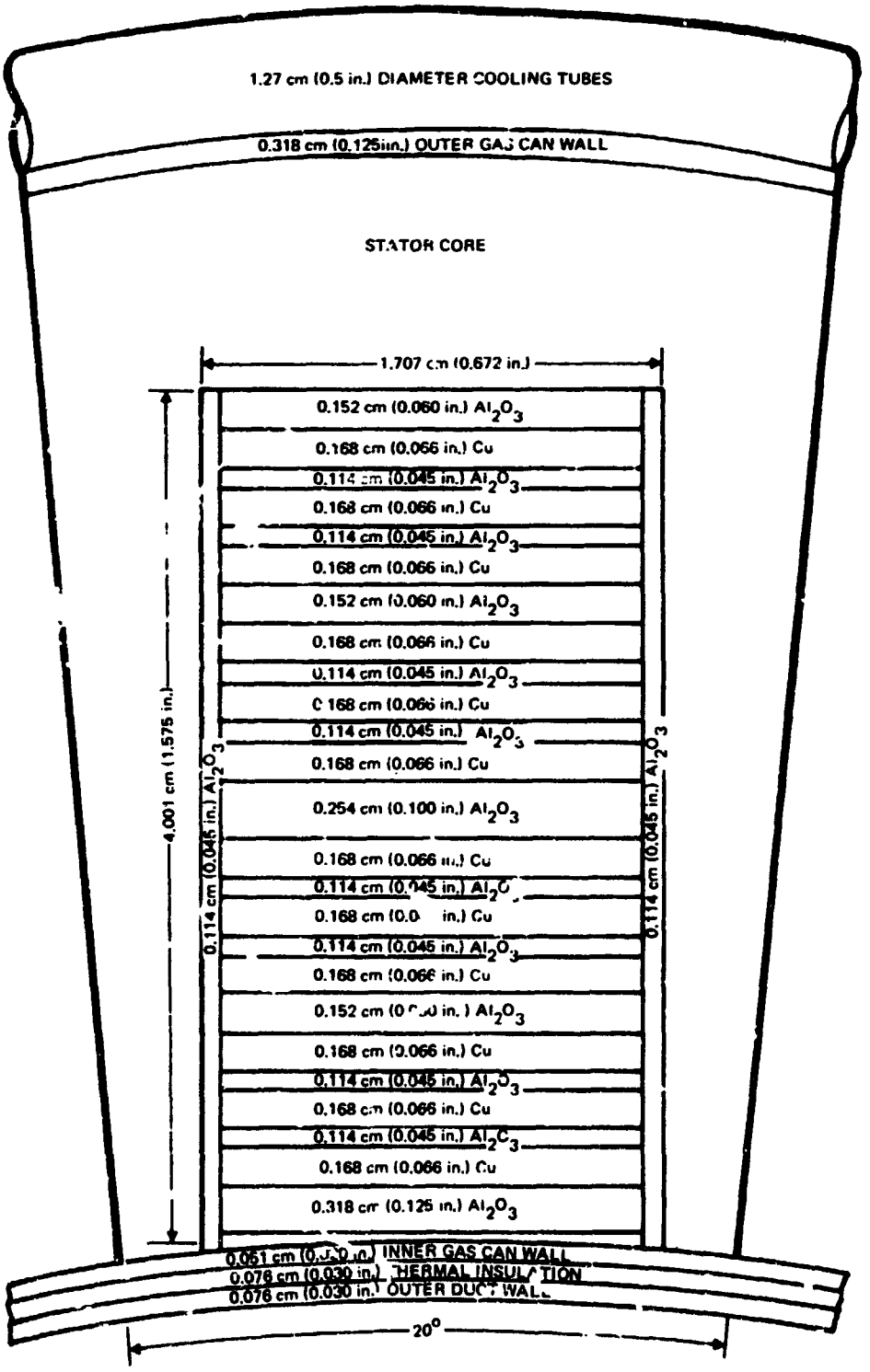

Figure 45. Schematic of Slot Geometry for ac Helical Induction Pump

L \ D	cm / in. 12.7 (5.0)	13.0 (5.1)	13.2 (5.2)	13.5 (5.3)	13.7 (5.4)	14.0 (5.5)	15.0 (5.9)
cm / in. 18 (7)	GAP cm / in. 1.78 (0.70) 2.14 (0.840) 2.39 (0.940) 2.54 (1.00)	GAP cm / in. 2.14 (0.840) 2.39 (0.940)	GAP cm / in. 2.14 (0.840)	GAP cm / in. 2.14 (0.840)	GAP cm / in. 2.14 (0.840)		
18.42 (7.25)		GAP cm / in. 2.39 (0.940)					
19 (7.5)		GAP cm / in. 2.39 (0.940)					
19.68 (7.75)		GAP cm / in. 2.39 (0.940)					
20 (8)		GAP cm / in. 2.39 (0.940)	GAP cm / in. 2.39 (0.940)	GAP cm / in. 2.39 (0.940) 2.14 (0.840) 1.91 (0.7[illegible])		GAP cm / in. 2.39 (0.940)	GAP cm / in. 2.39 (0.940)
23 (9)		GAP cm / in. 2.39 (0.940)					
25 (10)		GAP cm / in. 2.39 (0.940)	GAP cm / in. 2.14 (0.840) 1.88 (0.740) 2.39 (0.940)	GAP cm / in. 2.14 (0.840 1.88 (0.740) 2.39 (0.940) 2.03 (0.800)	GAP cm / in. 1.63 (0.640) 1.88 (0.740) 2.14 (0.840) 2.39 (0.940) 2.64 (1.040)	GAP cm / in. 2.14 (0.840)	
33 (13)			GAP cm / in. 2.39 (0.940)				
43 (17)			GAP cm / in. 2.39 (0.940)				

6530-5449

Figure 46. Design Matrix for ac Helical Induction PLPA

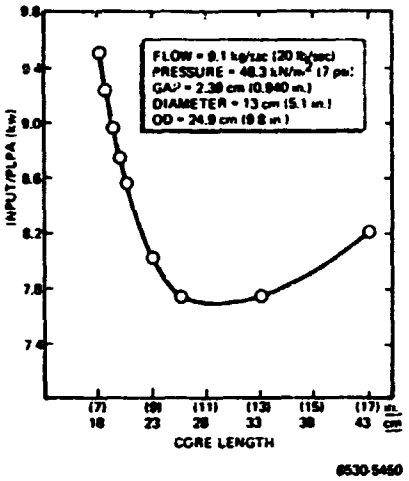

Figure 47. Power Input vs Core Length for Dual Helical PLPA

Figure 48. Power Input vs Bore Diameter for Dual Helical PLPA [25.4 cm (10 in.) stack length, 24.9 cm (9.8 in.) OD]

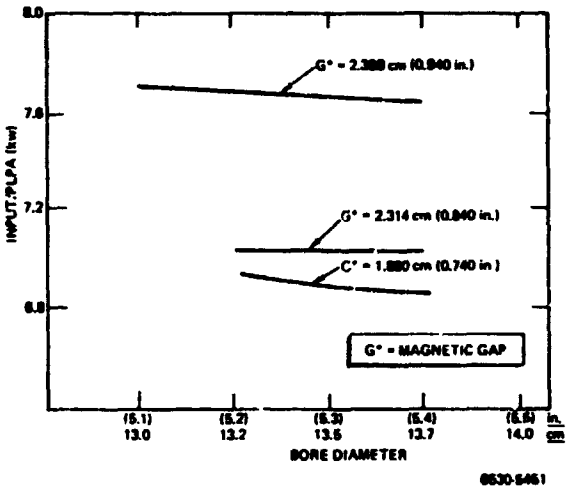

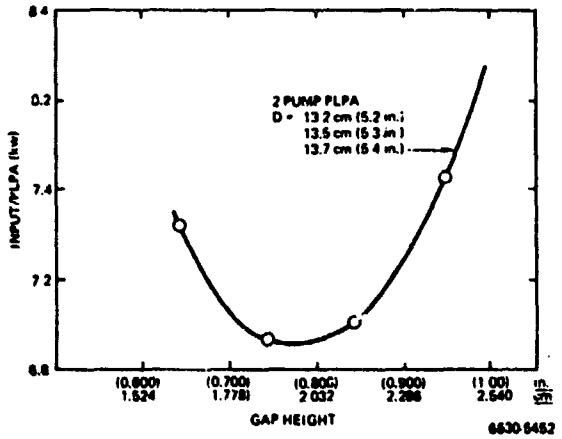

Figure 49. Power Input vs Gap Height for Dual Helical PLPA [25.4 cm (10 in.) stack length]

Based on these trend curves, interim PLPA reference designs were established. The interim dual pump design, referred to as Design No. 65, had a stack length of 25.4 cm (10 in.) with a 13.6 cm. (5.3 in.) stator bore and a 2.03 cm (0.8 in.), magnetic gap. The calculated performance is shown in Table 13, and the reduced flow performance is shown in Figure 50.

Additional optimization studies were subsequently made, in which slot configuration and conductor size were varied. Figure 51 is the matrix for this optimization study, and shows the values of strap thickness and width used. This optimization was performed in conjunction with the preparation of a detailed winding layout. The winding layout indicated the desirability of limiting the strap width at 1.27 cm (0.50 in.), to allow clearance between the coils in the end turn knuckle.

Figure 52 is the trend curve showing the variation of diameters, current density, and power input with copper depth. It appeared desirable to go to a 0.457-cm (0.180-in.) thick copper strap, but the height would take up the full allowed 40.64 cm (16 in.) of space. The copper depth selected was 0.279 cm (0.110 in.), to allow room for unexpected growth, mounting feet, and cooling coil variations. This selection also gave a good balance between stator OD (PLPA weight) and input power (efficiency). The design is known as No. 74. The performance of Design 74 is shown, along with its startup requirements, in Table 14. This unit is calculated for a slip of 0.65. Figure 53 shows the power variation with slip and indicates the optimum slip to be between 0.60 and 0.65. The reduced-flow, constant-frequency performance is shown in Figure 54.

Figure 55 shows the head-flow and input power - flow performance at constant voltage and frequency with three temperatures of pumped NaK. The variations in fluid resistivity, viscosity, and density account for the variation between the curves. The rated conditions are 610°C (1130°F) NaK at 9.07 kg/sec (20 lb/sec) and 48.3 kN/m^2 (7.0 psi) developed by the PLPA. Figure 56 is a performance curve of head and power input vs flow for various voltages. The stability, as represented by the intersection of the system curve and head-flow curve, is excellent for all voltages. This unit is quite adaptable to flow control by voltage control.

TABLE 13

ac DUAL HELICAL PLPA ERFORMANCE
(Y-Connected)

Stack Length [cm (in.)]	25.4 (10)
Stator Bore Diameter [cm (in.)]	13.6 (5.3)
Magnetic Gap [cm (in.)]	2.03 (0.8)
Number of Poles	2
Number of Slots	18
Input Power [kw/PLPA]	6.9
Amperes, Phase/Pump	230
Voltage, Phase/Pump	39
Power Factor	0.46
Frequency [Hz]	40
Efficiency [%/PLPA]	8.7

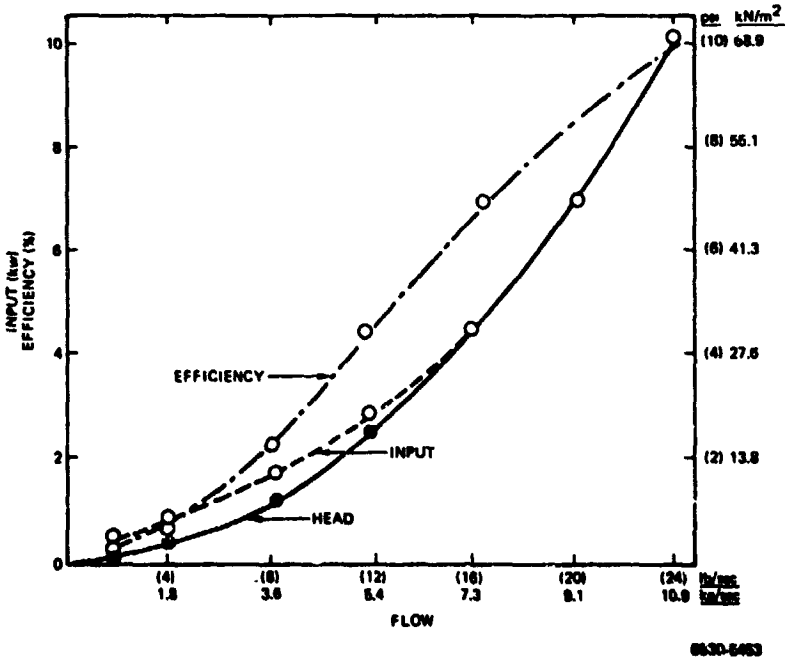

Figure 50. Head, Efficiency, and Input vs Flow for Dual Helical PLPA – Design No. 65 (Constant slip = 0.60)

STRAP THICKNESS \ STRAP WIDTH	cm 1.27 in. (0.50)	1.30 (0.511)	1.32 (0.521)	1.35 (0.531)
cm (in.)				
0.178 (0.070)				66*
0.203 (0.080)	85			67
0.299 (0.090)	84			68
0.241 (0.095)				69
0.254 (0.100)	83			70
0.279 (0.110)	74	73	72	71
0.305 (0.120)	75			
0.330 (0.130)	76			
0.356 (0.140)	77			
0.432 (0.170)	81			
0.483 (0.190)	82			
0.533 (0.210)	80			
0.635 (0.250)	78			
0.737 (0.290)	79			

*DESIGN NUMBERS

6530-5454

Figure 51. Design Matrix for Dual Helical PLPA

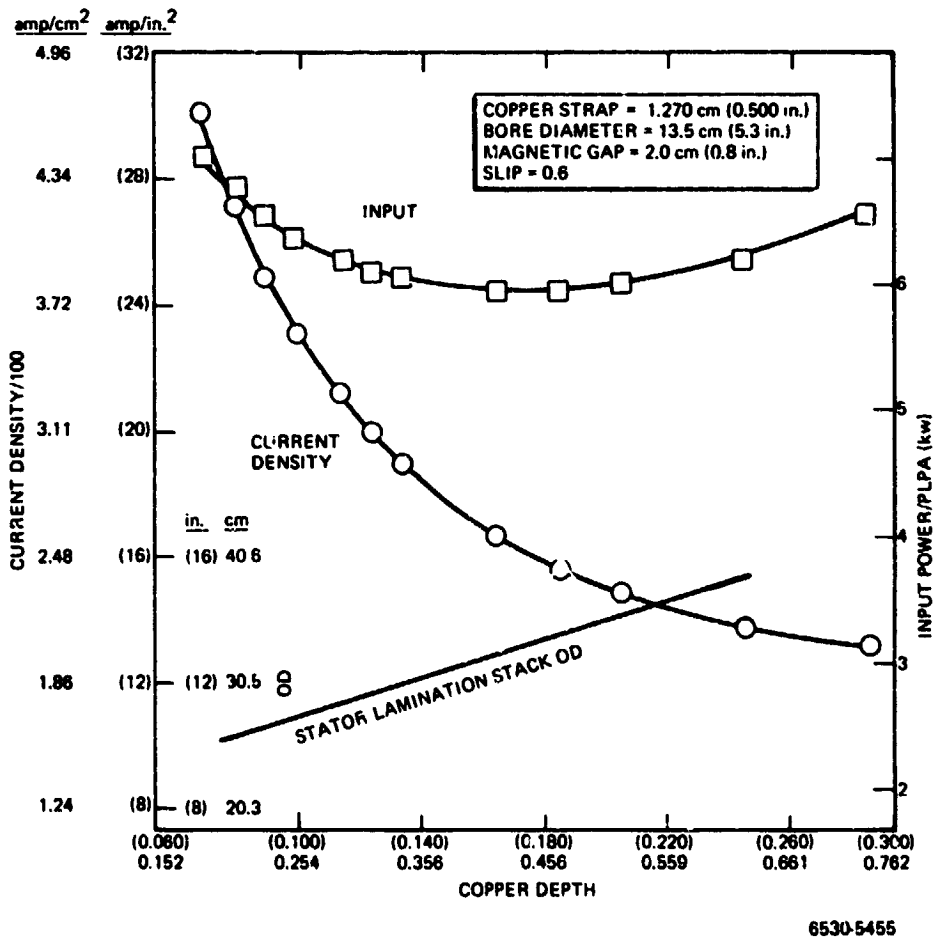

6530-5455

Figure 52. Variation of Pump Parameters With Copper Depth for Dual Helical PLPA

TABLE 14

ac DUAL HELICAL PLPA PARAMETERS - DESIGN NO. 74 (Y-Connected)

Design and Performance Summary	
Stack Length [cm (in.)]	25.4 (10)
Stator Bore Diameter [cm (in.)]	13.5 (5.3)
Stator OD [cm (in.)]	28.45 (11.2)
Magnetic Gap [cm (in.)]	20.0 (0.8)
Number of Poles	2
Number of Slots	18
Input Power/PLPA [kw]	6.6
NaK Flow Rate [kg/sec (lb/sec)]	9.1 (20)
NaK Head Rise [kN/m^2 (psi)]	48.3 (7)
Current [amps/phase/winding]	116
Line to Line Voltage [v]	43.4
Power Factor	0.37
Frequency [Hz]	46
PLPA Efficiency [%]	9.1
Slip	0.65

Startup Conditions (10% flow)	
Frequency [Hz]	46
Input Power/Winding [kw]	0.071
Power Factor	0.362
Current [amps/phase/winding]	42.6
Line to Line Voltage [v]	5.2

Figure 53.

Variation of Input Power With Slip for Dual Helical PLPA

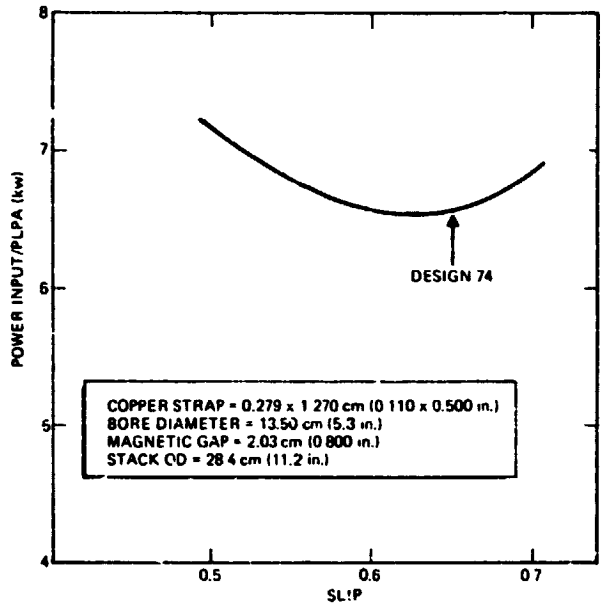

6530-5456

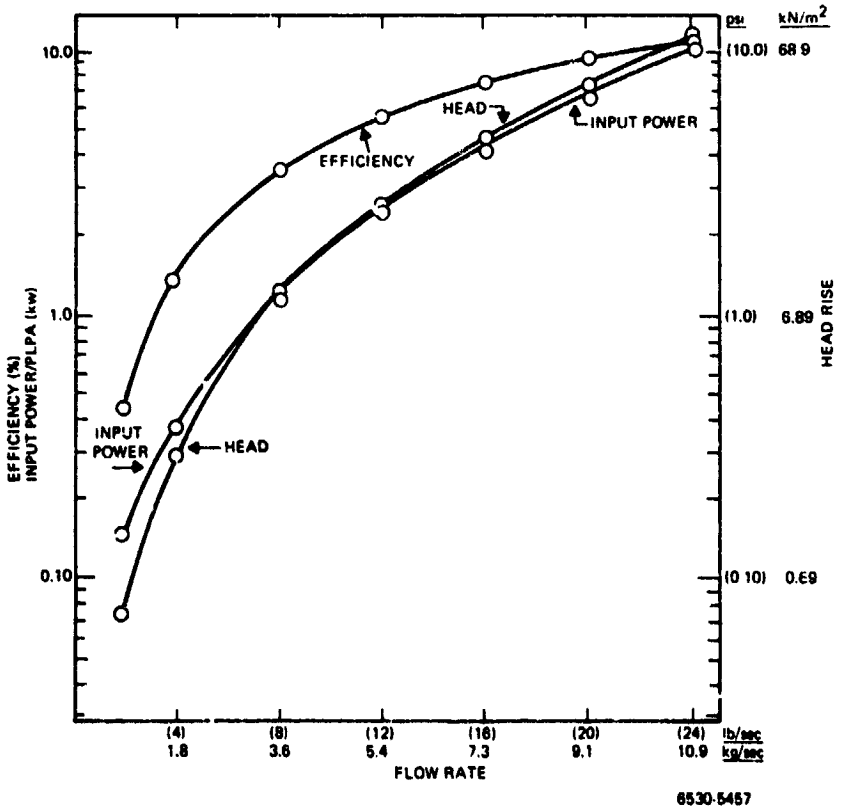

6530-5457

Figure 54.

Performance vs Flow Rate for Dual Helical PLPA [610°C (1130°F) NaK, 46 Hz]

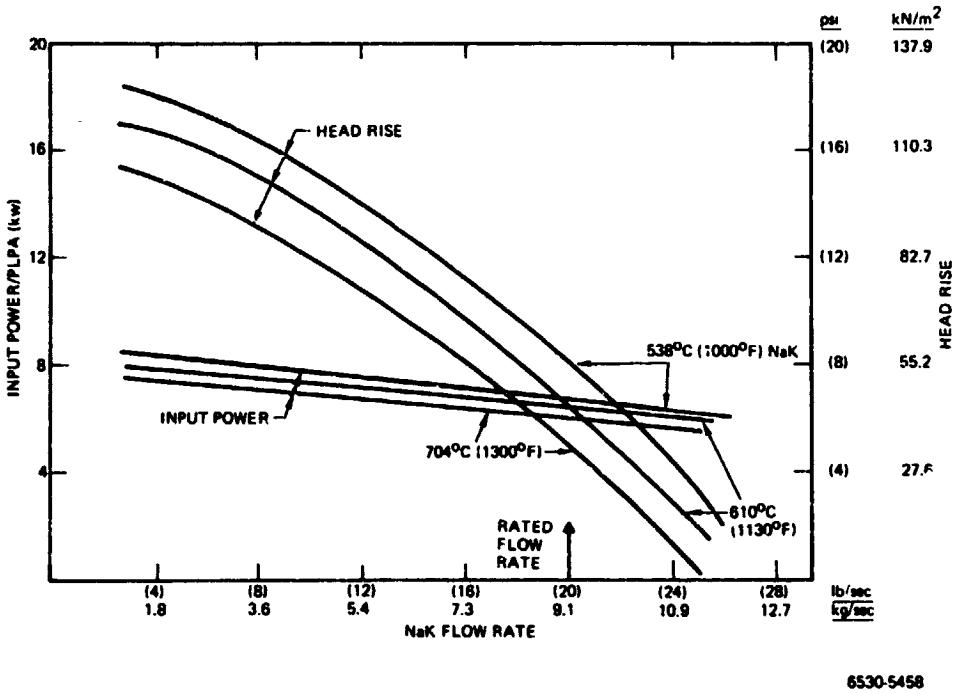

Figure 55. Input Power and Head vs Flow Rate and NaK Temperature at Constant Voltage for Dual Helical PLPA (Design No. 74, rated at 43.4 v and 46 Hz)

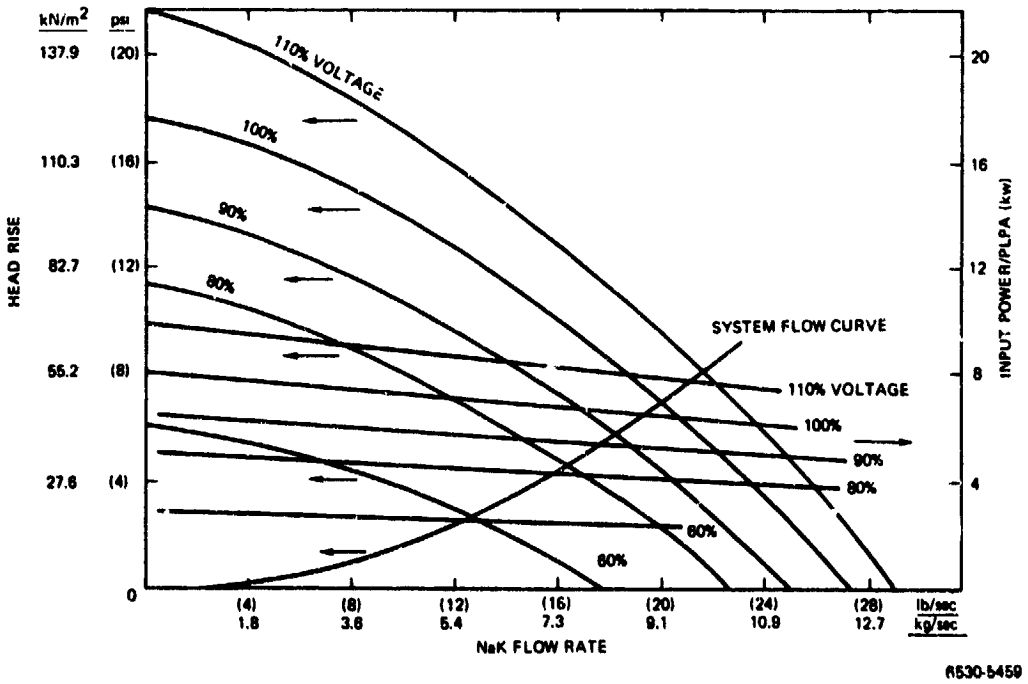

Figure 56. Head Rise vs Flow Rate for Dual Helical PLPA [Design No. 74, 610° C (1130° F) NaK rated at 43.4 v and 46 Hz]

1. Hydraulic Losses

The hydraulic loss of a flow circuit will depend upon the fluid characteristics, fluid velocity, and channel geometry. Calculation of total loss, therefore, requires separating the hydraulic circuit into elements having different geometries, and summating the loss of each element. Standard approaches, found in References 10 and 11, were used to calculate the losses.

The initial loss in the PLPA occurs in the guide vane and transition section, where the incoming axial velocity is changed in magnitude and direction to accommodate the flow of the fluid in the helix. This loss, as measured in meters of pumped head, was calculated from the expression:

$$h_1 = 0.04 \frac{V^2}{2g} \quad , \qquad \ldots(15)$$

where:

h_1 = head loss (m)

0.04 = empirically derived calculation constant

V = velocity of the exit fluid (m/sec)

2g = gravitational constant (m/sec^2)

This formula is of the form used for a trumpet inlet configuration, which approximates the guide vane and reducer loss. The loss in the helix, due to the small helix angle, can be approximated either by considering the helix as a length of pipe or as a coiled tube. Both approaches were applied. The "length of pipe" approach was used in the initial trend calculations (to be covered later), and the coiled tube calculations were used for the final detail evaluations of the PLPA.

The formula for the "length of pipe" loss is:

$$h_2 = \frac{f L V^2}{D2g} \quad , \qquad \ldots(16)$$

where:

h_2 = head loss (m of fluid)

f = friction factor

L = length of tube or pipe (m)

V = velocity in tube (m/sec)

D = equivalent diameter (m)

2g = gravitational constant (m/sec^2)

The value D is the equivalent diameter, based upon the geometric configuration of the fluid flow cross section, and is obtained from the hydraulic radius. The value f is obtained from a Moody diagram, which utilizes the Reynolds number and relative roughness to determine the friction factor.

The method developed for calculating hydraulic drop in coils, used to check the overall system after electrical sizing, is as follows:

$$\frac{L}{D} = R_t + (n - 1)\left[R_\ell + \frac{R_b}{2}\right] \quad , \qquad \ldots(17)$$

where:

L/D = equivalent length in diameter units

R_t = total resistances of one 90° bend in L/D units

n = equivalent number of 90° bends

R_ℓ = resistance due to length of a 90° bend

R_b = bend resistance of a 90° bend

Exit loss in the pump occurs as the guide vanes convert the fluid direction and velocity of the helix flow to the axial fluid direction as the fluid leaves the pump. This loss, as measured in meters of pumped fluid, was calculated as:

$$h_3 = \frac{0.20(V_1 - V_2)^2}{29} \quad , \qquad \ldots(18)$$

where:

h_3 = loss (m)

0.20 = an empirically derived constant

V_1 = incoming fluid velocity (m/sec)

V_2 = exit fluid velocity (m/sec)

29 = gravitational constant (m/sec^2)

The preceding formula is of the form applicable to a conical enlargement configuration which approximates the guide vane loss.

Various other straight runs and bend losses were determined by calculation methods based upon one or more of the preceding relationships.

Various sized tubing was considered for interconnecting the two pumps of the dual PLPA, and the results are shown in the following table:

Connecting Diameter	Hydraulic Loss in 2-Pump PLPA
2.54 cm (1 in.)	268.3 kN/m^2 (38.91 psi)
3.81 cm (1-1/2 in.)	54.4 kN/m^2 (7.89 psi)
5.08 cm (2 in.)	31.5 kN/m^2 (4.57 psi)
6.35 cm (2-1/2 in.)	27.5 kN/m^2 (3.99 psi)
7.62 cm (3 in.)	26.3 kN/m^2 (3.81 psi)

Based on the preceding results, a connecting tube with a diameter of 6.35 cm (2-1/2 in.) was selected for the reference design. The distribution of primary NaK hydraulic pressure losses are shown in Figure 57.

The losses shown for the helical sections were calculated, assuming that the passage was a continuous 720° bend of pipe. As with the linear pump, the highest losses occurred in the pump throats, where the NaK velocity was highest. Relative high losses also occurred in the 180° return pipe; but, as shown earlier, increasing its diameter to reduce the bend loss was offset by increased transition losses in the cone sections.

Based upon an auxiliary coolant circuit where both pumps are in series, two passages in parallel, and a 0.503 kg/sec (1.11 lb/sec) flow rate, coolant flow losses were calculated for various coolant tube diameters.

The resulting flow parameters were calculated for the auxiliary cooling coils:

Tube ID [cm (in.)]	1.75 (0.69)
Tube radius [cm (in.)]	15.24 (6)
Flow velocity [m/sec (ft/sec)]	1.189 (3.9)
Total equivalent length [m (ft)]	1.61 (5.3)
Total tube loss [m (ft)]	1.00 (3.27)
Total manifold entry and exit loss [m (ft)]	0.11 (0.333)
Total loss [kN/m^2 (psi)]	9.500 (1.38)

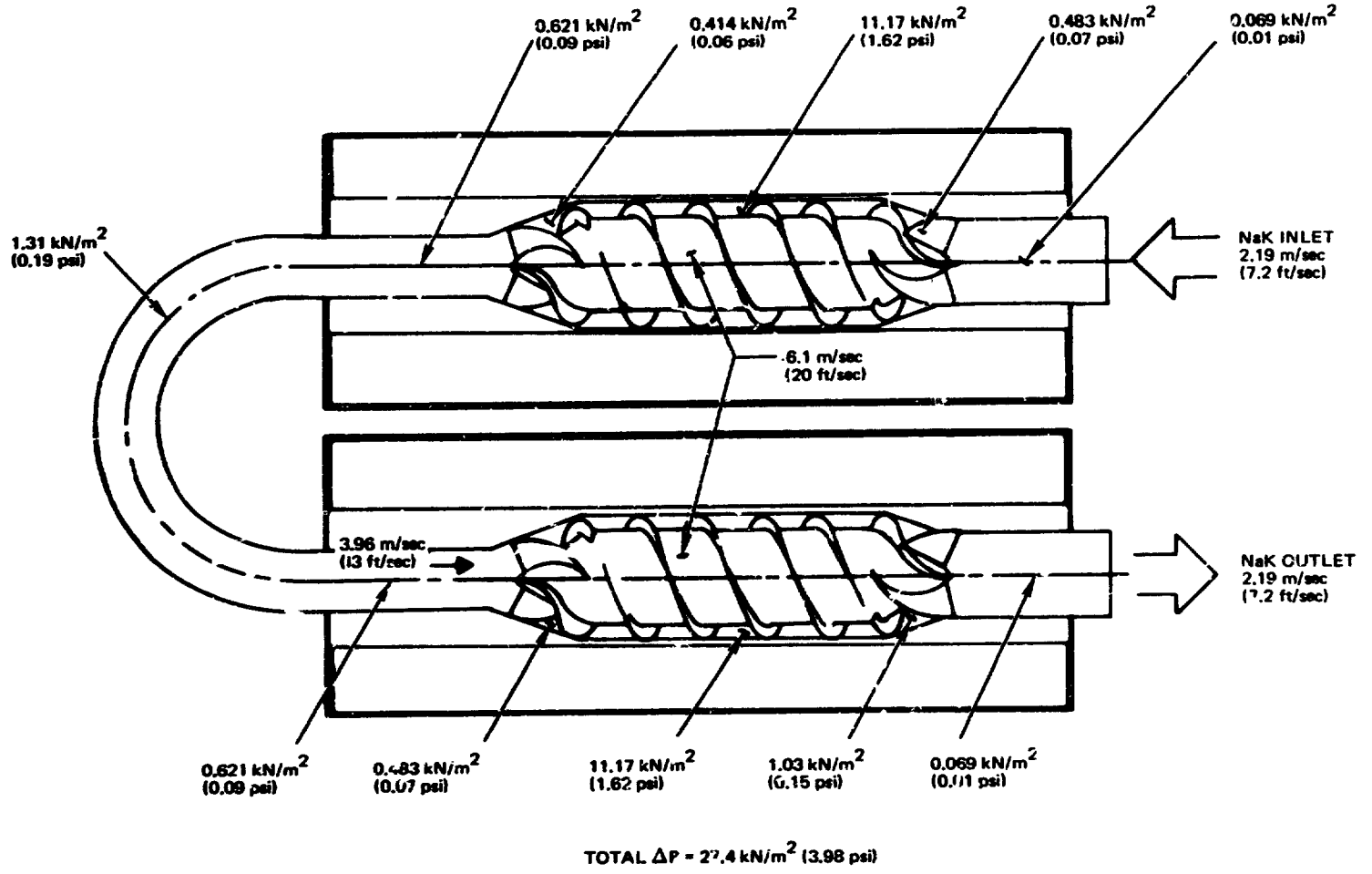

Figure 57. Hydraulic Pressure Loss – Helical Pump PLPA

2. Thermal Analysis

Thermal analysis was performed on earlier concepts and Design 74, to determine the expected temperatures of the windings and the major structural elements. Essentially, all of the heat generated in the pump electrical sections, and that leaking in from the 610° C (1130° F) NaK, must be rejected to the NaK coolant coils. The heat generated in the coils to be rejected must flow from the copper conductor, through the electrical insulation, to and through the lamination stack to the cooling coils.

In the slots, gaps will exist between the conductor and the insulation and between the insulation and the slot wall. A small, effective gap will exist between the lamination stack and the stator housing. Conversely, the heat flow from the hot NaK is inhibited by the thermal insulation and the gaps which will exist between the thermal insulation, the flow channel, the stator gas containment can, and the stator lamination stack. Heat transfer across each of the various gaps is a function of the actual contact area, the presence of a gas, or vacuum in the gap between the surfaces, and the emissivity and temperatures of the uncontacted area.[12-14] The actual contact area is a function of the physical properties of the contact material, the surface conditions and finish, the flatness of the material, and the contact pressure. In calculating the heat transfer across the gaps, a contact thermal conductance, shown schematically in Figure 58, was established for each of the various layers. In the schematic, heat flow would be evenly distributed at Stations a and f; while, in the area of the contacting surfaces, the conduction paths would be focused or concentrated. Typical temperature distribution along contacted and unattached areas are represented by Lines *l* and m, respectively. If there were a total metallurgical bond between the two parts, and the respective thermal conductivities, the line $T_a - T_x$ would be essentially a straight line. However, when the surfaces are in contact only at the higher asperities, there is a temperature drop, ΔT_c, across the joint. The contact thermal conductance, h_c, across the joint is then equivalent to the heat transfer per unit area divided by the temperature drop. The total heat flow across an interface can be represented by the following:

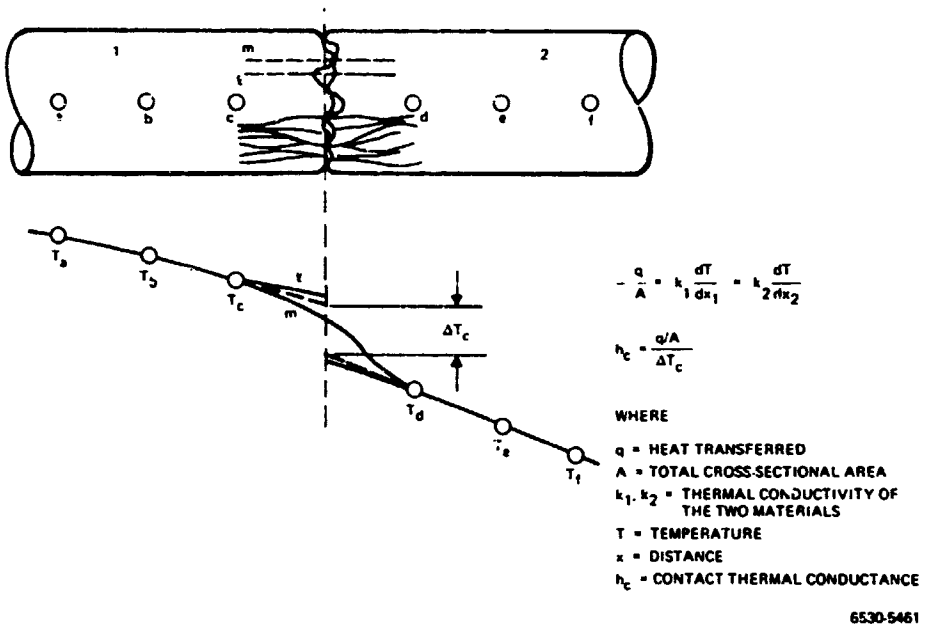

Figure 58. Temperature Distribution Through Surfaces in Contact

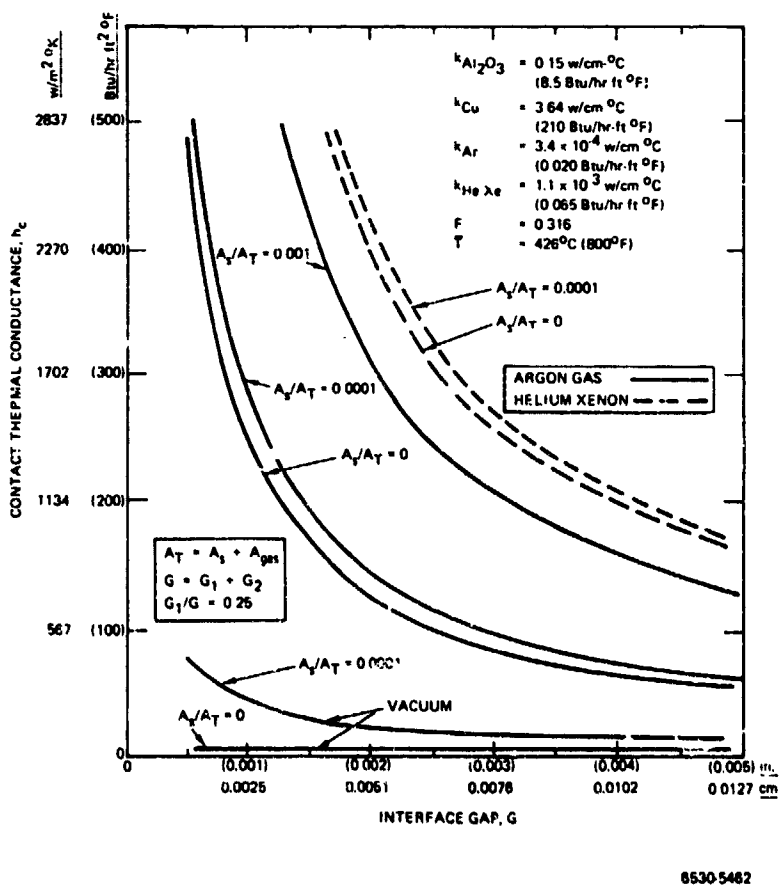

Figure 59. Thermal Conductance Across Interfaces

Total heat flow across interface:

$$Q_{1-2} = \left(\frac{A_s}{\frac{G_1}{k_1} + \frac{G_2}{k_2}} + \frac{k_{gas} A_{gas}}{G_1 + G_2} + 4\sigma A_{void} F_{1-2} \overline{T}^3 \right) (T_1 - T_2) \quad , \qquad \ldots(19)$$

where:

A_s = contact area

$A_{void} = A_{gas}$ = area taken up by gap

G_1 = average gap height of Material 1

G_2 = average gap height of Material 2

k_1 = thermal conductivity of Material 1

k_2 = thermal conductivity of Material 2

k_{gas} = thermal conductivity of gas in gap

σ = Stefan-Boltzmann Constant

$F_{1-2} = 1 / (1/\epsilon_1 + 1/\epsilon_2 - 1)$

where:

ϵ_1 = emissivity of Material 1

ϵ_2 = emissivity of Material 2

$\overline{T}$ = mean temperature of two materials

also:

$$Q_{1-2} = h_c A_T (T_1 - T_2) \quad . \qquad \ldots(20)$$

where: $A_T = A_s + A_{gas}$

Therefore:

$$h_c = \frac{A_s}{A_T} \left(\frac{1}{\frac{G_1}{k_1} + \frac{G_2}{k_2}} \right) + \frac{A_{gas}}{A_T} \left(\frac{k_{gas}}{G_1 + G_2} \right) + \frac{A_{void}}{A_T} \left(4\sigma F_{1-2} \overline{T}^3 \right) \quad . \qquad \ldots(21)$$

To increase thermal conductance across the gap, the area of contact must be increased by material deformation, or the gas gap reduced by higher mechanical loading. A plot of contact thermal conductance, as a function of gap height for various gas mixtures and contact area ratios, is shown in Figure 59. The

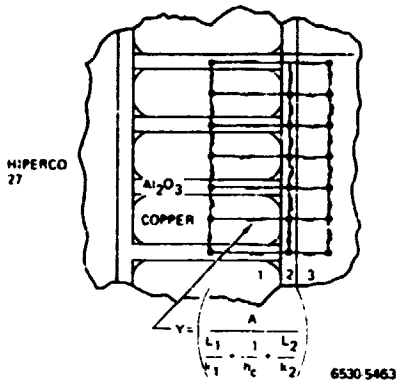

←Figure 60. Helical Pump Stator Slot Node Diagram — Design No. 74

Figure 61. Thermal Map—Helical Pump Slot With Argon Gas and Mica Thermal Insulation — Design No. 74

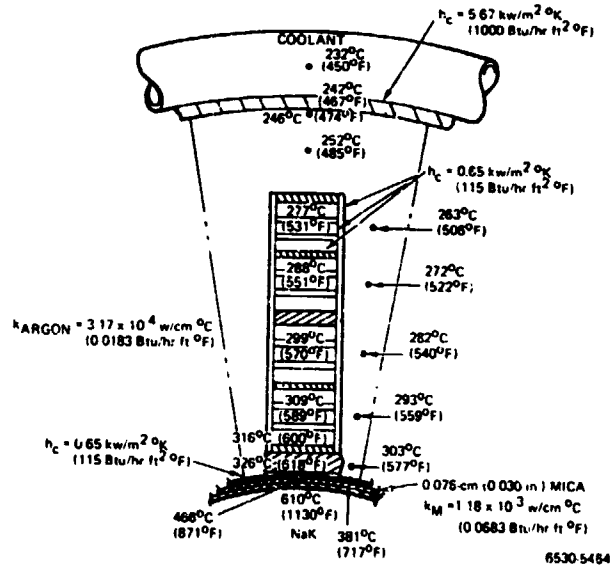

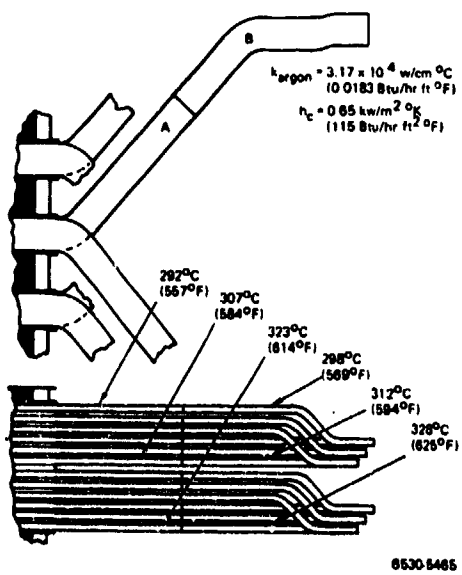

Figure 62. Thermal Map — Helical Pump End Turn With Argon Gas and Mica Thermal Insulation — Design No. 74 ←

bottom two curves are for evacuated gaps, and the thermal resistance is relatively high. The middle three curves are for argon-filled gaps, and it can be seen that increasing the ratio of contact area to total area from 0 to 0.001 more than doubles the thermal conductance. When the gaps are filled with a helium-xenon gas mixture, which has a thermal conductivity three times that of argon, the thermal conductance was raised by the same factor. Considering the manufacturing tolerances that would be used in the assembly of the electrical windings, a gap of 0.00635 cm (0.0025 in.) was assumed as being representative of the slot region. Contact thermal conductance of 5674 w/m^2-°K (1000 Btu/hr-ft^2-°F) was assumed for the interference fit between the stator start and outer gas containment wall.

Using appropriate values of gap parameters for the various gaps, and the material properties as listed in Appendix II, the pump thermal matrix was analyzed by the use of the thermal analyzer computer program (TAP code). A section of the matrix, as applied to the stator slot, is shown in Figure 60. Each path between each node is represented by an admittance term, Y, which is the reciprocal of the thermal resistance. Each node was assigned a heat generation rate and/or temperature. The logic of the TAP code follows.

The computer code applies the following finite-difference approximation equation to each of the nodes of the network for each time step or iteration:

$$T_{o,\theta+\Delta\theta} = T_{o,\theta} + \frac{\Delta\theta}{C_o}\left[Q + \sum(Y_i T_i) - \left(\sum Y_i\right) T_o\right] \quad , \qquad \ldots(22)$$

where:

C = capacitance of node

Q = heat generation rate of node

T = temperature of node

Y = admittance of a heat flow path

θ = time

Subscripts

σ = a node being iterated

θ = a value at time, θ

$\theta + \Delta\theta$ = a value at end of time step, $\Delta\theta$

o = designates the node which is being iterated at a given moment

i = designates a node connected to node o

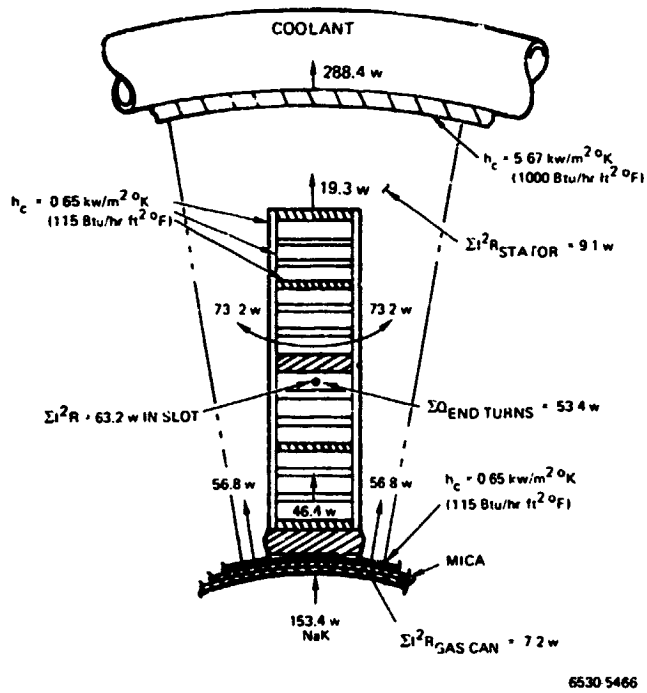

Figure 63. Heat Flow Map – Helical Pump Slot With Argon Gas and Mica Thermal Insulation – Design No. 74

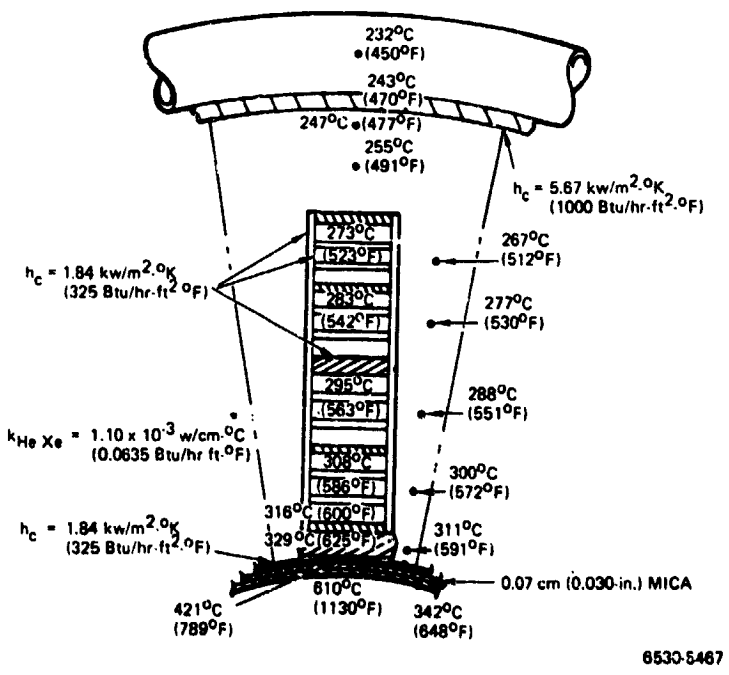

Figure 64. Effect of High Thermal Conductivity Gas on Helical Pump Slot Temperatures – Design No. 74

The finite-difference equation for iteration of zero-capacitance node is:

$$T_{o,\theta+\Delta\theta} = \frac{Q + \sum(Y_i T_i)}{\sum Y_i} \quad . \qquad \ldots(23)$$

The first case for the helical pump was run using argon cover gas and mica thermal insulation, and the results are shown in the steady-state temperature map, Figure 61. Using the thermal contact conductances and conductivities shown, the maximum copper temperature 316°C (600°F) occurred in the bar closest to the hot NaK duct. Temperatures in the stator iron ran ~17°C (30°F) lower than in the adjacent copper.

The hot-spot temperature of the winding occurred at the end turn of the bottom copper bar, Figure 62, and was ~14°C (25°F) higher than in the slot copper. This is because the primary heat transfer path is through the laminated Hiperco stack to the cooling coils. The end turns, being covered by layers of glass insulation tape and each other, have little chance of rejecting their heat by radiation or conduction directly to the cooling coils. No credit was taken for gas convection cooling which would contribute a heat transfer path during ground testing.

A heat flow map of the stator slot, Figure 63, shows that most of the heat is conducted laterally from the copper into the laminations, and then radially to the cooling coils. Nearly as much heat is conducted from the end turns into the slot as is generated in the slot. Approximately half the total heat being rejected to the cooling coils is coming from the hot NaK duct.

All of these temperatures are sufficiently low that no degradation of the materials was anticipated; however, a series of runs were made to determine the sensitivities of the temperatures to gap conductivities and thermal insulation effectiveness.

Substitution of a helium-xenon gas mixture, molecular weight of 40, for argon in the stator can had no appreciable change on the temperatures (Figure 64). Although the gas mixture had a thermal conductivity of nearly three times that of the argon, and increased the heat transfer across the gaps, it also allowed more heat to flow into the winding from the NaK duct. The net effect was a slight reduction in temperatures near cooling coils. This result might have been different, if a more effective thermal insulation were used between the

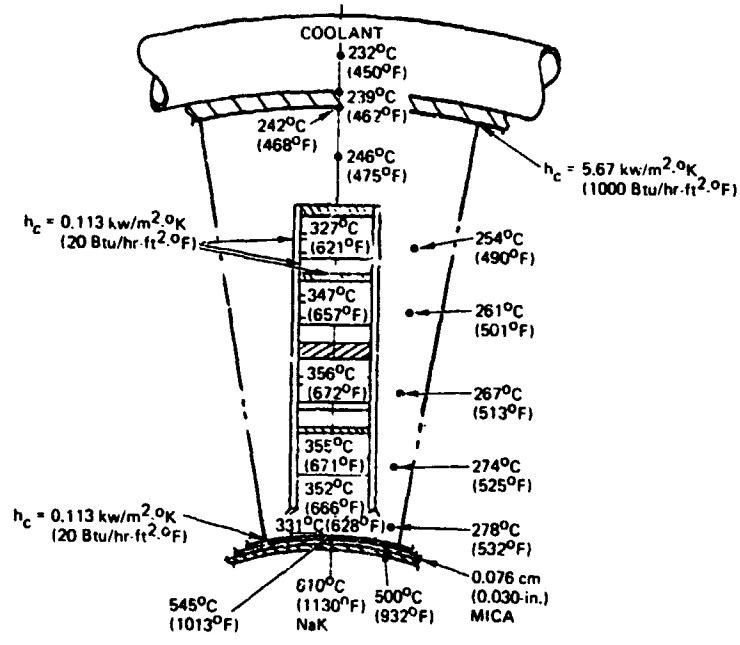

Figure 65. Effect of Vacuum on Helical Pump Slot Temperatures -- Design No. 74

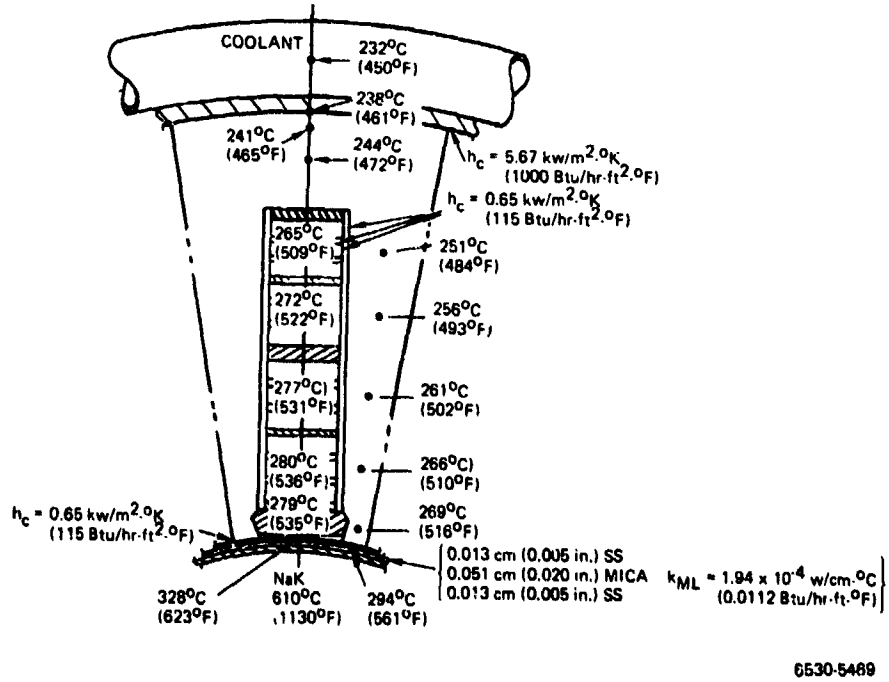

Figure 66. Effect of Multi-Layer Thermal Insulation on Helical Pump Slot Temperatures -- Design No. 74 With Argon Gas

NaK duct and stator gas can. No problem was anticipated with corona discharge with the helium gas, based upon Reference 15.

The effect of cover gas loss on slot temperatures is shown in Figure 65. Temperatures are between 39 and 50°C (70 and 90°F) higher than with argon in the gaps, but are still well within the capabilities of the materials.

When a more effective three-layer composite insulation system is used in place of the solid mica, the hot-spot temperatures are dropped nearly 33°C (60°F) (Figure 66). During detail design, an even more effective insulation system was planned, which would reduce temperatures even further.

A summary of the thermal analysis is shown in Table 15. The hot-spot temperatures were consistently in the end turns, which were 6 to 11°C (10 to 20°F) higher than the slot copper. All of the temperatures shown were well within materials capabilities, but temperatures would be further reduced with super thermal insulation and higher conductivity gases. The stator can temperature shown was used in the stress analysis.

3. Stress Analysis

It was decided, early in the preliminary design phase, to design the pump duct to meet the intent of Section III, Class I, of the ASME Boiler and Pressure Code, applying the high-temperature case criteria. Section VIII of the Code was applied to the gas containment elements and structural members. Because of the conservatism built into the Code, a design margin of 0 represents a high-integrity design. The applied loads on the various pump members and the allowable stresses will vary, depending on the particular mode of PLPA operation [i.e., vacuum operation with 610°C (1130°F) NaK, ground test NaK fill and drain, short-term operation at 649°C (1200°F) NaK]. The loadings on the various parts for these conditions are shown in Figures 67a, b, and c, and the stresses resulting from these loads at steady-state temperature conditions were analyzed. Standard formulas, found in the preceding codes and in References 16 and 17, were used to calculate stress levels and design margins.

Positive design margins were achieved in the elastic range for the primary NaK pressure boundary, Figure 68. The stress levels shown for the return pipe, Figure 69, indicated that additional flexibility would have to be achieved in the

TABLE 15

HELICAL PUMP THERMAL ANALYSIS SUMMARY – DESIGN No. 74

Case No.	Thermal Insulation*	Contact Coefficient [kw/m^2-°K (Btu/hr-ft^2-°F)]		Gas in Can	Peak Temperatures [°C (°F)]			
					Windings		Stator Can	
		Slot	Stator Can – Teeth Interface		Slot	End Turns	Below Slot	Below Teeth
1	Mica 0.076 cm (0.030 in.)	0.65 (115)	0.65 (115)	Argon	316 (600)	329 (625)	466 (871)	381 (717)
2	Mica 0.076 cm (0.030 in.)	1.84 (325)	1.84 (325)	He-Xe	316 (600)	324 (616)	421 (789)	342 (648)
3	Mica 0.076 cm (0.030 in.)	0.11 (20)	0.11 (20)	Vacuum	357 (675)	383 (721)	545 (1013)	500 (932)
4	Mica-SS Foil 0.076 cm (0.030 in.)	0.65 (115)	0.65 (115)	Argon	280 (536)	304 (580)	328 (623)	294 (561)

*Mica Thermal Conductivity = 1.18×10^{-3} w/cm-°C (0.0683 Btu/hr-ft-°F)
SS-Mica Sandwich Thermal Conductivity = 1.19×10^{-4} w/cm-°C (0.0112 Btu/hr-ft-°F)

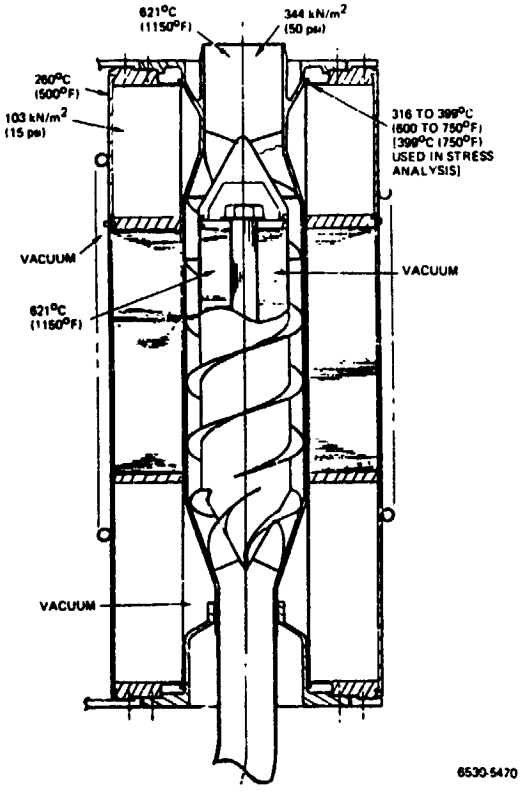

a. Continuous Operation

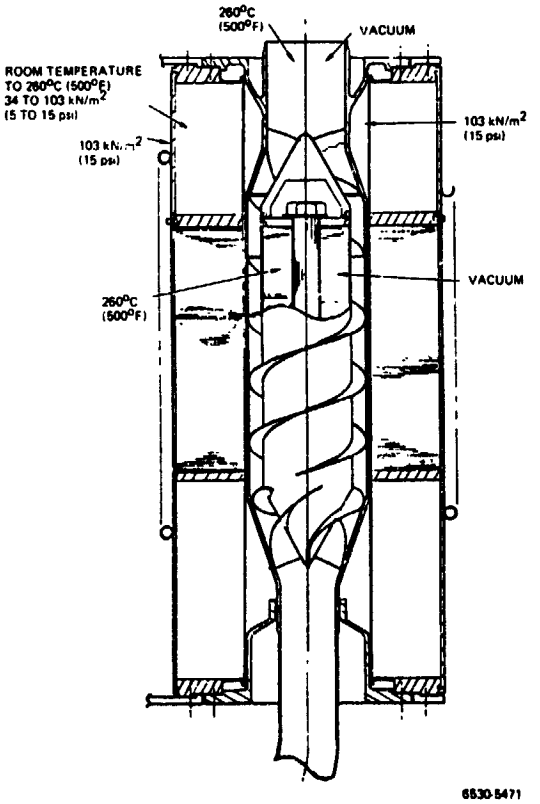

b. NaK Fill and Drain

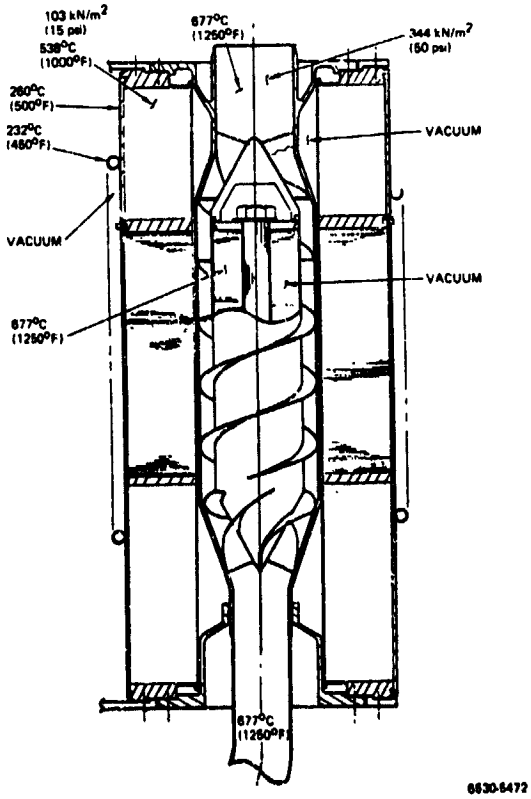

c. Short-Term Operation (100 hr)

Figure 67. Helical Pump Temperatures and Pressures

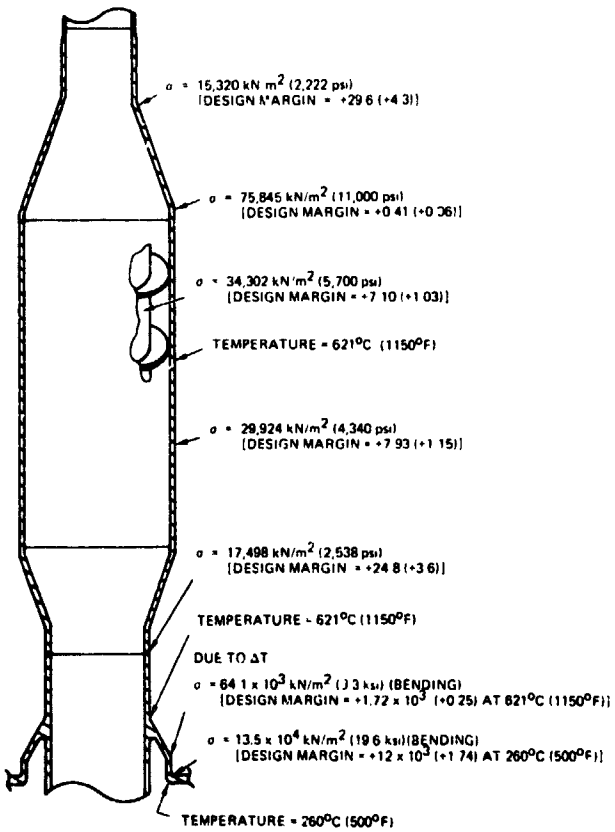

6530-5473

← Figure 68. Helical Pump Duct and Throat Design Margins

Figure 69. Helical Pump Duct Loop Design Stress →

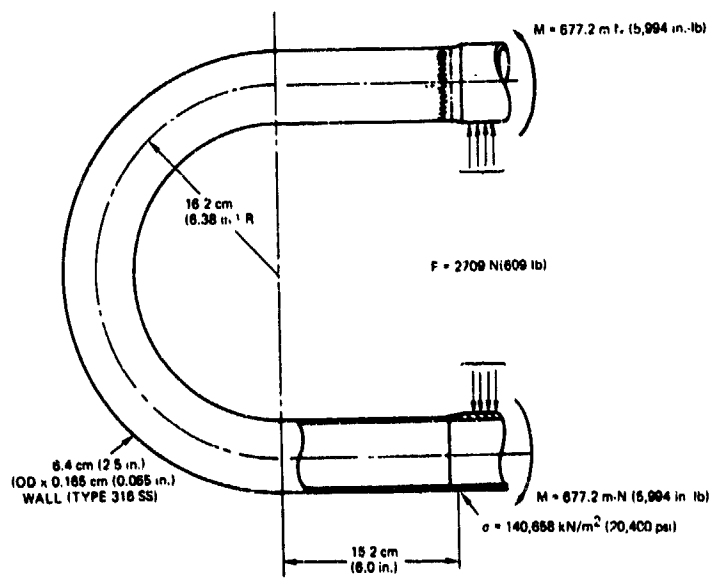

BASED UPON COMPUTER PROGRAM MEC – 21/7094
[LOOP AT 621°C (1150°F),
PLPA SUPPORT AT 260°C (500°F)]

6530-5474

loop, and/or a plastic analysis would have to be conducted. Figure 70 shows that the sliding duct support is rigid enough to prevent movement of the NaK duct in the stator bore; <0.0025 cm (0.001 in.) deflection would occur for the calculated loads.

The most difficult stress problem occurred in the thin inner gas can and its deflection diaphragm, Figure 71. The inner gas can must be kept as thin as possible, since it occupies the magnetic gap and can contribute to the electrical losses. Since the inner gas can operates 139° C (250° F) hotter than the outer can, some means of accommodating the differential thermal expansion must be provided. In the particular design, this was achieved by the use of a flexing diaphragm. The stress shown indicates that a plastic analysis would have to be conducted, to ascertain whether the design meets code. Another possibility was the use of alternate materials for certain structural members.

The effect of launch loads on the support structure is shown in Figure 72. All of the stresses shown are well below the yield strength of the Type 316 stainless steel frame or A-286 super alloy bolts, and no problem is anticipated in this area.

4. Dual Helical PLPA Design Features

The general design details of the final configuration, at the end of the preliminary design phase, are shown as Figures 73, 74, and 75.

A tie bolt is shown holding the center section laminations under compression. The washer at the bolt head is a close fit to the bolt, and welded to the conical flow guide section. The other end of the bolt is in a sliding guide, which allows for differential thermal growth between the washer and the NaK duct. A similar approach is used on the whole center body, in that the transition swirl vanes were welded only at one end to the outer transition cone. A sweat fit between the helix and outer NaK duct was not used, since it complicated designing to the codes. The entrance and exit pipes to the PLPA were welded to the end bells, while the other U-shaped loop was allowed to float. The inner duct and outer duct are supported without any reliance on the thermal insulation to carry the load. The end bells are welded to the stator shell which locates the stator and its bore, maintaining excellent control of the magnetic gap, which contains the

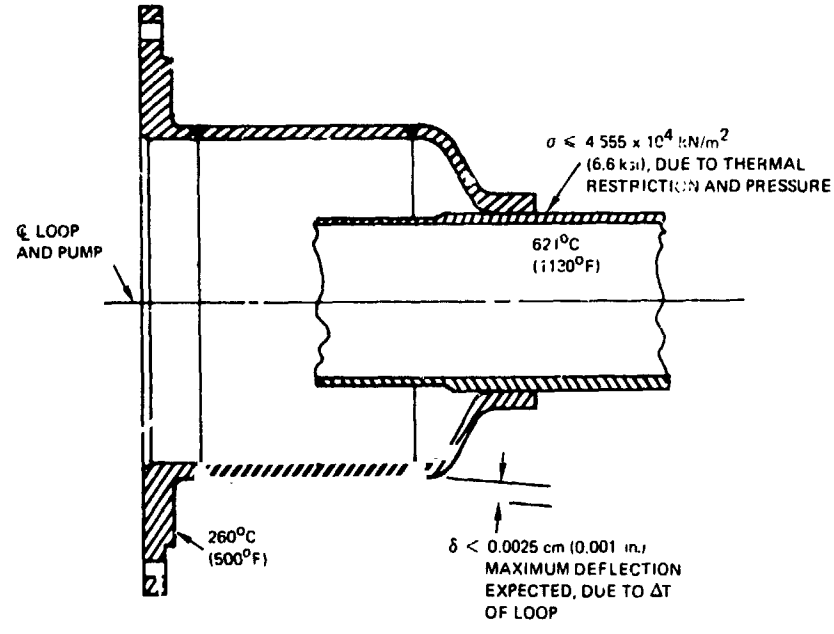

Figure 70. Helical Pump Duct Sliding Support

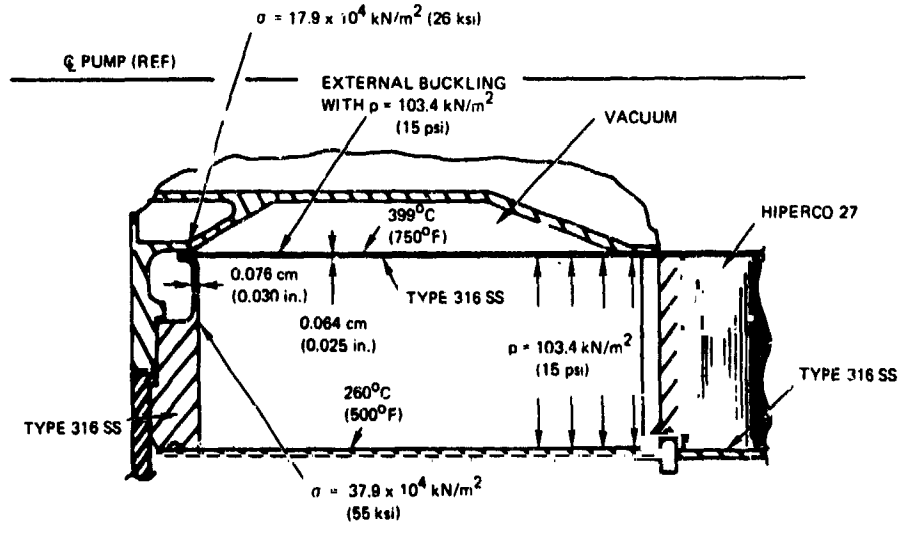

Figure 71. Helical Pump Gas Containment Can Design Stress

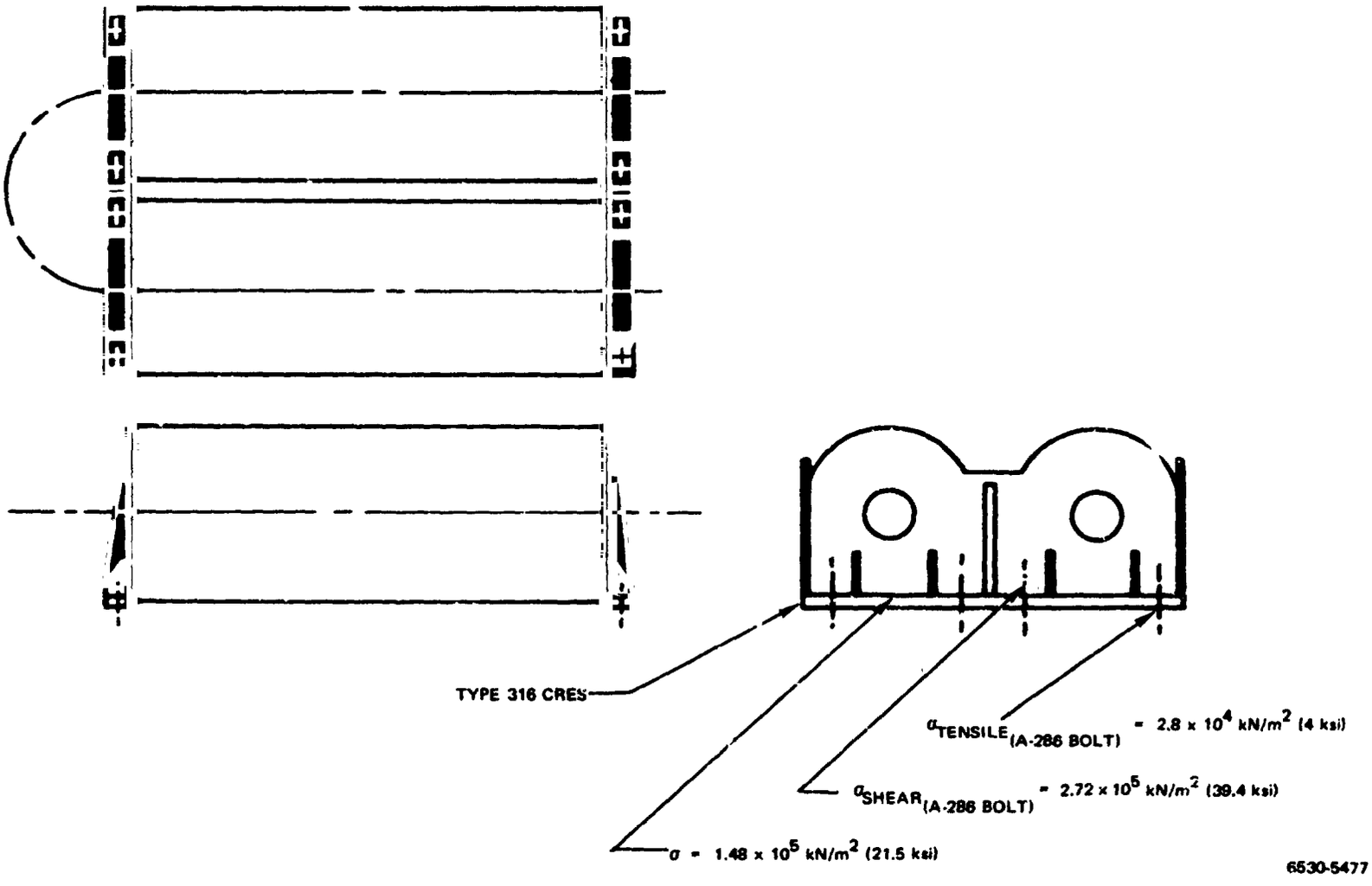

Figure 72. Effect of Room-Temperature Launch Loads on Helical Pump Support Bracket

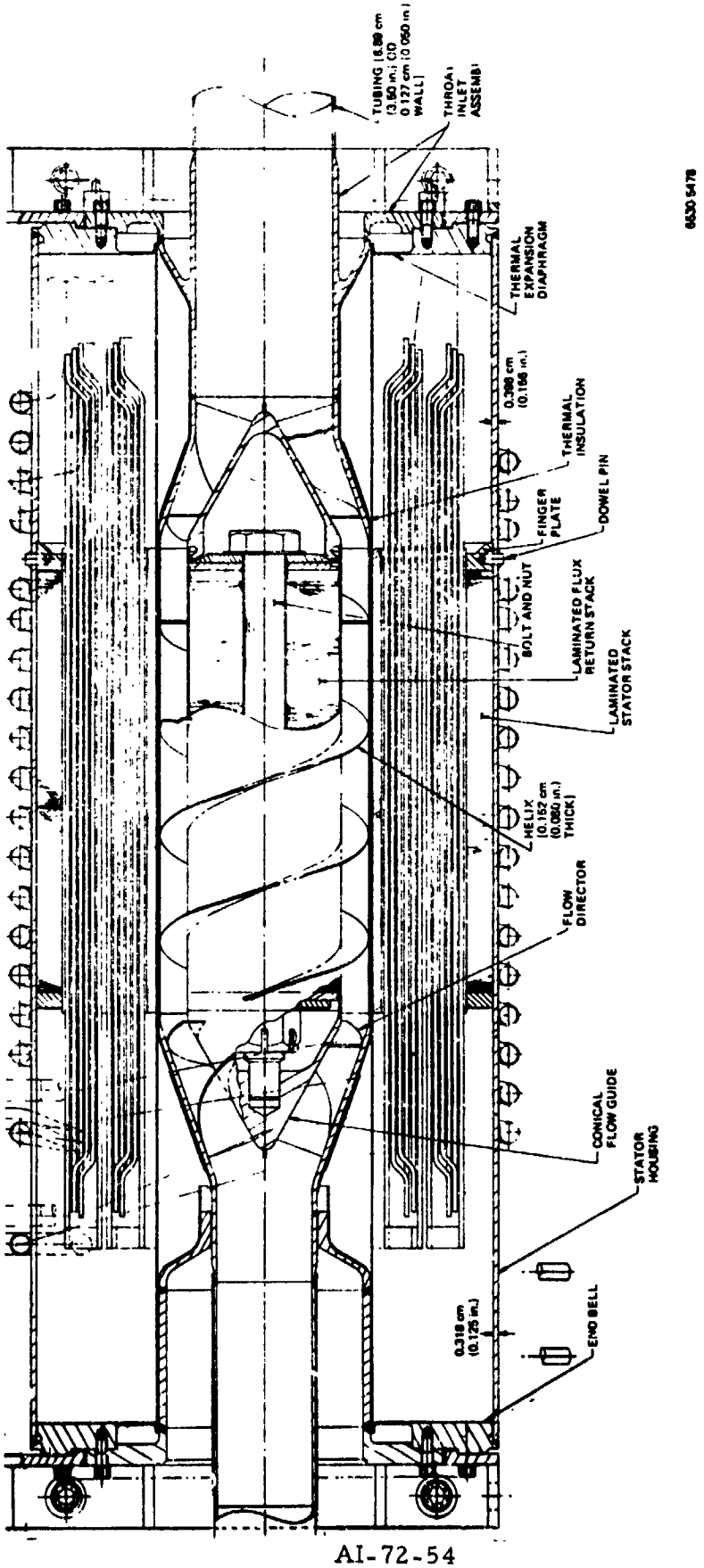

Figure 73. Plan View of Helical Pump (Dwg. N530310004)

AI-72-54

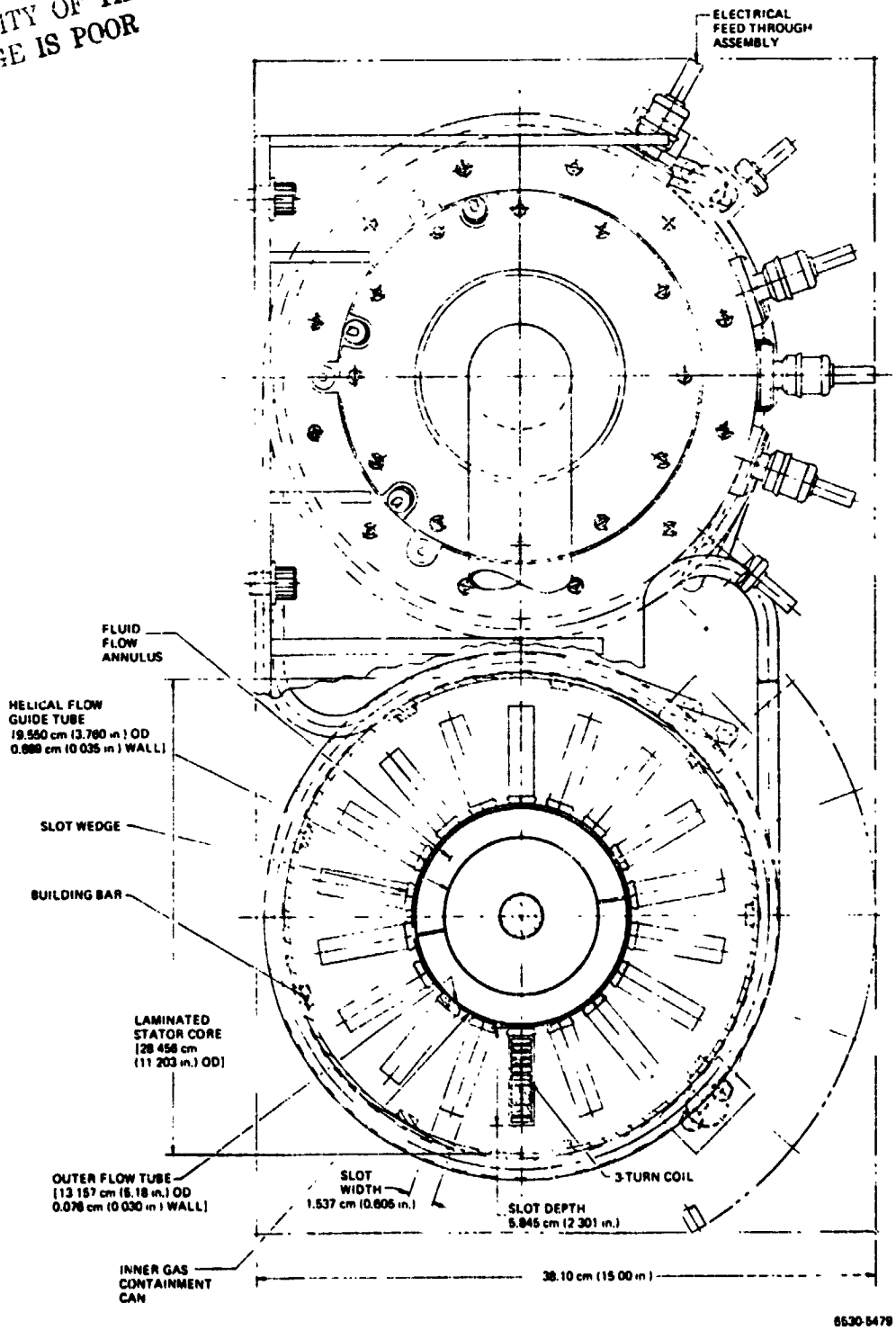

Figure 74. End View of Helical Pump (Dwg. N530310004)

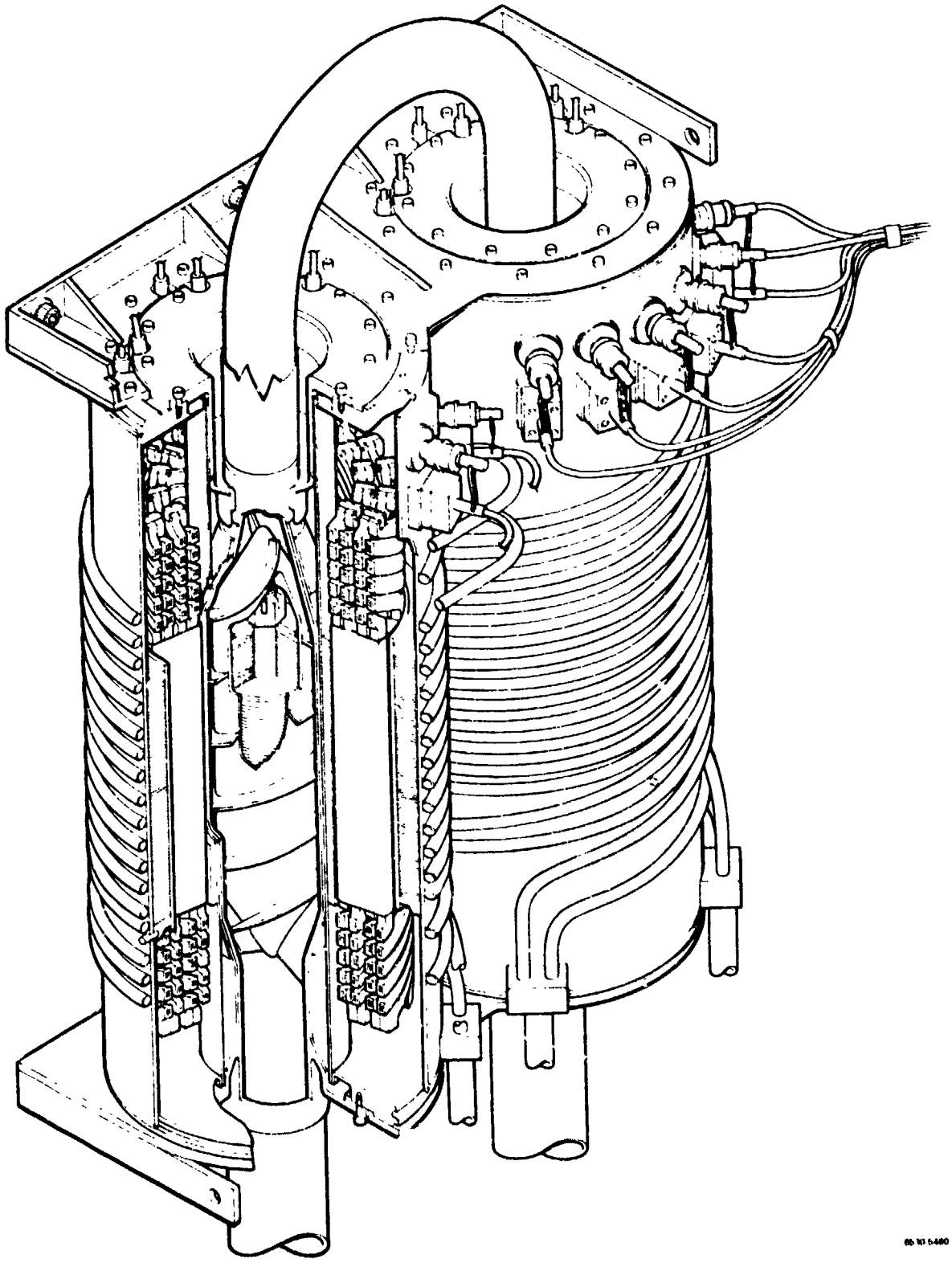

Figure 75. Cutaway Isometric of Dual Helical PLPA

gas can and thermal insulation. The thermal insulation in the helical section is manufactured as a cylinder, and mounted on the duct by attachment at the conical sections. Additional thermal insulation covers the remaining pipe and conical section.

TABLE 16

PLPA COMPARISON

Characteristics	2-Pump ac Helical PLPA No. 74, 25.4-cm (10-in.) Stack Length, 28.4-cm (11.2-in.) Stack Diameter	2-Pump ac Linear PLPA No. 66 15-cm (6-in.) Stack Width, 62.2-cm (24.5-in.) Stack Height
Efficiency/PLPA [%]	9.1	7.0
Pump Envelope [cm (in.)]	83.8 x 38.1 (33.0 x 15.0)	102.9 x 52.1 x 34.3 (40.5 x 20.5 x 13.5)
PLPA Envelope [cm (in.)]	102.6 x 70.6 x 38.1 (40.4 x 27.8 x 15.0)	143.0 x 105.4 x 34.3 (56.3 x 41.5 x 13.5)
PLPA Weight [kg (lb)]	399 (880)	630 (1390)
Some-Flow 5-year Reliability	0.998	0.997
Full-Flow 5-year Reliability	0.989	0.989
Maximum Winding Temperature [°C (°F)]	329 (625)	394 (742)
Design Predictability	Good	Fair
Fabrication Difficulty		
Windings	More Difficult	Simple
Laminations	Conventional	More Difficult
Duct	Moderate	Difficult

VI. ac PUMP SUMMARY COMPARISON

Upon completion of the preliminary design phase, a new comparison of the dual ac linear and helical PLPA's was made (see Table 16). The helical pump approach was shown to be superior in every regard to the linear PLPA. The efficiency of the helical pump had increased to 9.1% as the study progressed, due to lower hydraulic losses and lower winding temperatures than originally anticipated. On the other hand, the linear pump, for the reverse of these reasons, exhibited a lower efficiency (7.0%) at the end of the study. Volume of the helical PLPA was ~50% of that of the linear PLPA, and weighed 227 kg (500 lb) less. Estimated reliabilities of the two approaches were approximately equal; however, the hot spot temperature of the helical pump was calculated to be 65°C (117°F) lower. This lower temperature would increase the PLPA's chance of surviving any reduction of coolant flow, etc., and is definitely a desirable feature. Design predictability of the helical pump was considered good, since it was based primarily on standard electrical machine design techniques. The linear pump design, on the other hand, required the extrapolation of performance data from larger, non-flight-type EM pump tests. The assumptions required in the extrapolations tended to increase the development risk of the linear pump. Fabrication process development was considered approximately equal for the two approaches. Based upon the preceding comparisons, it was concluded that the best EM pump option to satisfy the PLPA requirements was the ac helical induction approach.

REFERENCES

1. D. C. Guentert and R. L. Johnsen, "Study of Brayton Cycle Power Generating System Using SNAP-8 Nuclear Reactor as an Energy Source," NASA TN-D-5751 (April 1970)

2. P. T. Kerwin, "Design Point Characteristics of a 15 to 80 Kwe Nuclear-Reactor Brayton Power System," NASA TMX-67811 (August 1971)

3. D. C. Guentert and R. L. Johnsen, "Predicted Performance of a 15-80 Kwe Reactor Brayton Power System over a Range of Operating Conditions," NASA TMX-67833 (August 1971)

4. P. E. Kueser et al., "Magnetic Materials Topical Report," NASA-CR-54091 (September 1964)

5. P. E. Kueser et al., "Electrical Conductor and Electrical Insulation Materials Topical Report," NASA-CR-54092 (October 1964)

6. N. F. Davies, "Developmental Irradiation Test of SNAP-8 Electrical Components (HF-8)," NAA-SR-11924 (July 16, 1966)

7. N. F. Davies, W. J. Kurzeka, and M. Warren, "Irradiation Test of SNAP Actuators, Position Sensors, and Limit Switches," NAA-SR-12042 (November 15, 1966)

8. O. J. Foust, Liquid Metals Handbook, Sodium and NaK Supplement, (U.S. Atomic Energy Commission, June 30, 1967)

9. Personal communication with J. P. Couch, NASA PLPA Project Manager

10. D. S. Ellis, Elements of Hydraulic Engineering (D. Van Nostrand, Inc., New York, 1947)

11. "Flow of Fluid Through Valves, Fittings, and Pipe," Technical Paper 410, Crane Co., Chicago (1957)

12. W. M. Rohsenow, Ed., Developments in Heat Transfer (MIT Press, Cambridge, Mass., 1964)

13. A. W. Brunot and F. F. Buckland, "Thermal Contact Resistance of Laminated and Mechanical Joints," Trans. ASME (April 1949)

14. M. Barzelay, K. N. Tong, and G. Hullo, "Thermal Conductance in Aircraft Joints," NASA Technical Note 3167 (1951)

15. G. Bollenbacker and E. Kempke, "Corona Inception Voltage in Statorettes With Various Gas-Solid Dielectric Systems," NASA TMX-2474 (January 1972)

16. R. J. Roark, Formulas for Stress and Strain (McGraw Hill Book Co., New York, N. Y., 1965

17. W. Griffel, Handbook of Formulas for Stress and Strain (F. Ungar Publishing Co., New York, N. Y., 1966)

APPENDIX I
RELIABILITY EQUATIONS

The reliability evaluation of the various pumping concepts required setting up equations which represented the failure of the different components. These equations are shown in the following sections.

A. HELICAL PUMP – DUAL PLPA – DOUBLE WINDING = 100% DEVELOPED PRESSURE RISE REQUIRED IN EACH PUMP

Probability of flow = [probability of 100% capacity + probability of 1 good winding in each pump and gas containment (can) good in both + probability of 1 good winding only in either pump and the proper can good] (probability 1 of 2 cooling coils being good) (probability throats are good)

$$P(\text{flow}) = \left[\left(2R_w^2 R_g - R_w^4 R_g^2\right) + \left(4R_w^2 - 8R_w^3 + 4R_w^4\right) R_g^2 + 4R_g\left(R_w - R_w^2\right)\left(2 - 2R_w + R_w^2 - R_g\right)\right]\left[R_T^2\left(2R_c - R_c^2\right)\right] \quad , \quad \ldots(A\text{-}1)$$

$$P(100\%) = \left(2R_w^2 R_g - R_w^4 R_g^2\right) R_T^2\left(2R_c - R_c^2\right) \quad , \quad \ldots(A\text{-}2)$$

where:

$P(\text{flow})$ = probability of some flow

$P(100\%)$ = probability of 100% flow

R_w = winding reliability = $\exp(-\lambda_w t)$

R_g = gas containment reliability = $\exp(-\lambda_g t)$

R_T = throat reliability = $\exp(-\lambda_T t)$

R_c = cooling coil reliability = $\exp(-\lambda_c t)$

λ = failure rate

t = time period

If gas containment is not critical (i.e., loss of gas does <u>not</u> cause pump failure), then Equations A-1 and A-2 become:

$$P\,(\text{flow}) = \left[\left(2R_w^2 - R_w^4\right) + \left(4R_w^2 - 8R_w^3 + 4R_w^4\right) + 4\left(R_w - R_w^2\right)\left(1 - 2R_w + R_w^2\right)\right]\left[R_T^2\left(2R_c - R_c^2\right)\right] \quad , \qquad \ldots(A\text{-}3)$$

$$P\,(100\%) = \left(2R_w^2 - R_w^4\right)\left[R_T^2\left(2R_c - R_c^2\right)\right] \quad . \qquad \ldots(A\text{-}4)$$

B. HELICAL PUMP – TRIPLE PLPA – SINGLE WINDINGS – 50% DEVELOPED PRESSURE RISE REQUIRED IN EACH PUMP

Probability of flow = (probability of 1 of 3 units operating) (probability of good throats) (probability of 1 of 2 cooling coils being good)

where:

R_p = pump reliability = $R_w R_g$

$Q_p = 1 - R_p = 1 - R_w R_g$

$$P\,(\text{flow}) = \left(R_p^3 + 3R_p^2 Q_p + 3R_p Q_p^2\right)\left[R_T^3\left(2R_c - R_c^2\right)\right]$$

$$= \left(R_p^3 + 3R_p - 3R_p^2\right)R_T^3\left(2R_c - R_c^2\right)$$

$$= \left(R_w^3 R_g^3 + 3R_w R_g - 3R_w^2 R_g^2\right)R_T^3\left(2R_c - R_c^2\right) \quad . \qquad \ldots(A\text{-}5)$$

$P\,(100\%)$ = probability of 2 of 3 units operating

$$= \left(R_p^3 + 3R_p^2 Q_p\right)R_T^3\left(2R_c - R_c^2\right) = \left(3R_p^2 - 2R_p^3\right)R_T^3\left(2R_c - R_c^2\right)$$

$$= \left(3R_w^2 R_g^2 - 2R_w^3 R_g^3\right)R_T^3\left(2R_c - R_c^2\right) \quad . \qquad \ldots(A\text{-}6)$$

Assuming gas containment loss does <u>not</u> fail pump, Equations A-5 and A-6 are:

$$P\,(\text{flow}) = \left(R_w^3 + 3R_w - 3R_w^2\right)R_T^3\left(2R_c - R_c^2\right) \quad , \qquad \ldots(A\text{-}7)$$

$$P\,(100\%) = \left(3R_w^2 - 2R_w^3\right)R_T^3\left(2R_c - R_c^2\right) \quad . \qquad \ldots(A\text{-}8)$$

C. LINEAR PUMP – DUAL PLPA – SINGLE CAN – 100% DEVELOPED PRESSURE RISE IN EACH PUMP

Probability of flow = (probability of 100% + probability of 1 winding in each pump good and cans good) (probability of 2 good throats) (probability of 1 of 2 cooling coils good)

where:

$$R_p = R_w^2 R_g$$

$$Q_p = 1 - R_w^2 R_g$$

$$P(\text{flow}) = \left[\left(2R_w^2 R_g - R_w^4 R_g^2\right) + \left(4R_w^2 - 8R_w^3 + 4R_w^4\right)R_g^2 + 4R_g\left(R_w - R_w^2\right)\left(2 - 2R_w + R_w^2 - R_g\right)\right]\left[R_T^2\left(2R_c - R_c^2\right)\right] \quad . \quad \ldots(A\text{-}9)$$

$$P(100\%) = \left(2R_w^2 R_g - R_w^4 R_g^2\right)R_T^2\left(2R_c - R_c^2\right) \quad . \quad \ldots(A\text{-}10)$$

If loss of gas containment does not fail pump,

$$P(\text{flow}) = \left[\left(2R_w^2 - R_w^4\right) + \left(4R_w^2 - 8R_w^3 + 4R_w^4\right) + 4\left(R_w - R_w^2\right)\left(1 - 2R_w + R_w^2\right)\right]R_T^2\left(2R_c - R_c^2\right) \quad . \quad \ldots(A\text{-}11)$$

$$P(100\%) = \left(2R_w^2 - R_w^4\right)R_T^2\left(2R_c - R_c^2\right) \quad . \quad \ldots(A\text{-}12)$$

D. LINEAR PUMP – TRIPLE PLPA – SINGLE CAN – 50% DEVELOPED PRESSURE RISE REQUIRED IN EACH PUMP

Probability of flow = (probability of 100% + probability of 1 winding in each of 3 units and the cans good + probability of 1 winding in 2 of 3 units and proper cans good + probability of 1 winding and its can good in 1 of 3 units) (probability of 3 good throats) (probability of 1 of 2 cooling coils good)

where:

$$R_p = R_w^2 R_g$$

$$Q_p = 1 - R_w^2 R_g$$

$$P\,(\text{flow}) = \left|\left(3R_w^4 R_g^2 - 2R_w^6 R_g^3\right) + 8R_g^3\left(R_w^3 - 3R_w^4 + 3R_w^5 - R_w^6\right)\right.$$
$$\left. + 6R_g\left(R_w - R_w^2\right)\right|\left|\left(1 - R_w\right)^2 + \left(1 - R_g\right)^2\right|\left|R_T^3\left(2R_c - R_c^2\right)\right| . \quad \ldots(A\text{-}13)$$

Probability of 100% = (probability of 2 of 3 units) (probability of 3 good throats) (probability 1 of 2 coils good)

$$P\,(100\%) = \left(R_p^3 + 3R_p^2 - 3R_p^3\right)R_T^3\left(2R_c - R_c^2\right) = \left(3R_p^2 - 2R_p^3\right)R_T^3\left(2R_c - R_c^2\right)$$
$$= \left(3R_w^4 R_g^2 - 2R_w^6 R_g^3\right)R_T^3\left(2R_c - R_c^2\right) \quad . \quad \ldots(A\text{-}14)$$

If gas loss does not fail pump,

$$P\,(\text{flow}) = \left|\left(3R_w^4 - 2R_w^6\right) + 8\left(R_w^3 - 3R_w^4 + 3R_w^5 - R_w^6\right)\right.$$
$$\left. + 6\left(R_w - R_w^2\right)\left(1 - R_w\right)^2\right|\left|R_T^3\left(2R_c - R_c^2\right)\right| . \quad \ldots(A\text{-}15)$$

$$P\,(100\%) = \left(3R_w^4 - 2R_w^6\right)R_T^3\left(2R_c - R_c^2\right) \quad . \quad \ldots(A\text{-}16)$$

E. LINEAR PUMP – DUAL PLPA – DOUBLE CAN – 100% PRESSURE RISE REQUIRED IN EACH PUMP

where:

$$R_p = R_w^2 R_g^2$$
$$Q_p = 1 - R_p = 1 - R_w^2 R_g^2$$

$$P\,(\text{flow}) = \left|2R_w^2 R_g^2 - R_w^4 R_g^4 + 4R_w R_g\left(1 - 3R_w R_g + 3R_w^2 R_g^2 - R_w^3 R_g^3\right)\right.$$
$$\left. + \left[\left(R_w R_g\right)\left(1 - R_w R_g\right)2\right]^2\right|R_T^2\left(2R_c - R_c^2\right)$$
$$= \left|4\left(R_w R_g\right) - 6\left(R_w R_g\right)^2 + 4\left(R_w R_g\right)^3 - \left(R_w R_g\right)^4\right|\left|R_T^2\left(2R_c - R_c^2\right)\right| .$$
$$\ldots(A\text{-}17)$$

$$P\,(100\%) = \left(2R_w^2 R_g^2 - R_w^4 R_g^4\right)R_T^2\left(2R_c - R_c^2\right) \quad . \quad \ldots(A\text{-}18)$$

If loss of gas does not fail pump,

$$P\,(\text{flow}) = \left(4R_w - 6R_w^2 + 4R_w^3 - R_w^4\right)\left[R_T^2\left(2R_c - R_c^2\right)\right] \quad . \qquad \ldots(A\text{-}19)$$

$$P\,(100\%) = \left(2R_w^2 - R_w^4\right)R_T^2\left(2R_c - R_c^2\right) \quad . \qquad \ldots(A\text{-}20)$$

APPENDIX II
THERMAL ANALYSIS ASSUMPTIONS

Thermal Conductivities [w/cm-°C (Btu/hr-ft-°F)]	
S Glass	0.01 (0.60)
Mica	1.18×10^{-3} (0.0683)
Thermal Insulation	
0.0127 cm (5 mils) SS foil 0.0508 cm (20 mils) mica 0.0127 cm (5 mils) SS foil	1.93×10^{-4} (0.0112)
Copper	3.63 at 371°C (210 at 700°F)
Laminated Hiperco-27	0.502 at 316°C (29.0 at 600°F)
Alumina	0.14 at 371°C (8.0 at 700°F)
Stainless Steel	0.225 at 538°C (13.0 at 1000°F)
Argon	3.17×10^{-4} at 371°C (0.0183 at 700°F)
Helium-Xenon Mixture (M.W. = 40)	1.10×10^{-3} at 399°C (0.0635 at 750°F)
Emissivities	
S Glass	0.80
Copper	0.40
Alumina	0.40
Internal Heat Generation Rates (I^2R)	
Helical Pump – Design No. 74	
Windings	0.207 w/cm (0.526 w/in.)
Laminations	1.10 w/kg (0.50 w/lb)
Inner Stator Can [25.4 cm (10 in.) length, equally distributed]	130 w
Linear Pump – Design No. 66	
Windings	0.055 w/cm (0.14 w/in.)
Per Tooth	2.3 w
Core (slot pitch basis)	1.5 w